



## Methods for Nitrogen Activation by Reduction and Oxidation

Iriawan, Haldrian; Andersen, Suzanne Z.; Zhang, Xilun; Comer, Benjamin M.; Barrio, Jesús; Chen, Ping; Medford, Andrew J.; Stephens, Ifan E.L.; Chorkendorff, Ib; Shao-Horn, Yang

*Published in:*  
Nature Reviews Methods Primers

*Link to article, DOI:*  
[10.1038/s43586-021-00053-y](https://doi.org/10.1038/s43586-021-00053-y)

*Publication date:*  
2021

*Document Version*  
Peer reviewed version

[Link back to DTU Orbit](#)

*Citation (APA):*  
Iriawan, H., Andersen, S. Z., Zhang, X., Comer, B. M., Barrio, J., Chen, P., Medford, A. J., Stephens, I. E. L., Chorkendorff, I., & Shao-Horn, Y. (2021). Methods for Nitrogen Activation by Reduction and Oxidation. *Nature Reviews Methods Primers*, 1, Article 56. <https://doi.org/10.1038/s43586-021-00053-y>

---

### General rights

Copyright and moral rights for the publications made accessible in the public portal are retained by the authors and/or other copyright owners and it is a condition of accessing publications that users recognise and abide by the legal requirements associated with these rights.

- Users may download and print one copy of any publication from the public portal for the purpose of private study or research.
- You may not further distribute the material or use it for any profit-making activity or commercial gain
- You may freely distribute the URL identifying the publication in the public portal

If you believe that this document breaches copyright please contact us providing details, and we will remove access to the work immediately and investigate your claim.

# Methods for Nitrogen Activation by Reduction and Oxidation

H. Iriawan<sup>1,2,9</sup>, S.Z. Andersen<sup>3,9</sup>, X. Zhang<sup>4,5</sup>, B. M. Comer<sup>6</sup>, J. Barrio<sup>2</sup>, P. Chen<sup>4†</sup>, A.J. Medford<sup>6†</sup>, I.E.L. Stephens<sup>2†</sup>, I. Chorkendorff<sup>3†</sup>, Y. Shao-Horn<sup>1,7,8†</sup>

<sup>1</sup>Department of Materials Science & Engineering, Massachusetts Institute of Technology

<sup>2</sup>Department of Materials, Imperial College London

<sup>3</sup>Department of Physics, Technical University of Denmark

<sup>4</sup>Dalian National Laboratory for Clean Energy, Dalian Institute of Chemical Physics, Chinese Academy of Sciences

<sup>5</sup>University of Chinese Academy of Sciences, Beijing, 100049, China

<sup>6</sup>School of Chemical & Biomolecular Engineering, Georgia Institute of Technology

<sup>7</sup>Department of Mechanical Engineering, Massachusetts Institute of Technology

<sup>8</sup>Research Laboratory of Electronics, Massachusetts Institute of Technology

<sup>9</sup>These authors have contributed equally

†Corresponding authors

## Abstract

The industrial Haber-Bosch process to produce ammonia ( $\text{NH}_3$ ) from dinitrogen ( $\text{N}_2$ ) is crucial for modern society. However,  $\text{N}_2$  activation is inherently challenging and the Haber-Bosch process has significant drawbacks, as it is highly energy intensive, not sustainable due to substantial  $\text{CO}_2$  emissions primarily from the generation of  $\text{H}_2$  and requires large-centralized facilities. New strategies of sustainable  $\text{N}_2$  activation, such as low-temperature thermochemical catalysis and (photo)electrocatalysis, have been pursued, but progress has been hindered by the lack of rigor and reproducibility in the collection and analysis of results. In this Primer, we provide a holistic step-by-step protocol, applicable to all nitrogen-transformation reactions, focused on verifying genuine  $\text{N}_2$  activation by accounting for all contamination sources. We compare state-of-the-art results from different catalytic reactions following the protocol's framework, and discuss necessary reporting metrics and ways to interpret both experimental and density functional theory results. This Primer covers various common pitfalls in the field, best practices to improve reproducibility and cost-efficient methods to carry out rigorous experimentation. The future of nitrogen catalysis will require an increase in rigorous experimentation and standardization to prevent false positives from appearing in the literature, which can enable advancing towards practical technologies for the activation of  $\text{N}_2$ .

## [H1] Introduction

### [H2] Importance of NH<sub>3</sub> for Population Growth

Nitrogen is essential to all forms of life and constitutes ~78 % of air in the form of dinitrogen (N<sub>2</sub>). However, the formidable strength of the N≡N triple bond (bond dissociation energy of 9.80 eV per bond at 298 K)<sup>1</sup> makes N<sub>2</sub> fixation into biologically-available forms extremely difficult<sup>2</sup>. N<sub>2</sub> fixation in nature occurs in two ways. Lightning can convert N<sub>2</sub> in air to nitrous oxides (NO<sub>x</sub>)<sup>3</sup>. More dominantly, nitrogenase enzymes can catalyse N<sub>2</sub> reduction to ammonia (NH<sub>3</sub>) by a multi-electron transfer process. The other process involves the hydrolysis of at least 16 equivalents of adenosine triphosphate (ATP) to produce 2 molecules of NH<sub>3</sub> and at least 1 molecule of dihydrogen (H<sub>2</sub>), alongside adenosine diphosphate (ADP) and phosphate (P<sub>i</sub>) release (N<sub>2</sub> + 8 H<sup>+</sup> + 8 e<sup>-</sup> + 16ATP → 2 NH<sub>3</sub> + H<sub>2</sub> + 16ADP + 16 P<sub>i</sub>)<sup>4</sup>. This system performs at up to 65% selectivity to NH<sub>3</sub> at 1 atm N<sub>2</sub> in the absence of N<sub>2</sub>O [REF<sup>4,5</sup>]. Yet, biological N<sub>2</sub> fixation is kinetically slow due to reliance on electron tunnelling<sup>6</sup> and is insufficient to sustain intensive modern agricultural practices<sup>7</sup>.

Prior to industrial production of NH<sub>3</sub> by the Haber-Bosch process, natural fertilizers came in the form of caliche from Chile and guano from Peru<sup>8</sup>. In 1898, Sir William Crookes deemed mass starvation to be the biggest challenge of the 20<sup>th</sup> century<sup>9</sup>, instigating the burgeoning interest in industrial N<sub>2</sub> activation. In 1903, the Birkeland-Eyde process became commercial<sup>7</sup>, utilizing electric arcs to fix atmospheric N<sub>2</sub> into nitric acid (HNO<sub>3</sub>), based on a method used by Henry Cavendish in 1784<sup>10</sup>. In 1908, Fritz Haber managed to synthesize NH<sub>3</sub> from N<sub>2</sub> and H<sub>2</sub> (N<sub>2(g)</sub> + 3H<sub>2(g)</sub> ⇌ 2NH<sub>3(g)</sub>, ΔG° = -32.9 kJmol<sup>-1</sup> (REF<sup>11</sup>), eq. 1) on a table-top machine, but it suffered from remarkably slow kinetics under standard temperature and pressure<sup>8</sup>. To boost the formation rate of NH<sub>3</sub> and tilt the equilibrium, Haber increased both temperature and pressure over an Os catalyst<sup>7</sup>. Subsequently, BASF bought the invention and Carl Bosch up-scaled the production in 1913<sup>7</sup> to the currently known Haber-Bosch process, which operates at 400-450 °C and 150-250 bar over a multi-promoted fused Fe catalyst<sup>12</sup>. This system can be referred to as Gen 1 (**Fig. 1**) and is currently the main commercially available process for NH<sub>3</sub> synthesis. A more active Ru-based supported catalyst was later developed, but it was not as widely adopted due to drawbacks such as high cost and low stability<sup>13</sup>. Gerhard Ertl elucidated the molecular mechanistic details of the catalytic N<sub>2</sub> reduction to NH<sub>3</sub> over Fe, enriching the understanding of the system<sup>14</sup>, for which he was awarded a Nobel Prize in 2007 (**Fig. 1**).

Industrial NH<sub>3</sub> production by the Haber-Bosch process is the backbone of modern society and is responsible for the population boom in the 20<sup>th</sup> century<sup>15-17</sup>. Current annual NH<sub>3</sub> production exceeds 170 million metric tonnes<sup>18</sup> (Mt) globally, of which ~80 % is used as synthetic fertilizer<sup>19</sup>, thereby providing sustenance for two-fifths of the global population<sup>20</sup>. Moreover, NH<sub>3</sub> is the source of every N atom in all synthetic chemicals<sup>21</sup>, a key reactant in the chemical industry<sup>22</sup> and a potential hydrogen energy carrier<sup>23,24</sup>. However, NH<sub>3</sub> production from the Haber-Bosch process is energy and emission intensive. Nearly all the required energy and emissions in NH<sub>3</sub> production originate from the generation of H<sub>2</sub>, most commonly from natural gas via steam-methane reforming<sup>25</sup> (0.75CH<sub>4(g)</sub> + 1.5H<sub>2</sub>O<sub>(l)</sub> ⇌ 3H<sub>2(g)</sub> + 0.75CO<sub>2(g)</sub>, ΔG° = +98.0 kJmol<sup>-1</sup> (REF<sup>11</sup>), eq. 2). For the methane-fed process, NH<sub>3</sub> production has a theoretical minimum energy input of 22.2 GJt<sub>NH<sub>3</sub></sub><sup>-1</sup> with the stoichiometric emission of 1.2 t<sub>CO<sub>2</sub></sub>t<sub>NH<sub>3</sub></sub><sup>-1</sup> (REF<sup>12</sup>). In comparison, modern NH<sub>3</sub> production plants using the best available technology consume 28-33 GJt<sub>NH<sub>3</sub></sub><sup>-1</sup> and emit 1.6 t<sub>CO<sub>2</sub></sub>t<sub>NH<sub>3</sub></sub><sup>-1</sup> (REF<sup>12,25</sup>), but the global average is 2.9 t<sub>CO<sub>2</sub></sub>t<sub>NH<sub>3</sub></sub><sup>-1</sup> (REF<sup>26</sup>) owing to the use of coal and oil-based feedstocks<sup>12</sup>. The annual global NH<sub>3</sub> production (>170 Mt) consumes about 1% of total world energy production and emits 1.4% of global CO<sub>2</sub> emissions<sup>18,25,27</sup>. Implementation of CO<sub>2</sub> sequestration processes

78 or other carbon offsets can reduce emissions but will add cost, plant complexity and energy losses<sup>28</sup>.  
79 Overall, sustainable alternatives for NH<sub>3</sub> production are required to address climate change challenges by  
80 reducing reliance on fossil fuels.

## 81 [H2] Decarbonization of N<sub>2</sub> activation

82 Replacing the generation of H<sub>2</sub> by steam-methane reforming with renewable water splitting ( $3\text{H}_2\text{O}_{(l)} \rightleftharpoons$   
83  $3\text{H}_{2(g)} + 1.5 \text{O}_{2(g)}$ ,  $\Delta G^\circ = +711.4 \text{ kJmol}^{-1}$  (REF<sup>11</sup>), eq. 3) can eliminate CO<sub>2</sub> emissions associated with the  
84 Haber-Bosch process<sup>12</sup>, referred to as Gen 2 (**Fig. 1**), resulting in an energy expenditure of  $\Delta G^\circ = +678.5$   
85  $\text{kJmol}^{-1}$  (REF<sup>11</sup>) for  $\text{N}_{2(g)} + 3\text{H}_2\text{O}_{(l)} \rightleftharpoons 2\text{NH}_{3(g)} + 1.5 \text{O}_{2(g)}$  (eq. 4). Operating the Haber-Bosch at reduced  
86 temperatures and pressures and coupling with renewable H<sub>2</sub> production via water electrolysis could make  
87 NH<sub>3</sub> production sustainable and reduce capital cost via smaller, local reactors. However, major challenges  
88 need to be addressed<sup>29</sup>, including: synthesizing NH<sub>3</sub> at milder conditions (pressures of 20-40 bar) to cope  
89 with the intermittent and low-pressure influent of H<sub>2</sub> from water electrolysis; sustainable separation of pure  
90 N<sub>2</sub> from air, as N<sub>2</sub> is presently separated from O<sub>2</sub> by combustion of unreacted methane; and the discovery  
91 of low-temperature thermochemical catalysts to achieve high yield per pass at moderate pressures.

92 Electrochemical reduction of N<sub>2</sub> and H<sub>2</sub>O to make NH<sub>3</sub> is an attractive strategy because NH<sub>3</sub> can be  
93 synthesized directly at the point of consumption, eliminating transportation cost and emissions and reducing  
94 issues of excess fertilizer run-off<sup>30,31</sup>. The energy expenditure of  $\Delta G^\circ = +678.5 \text{ kJmol}_{\text{fixed N}_2}^{-1}$  (eq. 4) or 19.9  
95  $\text{GJt}_{\text{NH}_3}^{-1}$  for such process can be provided by using (photo)electrochemical systems powered by solar or  
96 wind (Gen 3, see **Fig. 1**). Assuming 5% electrical-to-NH<sub>3</sub> efficiency (the calculation neglects upstream and  
97 downstream separations, see [Supplementary Information](#) for details), 40 m<sup>2</sup> of state-of-the-art solar cells  
98 operating at 20% efficiency should meet the average nutrient requirement of 100 kg of fixed N (expressed  
99 as monatomic nitrogen) per hectare of land per year, making this process sustainable and economical.<sup>32,33</sup>  
100 The current densities will need to be comparable to those of the state-of-the-art electrolyzers to keep down  
101 capital costs; the US Department of Energy has a target<sup>34</sup> of 300 mA cm<sup>-2</sup><sub>geo</sub> at 90% **Faradaic efficiency**  
102 **[G]**.

103 The reduction of N<sub>2</sub> can also be facilitated by non-thermal plasmas, where vibrational excitations of ground-  
104 state N<sub>2</sub> via collision with high-energy electrons can decrease the N<sub>2</sub> **activation barriers [G]**<sup>35</sup>. Typically,  
105 microwave and **dielectric barrier discharge [G]** (DBD) reactors have been used, where the NH<sub>3</sub> synthesis  
106 rate can be increased through heterogeneous catalysis<sup>36</sup>. Kim *et al.* have reported among the highest energy  
107 efficiencies of 25-35 g<sub>NH<sub>3</sub></sub> kWh<sup>-1</sup> (100-140 GJ t<sub>NH<sub>3</sub></sub><sup>-1</sup>) using a DBD reactor and promoted Ru catalyst<sup>37</sup>, but  
108 the challenges lie in the uncompetitive energy efficiency compared to commercial Haber Bosch (28-33 GJ  
109 t<sub>NH<sub>3</sub></sub><sup>-1</sup>) and NH<sub>3</sub> decomposition<sup>38</sup>. Additionally, recent reports suggest a mechanocatalytic method of NH<sub>3</sub>  
110 synthesis under (near) ambient conditions<sup>39,40</sup>, by ball-milling the catalysts under N<sub>2</sub> and subsequently  
111 introducing H<sub>2</sub>, showing early promise of comparable energy efficiency to the Haber-Bosch<sup>39</sup>.

112 Electrochemical oxidation of N<sub>2</sub> by electrolysis to fixate N<sub>2</sub> ( $\text{N}_{2(g)} + \text{H}_2\text{O}_{(l)} + 2.5\text{O}_{2(g)} \rightleftharpoons 2\text{HNO}_{3(aq)}$ ,  $\Delta G^\circ =$   
113  $+14.6 \text{ kJmol}^{-1}$ , eq. 5) expends much less energy than  $\Delta G^\circ = +678.5 \text{ kJmol}^{-1}$  (REF<sup>11</sup>) for the reductive  
114 counterpart (eq. 4). Such process can in principle replace the synthesis of NH<sub>3</sub> and subsequent oxidation of  
115 NH<sub>3</sub> by the Ostwald Process ( $2\text{NH}_{3(g)} + 4\text{O}_{2(g)} \rightleftharpoons 2\text{HNO}_{3(aq)} + 2\text{H}_2\text{O}_{(l)}$ ;  $\Delta G^\circ = -663.9 \text{ kJmol}^{-1}$  (REF<sup>11</sup>, eq. 6)  
116 for the production of nitric acid (aqueous HNO<sub>3</sub> is fully ionized), a primary commodity chemical of  
117 oxidized N<sub>2</sub><sup>41</sup>. The remarkable difference in the energy expenditure for N<sub>2</sub> fixation between reduction and  
118 oxidation can be noted clearly by **standard potentials [G]** of **electrochemical half-cell reactions [G]** plotted

119 on the standard hydrogen electrode (SHE) scale and also on the absolute electron energy scale referenced  
120 to the free electron in vacuum<sup>42</sup>, as shown in **Fig. 2a**. The standard potential for N<sub>2</sub> reduction (N<sub>2(g)</sub> + 6H<sup>+</sup>  
121 + 6e<sup>-</sup> → 2NH<sub>3(g)</sub>, 0.06 V<sub>SHE</sub>, -4.50 eV) is considerably higher than that of water splitting to generate O<sub>2</sub>  
122 (2H<sub>2</sub>O<sub>(l)</sub> → O<sub>2(g)</sub> + 4H<sup>+</sup><sub>(aq)</sub> + 4e<sup>-</sup>, 1.23 V<sub>SHE</sub>, -5.67 eV). The difference indicates the energy need of pumping  
123 electron energy from -5.67 eV to -4.50 eV for each electron transferred, in agreement with standard reaction  
124 free energy of +678.5 kJmol<sup>-1</sup> for N<sub>2(g)</sub> + 3H<sub>2</sub>O<sub>(l)</sub> ⇌ 2NH<sub>3(g)</sub> + 1.5O<sub>2(g)</sub> (with 6 electrons transferred from the  
125 cathodic to anodic half reactions). On the other hand, the standard potential for N<sub>2</sub> oxidation (N<sub>2(g)</sub> + 6H<sub>2</sub>O<sub>(l)</sub>  
126 → 2NO<sub>3<sup>-</sup>(aq)</sub> + 12H<sup>+</sup><sub>(aq)</sub> + 10e<sup>-</sup>, 1.24 V<sub>SHE</sub>, -5.68 eV) is very similar to that of water splitting to generate O<sub>2</sub>  
127 (2H<sub>2</sub>O → O<sub>2(g)</sub> + 4H<sup>+</sup> + 4e<sup>-</sup>, 1.23 V<sub>SHE</sub>, -5.67 eV), where minimum energy is required to activate N<sub>2</sub> and H<sub>2</sub>O  
128 to make NO<sub>3<sup>-</sup></sub> from the thermodynamic standpoint.

129 Since N<sub>2</sub> activation is the challenging step, once N<sub>2</sub> is activated, N-containing compounds can easily be  
130 converted to other N-containing compounds. To this end, direct conversion to nitric oxide (NO) from N<sub>2</sub>  
131 and O<sub>2</sub> via plasma driven processes<sup>43</sup> does not require NH<sub>3</sub> synthesis as an included step. The most  
132 technologically mature form of N<sub>2</sub> oxidation is the Birkeland-Eyde process, which is assisted by **electric**  
133 **arc-generated hot plasma**[G]<sup>44,45</sup>. High-temperature thermal plasmas are not energy-competitive<sup>46</sup> and  
134 require rapid quenching to prevent NO decomposing back to N<sub>2</sub><sup>47</sup>. Researchers are paying increasing  
135 attention to the use of warm and cold (non-thermal) plasmas, as its theoretical energy consumption<sup>48</sup> is  
136 more than two-fold lower than that from N<sub>2</sub> and CH<sub>4</sub>, yet a technological bottleneck lies in low conversion  
137 to product<sup>49</sup>. More recently, a growing number of studies are dedicated to the electron and photon assisted  
138 conversion of N<sub>2</sub> to nitrate (NO<sub>3<sup>-</sup></sub>)<sup>50-56</sup> but seem to suffer significant kinetic limitations similar to the  
139 reductive counterpart.

## 140 [H2] Origin to N<sub>2</sub> activation challenges

141 Activating N<sub>2</sub> by reduction to make NH<sub>3</sub> is kinetically difficult, which demands much more energy than  
142 what is needed thermodynamically to drive reactions at high rates to make these processes economical.  
143 Catalyzing N<sub>2</sub> fixation has been limited largely by the cleavage of the N≡N bond due to the inertness of  
144 N<sub>2</sub> (REF<sup>2</sup>), as related to the high triple bond strength (9.80 eV), high ionization potential (15.84 eV), low  
145 electron affinity (-1.90 eV) and nonpolarity. Ru is considered the most active elemental heterogenous  
146 catalyst for thermochemical NH<sub>3</sub> synthesis (the Haber-Bosch process). The energetics of the possible  
147 elementary steps are examined. The free energy profile for an associative mechanism on Ru(0001) terrace,  
148 which involves N<sub>2</sub> bond cleavage via a hydrogenated intermediate (similar to nitrogenase<sup>6</sup>), is shown in  
149 **Fig. 2a**. The protonation of adsorbed \*N<sub>2</sub> to \*N<sub>2</sub>H (step 1-2, where \* denotes adsorbed species) has the  
150 largest thermodynamic barrier, i.e. the largest energy difference between sequential states, of 1.1 eV  
151 compared to the other elementary steps. This \*N<sub>2</sub> protonation step to \*N<sub>2</sub>H is considered rate-limiting by  
152 invoking the Brønsted–Evans–Polanyi relationship<sup>57</sup>, which linearly correlates the activation barriers to the  
153 reaction energies. In contrast, Ru(0001) step sites adsorb N<sub>2</sub> more strongly than terrace sites and the  
154 thermodynamic barrier at the step sites for \*N<sub>2</sub> to \*N<sub>2</sub>H is much lower (~0.35 eV) as a result of stronger  
155 adsorption on a more undercoordinated site. In addition, the process can be understood commonly via a  
156 dissociative mechanism<sup>58-60</sup>, where N<sub>2</sub> is cleaved upon adsorption into atomic N, and then hydrogenated to  
157 release NH<sub>3</sub>. Although the dissociation of N<sub>2</sub> to 2\*N is thermodynamically favored, this step has a  
158 significant activation barrier, and occurs only at step sites as a result of the prohibitively high activation  
159 barrier for N<sub>2</sub> dissociation on terrace sites<sup>61,62</sup>. Experimentally, the apparent activation barrier on a clean  
160 Ru(0001) single crystal (containing step site density of ~1%) is 0.4 eV and increases to 1.3 eV when small

161 amounts of Au, which preferentially decorate step sites, is introduced, which demonstrates that the rate of  
162 N<sub>2</sub> dissociation is completely dominated by steps<sup>62</sup>. It is worth noting that an activation energy found from  
163 the Arrhenius plot corresponds to the potential energy barrier that only captures the enthalpy term. Thus, to  
164 evaluate the free energy of activation (displayed in **Fig. 2a**), the energy associated with the loss of gas phase  
165 entropy of N<sub>2</sub> as it is bound on the surface has to be included (see Creating free energy diagrams under  
166 Results for further details). Moreover, there are also significant uphill steps for the reduction of \*NH<sub>2</sub> to  
167 NH<sub>3(g)</sub> (step 6-8) at the step sites on Ru(0001), signifying the cost of creating free sites. The apparent  
168 activation energy is the sum of both the activation energy of the rate-limiting step and the cost of making  
169 free sites in a non-trivial manner<sup>61,63</sup>; this is the origin of the Sabatier principle.

170 Activating N<sub>2</sub> by oxidation is equally challenging, and very few systematic investigations on the oxidative  
171 N<sub>2</sub> fixation have been reported in the literature<sup>67,68</sup>. A reasonable starting point would be to consider a series  
172 of hydroxylation-deprotonation steps as computed for N<sub>2</sub> oxidation on rutile RuO<sub>2</sub>(110)<sup>56</sup> in **Fig. 2a**, which  
173 shows N<sub>2</sub> activation to \*N<sub>2</sub>OH is the most uphill step (1.9 eV), suggesting a large kinetic barrier.

174 An important distinction between electrochemical and non-electrochemical steps should be made when  
175 interpreting free energy diagrams. Electrochemical steps, such as those involving proton-electron transfers  
176 (see all steps in **Fig. 2a** except for N-N dissociation, adsorption and desorption), are affected by applied  
177 potential. The overpotential required to bring the most uphill electrochemical step downhill is plotted in  
178 **Fig. 2b** (blue, circle) for associative N<sub>2</sub> reduction on transition metal terraces. In addition to the  
179 thermodynamic barrier, electrochemical steps can possess an additional kinetic barrier. For example, the  
180 intrinsic electrochemical barrier (at  $\Delta G_{step} = 0$ ) for the \*N + e<sup>-</sup> + H<sup>+</sup> → \*NH step on transition metal terraces  
181 were calculated as ~0.7 eV regardless of the free energy difference between the two states (\*N and \*NH),  
182 and thus insensitive to the metal identity<sup>66</sup>. An intrinsic barrier of 0.7 eV for all proton-electron transfer  
183 steps is used in **Fig. 2a**. Non-electrochemical steps, such as N-N dissociation (step 0-1 of the dissociative  
184 N<sub>2</sub> reduction, **Fig. 2a**), adsorption (step 0-1 of the associative N<sub>2</sub> reduction/oxidation) and desorption (step  
185 7-8 of N<sub>2</sub> reduction), are not affected by applied potential.

186 The rate-limiting step, known as the maximum barrier along the reaction pathway whose rate is significantly  
187 slower than those of the other elementary steps, is a feature of interest as it governs the rate of the overall  
188 reaction. The rate constant (*k*) of the elementary step is given by **eq. 7** from transition state theory

$$189 \quad k = v \exp\left(\frac{-\Delta G^\ddagger}{k_B T}\right) \quad (\text{eq. 7.})$$

190 where the prefactor *v* equals  $k_B T/h$  (~10<sup>13</sup> s<sup>-1</sup> at 25 °C). The rate of reaction for heterogeneous catalysis,  
191 expressed in mol cm<sub>cat</sub><sup>-2</sup> s<sup>-1</sup>, is connected to the rate constant by multiplying that with the concentrations of  
192 reactants or with their surface concentrations if the rate limiting step is the first step or involves surface  
193 intermediates, respectively. This rate can be converted to the turnover frequency (mol site<sup>-1</sup> s<sup>-1</sup>) by dividing  
194 the site area density of the catalyst (sites cm<sub>cat</sub><sup>-2</sup>), to mass activity (mol g<sub>cat</sub><sup>-1</sup> s<sup>-1</sup>) by multiplying the specific  
195 surface area (cm<sub>cat</sub><sup>2</sup> g<sub>cat</sub><sup>-1</sup>), and to geometric-area-normalized activity (mol cm<sub>geo</sub><sup>-2</sup> s<sup>-1</sup>) by multiplying the  
196 roughness factor (cm<sub>cat</sub><sup>2</sup> cm<sub>geo</sub><sup>-2</sup>).

197 To rationalize a catalyst's viability, one can calculate the rate constant to estimate the rate and establish the  
198 point at which the barrier on a catalyst becomes prohibitive, which will be defined below. In using eq. 7,  
199 we note that the errors due to the level of theory and a free energy correction of ~0.25 eV<sup>67,68</sup> correspond to  
200 ~5 orders of magnitude difference in rate. Generally, an active catalyst would have a **turnover frequency**



201 [G] greater than  $1 \text{ s}^{-1}$ , which corresponds to a barrier of  $\sim 0.75 \text{ eV}$  at room temperature. Therefore, free  
202 energy diagrams for electrochemical  $\text{N}_2$  fixation under ambient conditions that involve an uphill step greater  
203 than  $1.5 \text{ eV}$  at the operating potential indicate non-viable catalysts, particularly if kinetic barriers have been  
204 neglected. However, a more quantitative and accurate description requires higher forms of simulation to  
205 capture the system's complexity, such as kinetic Monte Carlo simulation or microkinetic modelling; the  
206 latter shown in **Fig. 2b** for the thermochemical route of  $\text{NH}_3$  synthesis. For the electrochemical route, we  
207 refer readers to REF<sup>66</sup> for the full **microkinetic model [G]**.

208 The difficulty of finding catalysts with fast kinetics for  $\text{N}_2$  fixation can be explained by the “scaling  
209 relations”<sup>69</sup>, where the energetics of different elementary steps (**Fig. 2a**) cannot be controlled independently  
210 on a given surface. Such scaling relations can be manifested in the volcano dependence of catalytic activity  
211 on the adsorption energy of surface reaction intermediates. For example, the catalyst activity, computed via  
212 the **mean-field kinetic model [G]** of the dissociative mechanism, exhibits a volcano dependence on the N  
213 adsorption energy (**Fig. 2b**, circle, red)<sup>69</sup>. On the right side of the volcano  $\text{N}_2$  dissociation is rate-limiting  
214 for weak-binding surfaces, and on the left side there is a low barrier for  $\text{N}_2$  dissociation for strong-binding  
215 surfaces, but the surface is poisoned by N species. Fe, Ru and CoMo alloy exhibit the highest activity and  
216 further enhancement can be achieved by using alkali (electronic) promoters<sup>70,71</sup>. However, efficient and  
217 low-pressure Haber Bosch requires more active catalysts beyond the constraints set by the volcano<sup>72</sup>.

218 Scaling relations also constrain electrochemical  $\text{N}_2$  reduction. The overpotential needed to have all the  
219 elementary reaction steps downhill for the associative mechanism (**Fig. 2b**, circle, blue), exhibit a volcano  
220 relationship with the N binding energy on metal surfaces<sup>73,74</sup>. More importantly, electrochemical  $\text{N}_2$   
221 reduction in aqueous electrolytes has to compete with electrochemical  $\text{H}_2$  evolution as both reactions have  
222 similar standard potentials and electron energy on the absolute energy scale (**Fig. 2a**). This competition is a  
223 disadvantage, as the kinetics of water reduction to produce  $\text{H}_2$  is much faster than that reduction of  $\text{N}_2$  to  
224  $\text{NH}_3$ , as seen in the comparatively lower overpotential for  $\text{H}_2$  evolution (**Fig. 2b**, blue, triangle), translating  
225 to many orders of magnitude difference in the estimated rate (**Fig. 2b**). In addition, the bond strength of any  
226 given metal surface to H (a sole intermediate of  $\text{H}_2$  evolution) is stronger and linearly correlates with N-  
227 containing intermediates of  $\text{N}_2$  reduction<sup>32</sup>, which indicates that the surface will be poisoned by  $^*\text{H}$ <sup>75</sup> and is  
228 likely responsible for negligible  $\text{NH}_3$  reported in aqueous systems<sup>76,77</sup>. Although a study on wider  $\text{N}_2$   
229 electrooxidation trends has yet to be reported, a similar scaling relation between the reactant activation and  
230 subsequent hydroxylation or desorption steps is expected, as well as scaling with  $^*\text{O}_2$  intermediates of the  
231 competing  $\text{O}_2$  evolution.

232 Alternative strategies have been explored to overcome the activity and selectivity challenges in  $\text{N}_2$   
233 reduction. Excellent activities using transition metal-LiH composite catalysts in thermochemical  $\text{NH}_3$   
234 catalysis have been reported. In these systems, two active centers are present; transition metal sites to cleave  
235 the  $\text{N}_2$  bond, and LiH to aid N hydrogenation and subsequent  $\text{NH}_3$  desorption<sup>78</sup>. In electrochemical  $\text{NH}_3$   
236 synthesis, the lithium-mediated approach has emerged, where the  $\text{N}_2$  reacts with metallic Li to form  $\text{Li}_3\text{N}$ ,  
237 followed by nitride protonation to evolve  $\text{NH}_3$ , including continuous lithium-mediated  $\text{N}_2$  reduction in non-  
238 aqueous solvents<sup>79–82</sup> or a lithium-nitride cycling scheme<sup>83,84</sup> (**Fig. S2**, see Supplementary Information). The  
239 Li-mediated approach has decoupled reactant activation and subsequent protonation steps, while the non-  
240 aqueous solvent and the in-situ formation of protective solid-electrolyte-interphase layer restrict proton  
241 availability to the active site<sup>82,83</sup>, potentially responsible for the high yields.



## [H2] The need for a strict protocol

Progress in (photo)electrochemical  $N_2$  fixation can benefit from developing a more rigorous protocol of measurements and product quantification, as state-of-the-art yields of  $NH_3$  (and  $NO_3^-$ ) from these processes are significantly lower than thermochemical  $NH_3$  production (see Results) while contamination (possible sources summarized in **Table 1**) can be present at similar or greater concentration levels than the measured product<sup>76</sup>. In addition, the  $NH_3$  yields for low-temperature and/or low-pressure thermal catalysis exponentially drops, and accurate activity measurements can suffer from adventitious N contamination, N and/or H leaching and non-catalytic  $NH_3$  generation<sup>85</sup>, where such uncertainties in catalytic activity measurements can propagate into subsequent kinetic analyses.

The field has been plagued with false positives. The first observation of electrochemical  $N_2$  fixation was in 1807 reporting production of  $NH_3$  and  $HNO_3$  by passing current through distilled water<sup>86</sup>, but was proven non-reproducible some 90 years later<sup>87</sup>. In 1995, the inability to reproduce reported photochemical  $NH_3$  synthesis using  $TiO_2$  under rigorous measurements was rigorously reported<sup>88</sup>. More recently, Sn(II) phthalocyanine catalysts were tested in 2017 for electrochemical  $N_2$  reduction, concluding that the  $NH_3$  initially measured arose from decomposition of the catalyst<sup>89</sup>. Work on nanoscale  $Fe_2O_3$  in molten hydroxide citing adventitious  $NH_3$  synthesis from trace  $NO_x^-$  contaminants in their electrode material was later retracted from *Science* in 2020<sup>90</sup>. Others have retested and reported no electrochemical activity for VN<sup>91</sup>, and Bi and Au catalysts<sup>92</sup>, reported previously to have high activity<sup>93-95</sup>, after accounting for N-leaching from the VN catalyst and properly cleaning the supplied  $N_2$  gas for  $NH_3$  and  $NO_x$  impurities.

The ubiquity of contamination sources calls for an exceptional scrutiny. In this Primer, we introduce a general protocol focused on confirming genuine activation of inert  $N_2$  and elaborate details in performing catalytic measurements (Experimentation). We then evaluate state-of-the-art results, primarily focused on (photo)electrochemical and thermochemical systems using the protocol's framework, and discuss best practices in reporting and interpreting both experimental and **density functional theory [G]** (DFT) data (Results). The potential uses of these  $N_2$  activation reactions are discussed in the context of current practices, highlighting the importance of research in these areas (Applications), and we explore factors affecting reproducibility, thereby establishing reporting standards (Reproducibility and Data Deposition). Finally, we discuss ways to overcome cost-limitations of performing repeated isotope-labelled experiments (Limitations and Optimizations), and outline future directions in  $N_2$  activation research including community-wide adoption of rigorous protocol, in situ measurements for mechanistic understanding and field-specific needs (Outlook).

## [H1] Experimentation

A general protocol for carrying out electrochemical, photo(electro)chemical, and thermochemical  $N_2$  activation experiments is presented, which can be applied across all  $N_2$  activation fields. The unified protocol is followed by an in-depth discussion of the experimental setups and necessary measurements, and different methods of product detection to determine product synthesis.

## [H2] Protocol for N<sub>2</sub> reduction and oxidation

The general protocol highlighted in **Fig. 3** is applicable to any N<sub>2</sub> activation reaction and is based on the principle that one should always be wary of contamination, which should be accounted for accordingly.

The first step involves the experiment setup and is run with N<sub>2</sub>. If no product is measured, re-iterations with new parameters or catalysts is necessary, until the desired product is detected. To account for possible contamination sources, one must measure or estimate the total equivalent N mass of the system,  $mass_{sys}$ , which includes  $mass_{N,cat}$ ,  $mass_{N,electrolyte}$ ,  $mass_{N,absorber}$  and  $mass_{N,gas}$ . Precise definitions of these terms are outlined in **Box 1**.

The amount of N in the product measured must exceed the amount of N in  $mass_{sys}$  by a factor of 2 ( $mass_{prod} > 2 mass_{sys}$ ) – to account for unexpected sources of contamination– and  $mass_{prod}$  should be well above  $mass_{N,cat}$  for synthesis to be classified as effective. The product concentration ( $C_{prod}$ ) in the electrolyte or gas stream must be higher than 100 ppm, as this amount would easily be detectable by olfaction as per the NH<sub>3</sub> detection limit<sup>96</sup> and greater than a common source of contamination in the lab, in which case unaccounted sources of contamination (for example, glassware, breath, laboratory air, etc.) could be excluded.

If both criteria are met, repeated testing is necessary with independently prepared samples to confirm reproducibility. If these criteria were not met, the measured yield of product might stem from contamination, and further evidence of product synthesis via quantifiable isotope-labelling experiments is necessary. First, one must test using an inert gas (such as Ar, although any clean inert gas can be used) and test N<sub>2</sub> in the absence of a driving force. These conditions can range from operating an open circuit potential for electrochemical systems, analysis under dark illumination for photo(electro)chemical systems or in the absence of applied heat for thermochemical systems. Operating under these driving force-free conditions is essential to account for sources of contamination in the experimental set-up, as this should give significantly less to no product compared to N<sub>2</sub> with a driving force. Repeated identical testing of independently prepared batches also follows to ascertain reproducibility and determine the level of inherent contamination (if any) in the system. A stability test is also needed to eliminate the possibility of non-catalytic generation of the product, such as N-leaching from an N-containing catalyst. Once all sources of contamination have been accounted for, quantitative isotopic labelling experiments is necessary. Two separate quantification techniques must be used to detect the product, where at least one of these methods is isotopically sensitive, and repeated and reproducible overlap between the use of <sup>14</sup>N<sub>2</sub> and <sup>15</sup>N<sub>2</sub> over multiple points must be observed (see Results). It is important to include a proper gas cleaning procedure, as isotope labelled <sup>15</sup>N<sub>2</sub> gas can contain significant levels of NO<sub>x</sub> and NH<sub>3</sub> impurities<sup>97</sup>.

Kinetics parameters, such as activation energy and **reaction orders [G]** in the kinetic regime, are a key metric to report when studying thermochemical catalysis. The kinetics measurements should be carried out far from the equilibrium, where mass and heat transfer limitations are minimized, to avoid the reaction reversing. Measurements that enable extracting the activation energy and reaction orders are extremely beneficial for elucidating the reaction mechanism. In particular, the effect of NH<sub>3</sub> concentration on the reaction orders and the apparent activation energy must be accounted for (see Results). Electrochemical and photo(electro)chemical systems can also benefit from kinetic measurements, although this is not common in the literature. To this end, reliable determination of the partial current density toward NH<sub>3</sub> for a given system might be highly inaccurate owing to historic contamination issues in the field, which makes obtaining these measurements difficult. Measuring parameters such as the pH dependence of the N<sub>2</sub> reduction activity might provide insights on the reaction path and mechanism<sup>98</sup> using rigorous

323 experimentation. The only published and proven work reporting kinetic measurements have investigated  
324 the effect of proton and N<sub>2</sub> concentration and their respective reaction orders in the lithium-mediated  
325 system<sup>81</sup>. Tafel analysis [G] can be a powerful tool for elucidating rate determining steps, but overly  
326 simplified assumptions will lead to an inaccurate description of the electrocatalysis<sup>99</sup>, so researchers should  
327 apply caution when interpreting Tafel slopes as they may contain many artefacts<sup>100</sup>. Overall, great care  
328 should be taken with reporting a clear definition of the kinetic parameters and kinetic models used<sup>101</sup> when  
329 including these sets of measurements.

## 330 [H2] Experimental setup

### 331 [H3] Electrochemical measurements

332 Electrochemical measurements are typically conducted in a cell setup as depicted in **Fig. 4a**, into which gas  
333 streams are introduced. Feed gases (Ar, <sup>14</sup>N<sub>2</sub>, and <sup>15</sup>N<sub>2</sub>) must be cleaned prior to use as they can contain  
334 significant amounts of activated N-species (such as NH<sub>3</sub>, NO<sub>x</sub> and N<sub>2</sub>O) as contaminants<sup>97,102</sup>. This purifying  
335 process involves using a reduced Cu catalyst and freeze trap<sup>76</sup> or commercial gas purifiers. One can also  
336 choose to not clean the gas and measure all the N-containing contaminants to include in the value for  
337 *mass<sub>N,gas</sub>*. In the electrochemical cell, the working electrode (WE) will either facilitate N<sub>2</sub> reduction or  
338 oxidation, while the counter electrode (CE) runs the respective counter reaction, depending on the reaction  
339 being evaluated. Meanwhile, the reference electrode (RE) determines the potential at the surface of both  
340 other electrodes. In aqueous electrolytes, numerous commercial REs are available<sup>103</sup> and should be  
341 calibrated against the reversible hydrogen electrode (RHE) by measuring the equilibrium potential for H<sub>2</sub>  
342 oxidation and its evolution on a Pt electrode. Alternatively, a well-known RE such as saturated calomel  
343 electrode (SCE) in aqueous electrolytes, or Li in non-aqueous electrolytes can be utilized, with a conversion  
344 to RHE. Calibrating the RHE in non-aqueous electrolytes can be challenging<sup>104</sup>, but is possible because the  
345 H<sub>2</sub> oxidation and evolution potential is measurable for lithium-mediated N<sub>2</sub> reduction<sup>80</sup>. The same REs as  
346 those used in the battery literature can be used when measuring N<sub>2</sub> reduction in non-aqueous electrolytes,  
347 such as metallic Li<sup>105</sup>, and calibrate the RE to the RHE scale in their electrolyte of choice in a separate  
348 measurement.

349 As activated N-species are ubiquitous, electrochemical and photo(electro)chemical systems are prone to  
350 contamination. Possible sources of contamination are shown in **Table 1**, along with a recommended method  
351 of elimination. Specifically, the commonly used Nafion membrane has been shown to contaminate the  
352 setup<sup>76,106,107</sup> and degrade in the presence of NH<sub>3</sub><sup>108,109</sup>, so extra care must be taken if using this membrane.  
353 For a porous membrane like Celgard, an NH<sub>3</sub> crossover between electrode compartments has been observed  
354 under applied potential condition<sup>77</sup>, which may lead to irreproducible yields especially during a long-term  
355 evaluation. Caution must be taken when using a downstream acid trap in collecting the residual NH<sub>3</sub> from  
356 the gas stream as an acidic solution can readily absorb NH<sub>3</sub> from the environment. Overall, the extent to  
357 which all of these factors influence product quantification must be assessed when reporting catalyst  
358 performance.

359 Control experiments, such as testing using Ar with a driving force and N<sub>2</sub> without a driving force with time-  
360 dependent experiments, are needed. All adventitious sources of activated N<sub>2</sub> can be avoided by the use of  
361 purified isotopically labelled <sup>15</sup>N<sub>2</sub>, and the subsequent measurement of <sup>15</sup>NH<sub>3</sub> or <sup>15</sup>NO<sub>x</sub> by an isotope  
362 sensitive method<sup>76,77</sup>. Liquid samples from the electrolyte should be investigated, repeated for  
363 reproducibility and quantified via at least two separate methods, and the yield produced using <sup>15</sup>N<sub>2</sub> must be  
364 comparable to the yield measured with <sup>14</sup>N<sub>2</sub>.

365 Chronopotentiometric (CP) and/or chronoamperometric (CA) measurements show the stability of the  
366 system over time, and representative data for these should be reported, with a description of whether **Ohmic**  
367 **correction [G]** is utilized. When probing the potential across the electrochemical interface in question, an  
368 **iR-correction**, based on the pre- or post-testing ohmic drop, is generally encouraged as it can eliminate the  
369 system-dependent effects, such as electrolyte conductivity and electrode geometry. However, such  
370 correction must be done with caution especially if the ohmic drop varies during testing owing to factors  
371 such as bubble formation, rising electrolyte levels, temperature variation, build-up of non-conducting  
372 phases observed in the Li-mediated process, among others. In such cases, the potential should be reported  
373 as a range of values rather than a single point. Once the synthesized product is detected, the product yield  
374 and Faradaic efficiency can be calculated as a function of potential vs RHE, enabling the determination of  
375 the optimum for each of these factors in the system. Moreover, the difference between the operating  
376 potential and the equilibrium voltage approximates the overpotential, a critical figure-of-merit. The  
377 overpotential for N<sub>2</sub> reduction to NH<sub>3(g)</sub> is independent of pH and the electrolyte. The Nernstian shift in the  
378 equilibrium potential occurs due to a change in product and reagent concentrations that affect the overall  
379 pH of the solution, and can be taken into account via the actual amount of NH<sub>3</sub> produced. Relative to  
380 standard conditions, the equilibrium concentration of NH<sub>3(aq)</sub> or NH<sub>4<sup>+</sup>(aq)</sub> can be determined by  
381 thermodynamic data (solvation energy) or measured directly via NMR<sup>110</sup>. At pH = 0, the difference between  
382 the standard equilibrium potential N<sub>2(g)</sub>/NH<sub>4<sup>+</sup>(aq)</sub> is 0.27 V vs RHE, though at pH = 14, the standard  
383 equilibrium potential of N<sub>2(g)</sub>/NH<sub>3(aq)</sub> is ~0.1 V vs RHE<sup>11</sup>. However, this Nernstian shift is insignificant  
384 when there is a large overpotential for N<sub>2</sub> reduction, such as the case for non-aqueous lithium-mediated  
385 NH<sub>3</sub> synthesis.

### 386 [H3] Thermochemical measurements

387 Thermochemical measurements are usually conducted in a fixed-bed flow system as shown in **Fig. 4b**,  
388 where the catalyst is loaded into the reactor and pretreated under specified conditions. The reactant gases  
389 (N<sub>2</sub> and H<sub>2</sub>) are passed over the catalyst bed with a certain space velocity, such that the reaction rates are  
390 not limited by gas transport. The reactant gases may need purification by in-line gas purifiers to reduce the  
391 content of impurities (for example, H<sub>2</sub>O, O<sub>2</sub>, CO<sub>2</sub>) to sub-ppm level, as these might affect the surface of the  
392 active catalyst by poisoning the available active sites. The measurements should be conducted under steady-  
393 state conditions as a function of temperature and pressure. The produced NH<sub>3</sub> is typically trapped in a  
394 downstream diluted sulfuric acid solution, which is then quantified by using ion chromatography or a  
395 conductivity meter. The related parameters (such as NH<sub>3</sub> synthesis rate and yield) can be obtained once the  
396 amount of produced NH<sub>3</sub> is determined.

397 Reactors made of stainless steel are commonly employed for pressurized reactions. Transition metals  
398 (including Fe, Cr, Ni) in the reactor may not be inert, and could interfere in the NH<sub>3</sub> synthesis by interacting  
399 with the catalyst. It is recommended to use a reactor made of, or lined with, inert material such as quartz to  
400 exclude the contribution of a “reactive reactor”<sup>111</sup>. A blank test (without catalyst loading) should be  
401 performed prior to catalyst evaluation, to make sure there is no detectable NH<sub>3</sub> contamination present in the  
402 system. In addition, benchmark catalysts, such as Cs-promoted Ru/MgO should be prepared and tested,  
403 with an activity comparable to that previously reported (Cs–Ru/MgO with 3–6 wt.% Ru loading should  
404 have an NH<sub>3</sub> formation rate from 8–14 mmol g<sub>cat</sub><sup>-1</sup> h<sup>-1</sup> at 400 °C and 10 bar)<sup>112–114</sup>. These two experiments  
405 are important for validating the testing system.

406

## 407 [H2] Product detection and Isotope Labelling

### 408 [H3] Non-isotopic product detection

409 UV-Vis spectroscopy allows the fast and easy quantification of  $\text{NH}_3$  through the colorimetric reactions of  
410 either indophenol blue or Nessler's reagents, with a detection limit down to 10 ppb ( $\sim 0.5 \mu\text{M}$ )  $\text{NH}_3$  (**Fig. 5**  
411 **a, b**). The method induces a chemical reaction between  $\text{NH}_3$  and the reagents of choice, leading to the  
412 formation of a colorful dye that is quantifiable via UV-vis spectroscopy with a peak value at 640 nm for  
413 indophenol blue and 425 nm for Nessler's reagents<sup>115</sup>. Despite the simplicity of these techniques,  
414 interferences in the chemical reaction forming the colorful dye may be caused by the presence of different  
415 ions in the media ( $\text{Fe}^{3+}$ ,  $\text{Co}^{2+}$  to  $\text{S}^{2-}$ , etc.), the reaction time and diverse pH conditions, which may impede  
416 accurate quantification of  $\text{NH}_3$ <sup>116</sup>. Nevertheless, some of these can be overcome by using Seignette reagent  
417 (also known as Rochelle salt), which allows the analysis of samples with high salinity<sup>117</sup>. Similar in  
418 principle to indophenol-based detection, the salicylate method is also commonly used to detect  $\text{NH}_3$ .  
419 Recently, a convenient methodology to correct the effect of strong  $\text{Fe}^{3+}$  interference by using an interference  
420 model requiring only three experimental curves was reported<sup>118</sup>.

421 The Griess assay is widely adopted for the quantification of  $\text{NO}_2^-$ . To quantify  $\text{NO}_3^-$ , the sample can be  
422 reduced to  $\text{NO}_2^-$  using Zn powder<sup>119</sup>. However, this method should be used with caution as it suffers from  
423 a comparatively high limit of detection of 500 ppb ( $\sim 10 \mu\text{M}$ ) and interferences with  $\text{Fe}^{3+}$ ,  $\text{Cu}^{2+}$ ,  $\text{S}^{2-}$  or  $\text{I}^-$ .

424 A conductivity meter provides a facile and widely adapted method in thermochemical reactions for  
425 quantifying  $\text{NH}_3$  with a 1 ppm detection limit (**Fig. 5a, c**). The concentration of  $\text{NH}_3$  from the outlet gas  
426 trapped in a diluted sulfuric acid solution can be determined by measuring the decrease in ion conductivity  
427 of the solution, which corresponds to the conversion of  $\text{H}^+$  to  $\text{NH}_4^+$ . A calibration curve of the change of  
428 conductivity and the amount of  $\text{NH}_3$  produced should be determined under a given temperature and  
429 concentration of the solution. It is important to maintain a constant temperature and concentration of the  
430 solution in each measurement as each of these parameters have strong influences on the ion conductivity in  
431 the solution<sup>120</sup>.

### 432 [H3] Isotopic Product detection

433 Nuclear Magnetic Resonance (NMR) is one of the most widely used techniques for determining the  
434 chemical composition of a sample, and can accurately detect  $\text{NH}_3$  down to 50 ppb ( $\sim 3 \mu\text{M}$ ), as shown in  
435 **Fig. 5a, d**. It utilizes the magnetic properties of nuclei with non-zero spins and non-zero magnetic dipole  
436 moments. The sample composition can be determined based on the characteristic radio frequency (RF)  
437 pulse required for the excitation of the nuclei<sup>121</sup>. As the area of the signal is proportional to the number of  
438 nuclei affected by the applied RF pulse, the concentration of the sample can be inferred based on calibration  
439 curves.  $^1\text{H}$  NMR can be used to differentiate isotopes of  $^{14}\text{NH}_3$  and  $^{15}\text{NH}_3$ . Due to the difference in spin  
440 between  $^{14}\text{N}$  and  $^{15}\text{N}$ , the scalar interaction of  $^1\text{H}$  will lead to respectively a triplet peak with a characteristic  
441 spacing of 52 Hz, and a doublet peak with a splitting of 73 Hz. For non-aqueous systems, the use of organic  
442 solvents might interfere with the detection of the  $\text{NH}_3$  signal, however, different methods for solvent signal  
443 suppression have been reported<sup>76,122</sup>.

444 In principle, the quantification of  $^{14}\text{NO}_3^-$  and  $^{15}\text{NO}_3^-$  can be performed using N-NMR. However, the low  
445 production yield of the experiment coupled with the unfavorable NMR properties of  $^{15}\text{N}$  (low gyromagnetic  
446 ratio and long T1 relaxation constants)<sup>123</sup>, implies that long-duration electrochemical experiments must be  
447 performed to allow reproducible quantification at multiple points. One study covering  $\text{N}_2$  oxidation has  
448 used  $^{15}\text{N}$ -NMR<sup>56</sup>, but required  $>100$  ppm concentration of  $\text{NO}_3^-$  for detection, which was achieved via a 50



449 hour experiment. Finding a more convenient isotopic  $\text{NO}_3^-$  detection method is a gap that must be addressed  
450 to enable measuring advances in electrochemical  $\text{N}_2$  oxidation more easily.

## 451 [H1] Results

452 A state-of-the-art overview of electrochemical, photo(electro)chemical and thermochemical  $\text{N}_2$  activation  
453 applying the protocol from the Experimentation section to determine levels of contamination is described.  
454 Important reporting metrics and issues hindering progress in the field is covered in this section, along with  
455 interpretation of both experimental and density functional theory results.

## 456 [H2] Evaluation of $\text{N}_2$ Catalysis Experiments

457 Product yields ( $mass_{prod}$ ), namely  $\text{NH}_3$  for  $\text{N}_2$  reduction and  $\text{NO}_3^-$  for  $\text{N}_2$  oxidation, relative to the size of the  
458 system from which N-contaminants may originate ( $mass_{sys}$ ) are shown in **Fig. 6a**. Thermochemical systems  
459 typically produce several orders of magnitude more  $\text{NH}_3$  (especially at temperatures  $>300\text{ }^\circ\text{C}$ ) compared to  
460  $mass_{sys}$ . As a result, these systems can cross the  $mass_{prod} > 2\ mass_{sys}$  line within the first few hours of  
461 experimentation, and have experimental durations upwards to 100 hours (see Supplementary Information  
462 for a demonstration). The ease with which product yields in thermochemical experiments surpass the size  
463 of the system ( $mass_{prod} \gg 2\ mass_{sys}$ ) supports why contamination issues are not prevalent in thermal  
464 catalysis, and also inherently points towards an intrinsically high catalyst activity.

465 In contrast, electrochemical, photochemical and photoelectrochemical experiments typically show yields  
466 of  $\text{NH}_3$  or  $\text{NO}_3^-$  in orders of magnitude less than the size of the system ( $mass_{prod} \ll 2\ mass_{sys}$ ). None of  
467 these catalytic systems fulfill the  $mass_{prod} > 2\ mass_{sys}$ , and would require several orders of magnitude longer  
468 experimentation times (with proper gas cleaning) to afford more product. To this end, some suspiciously  
469 high yield rates from recent (photo)electrochemical studies have been reported (**Fig. 6b**), including the Bi  
470 point<sup>95</sup> operating at only  $-0.7\ \text{V}_{\text{RHE}}$ , which reported production rates higher than some very active  
471 thermochemical catalysts operating at elevated pressure and temperature conditions. These results should  
472 have raised some concerns due to the reported high computed barrier ( $>2\ \text{eV}$ ) and the selectivity challenge  
473 against  $\text{H}_2$  evolution<sup>32</sup> (see **Fig. 2b**). As the flagged point has been shown as non-reproducible<sup>92</sup>, this  
474 example serves to highlight how adventitious N sources can lead to non-genuine  $\text{N}_2$  fixation and inflate the  
475 reported yield rates. Comparison of the reported intrinsic activity (turnover frequency) with thermochemical  
476 catalysts also shows this conclusion (see **Fig. S3** in Supplementary Information) and can be used to screen  
477 potential false positives. In most cases, the catalytic activity of electro/photocatalysts are much lower than  
478 the thermal counterpart and so hundreds of hours of experimentation are required to surpass  $mass_{sys}$  (see  
479 Supplementary Information for demonstration). Therefore, quantitative isotope-labelling experiments,  
480 along with a proper gas-cleaning protocol, is a convenient and unambiguous way to verify genuine  $\text{N}_2$   
481 fixation, thereby proving the origin of the activated N.

482 Non-aqueous electrolytes are the only known conditions in which genuine electrochemical  $\text{N}_2$  reduction  
483 under standard temperature and pressure is reliably demonstrated to date, and the Li-mediated system is  
484 therefore the only benchmark system that can be used for this process<sup>76,81,82</sup>. Several generations of  
485 breakthroughs are still needed to enhance reaction kinetics and achieve viable photo- and (photo)electro-  
486 catalytic performances for commercial applications<sup>124</sup>. Advances in catalyst and electrolyte design are  
487 therefore required<sup>125</sup>, but low product concentrations ( $mass_{prod}$ )<sup>76,126</sup> in these fields means a rigorous  
488 experimental protocol must be followed to ensure the integrity of reported experimental results.

489 The current goal in thermochemical  $\text{NH}_3$  production is to decrease the temperature and pressure, enabling  
490 milder operational conditions compared to current Haber-Bosch plants<sup>12</sup>. However, lowering the  
491 temperature leads to an exponential decrease in the formation rate, which increases the possibility of  
492 contamination, particularly if the catalyst contains activated N. Also, the  $mass_{prod}$  for these low-temperature

493 systems becomes so low that they fall below the  $mass_{prod} > 2 mass_{sys}$  threshold and are comparable to some  
494 of the more active electrochemical systems, necessitating isotope measurements. We note that the integrity  
495 of the reported formation rate must be rigorously evaluated especially at the low production points, because  
496 if the activity measurement is based on incorrect yields of  $NH_3$ , the error will propagate to the subsequent  
497 kinetic analysis.

## 498 [H2] Electro- and Photo(electro)-chemical Reactions

### 499 [H3] Reporting metrics of experimental results

500 To measure the catalytic performance, CA and/or CP measurements are carried out and the product  
501 concentration is determined, enabling a calculation of the yield and Faradic efficiency of the process.  
502 Typically, a metric such as the partial current density or formation rate is plotted as a function of applied  
503 current or potential, and the Faradaic efficiency is overlaid on a separate y-axis, displaying the maximum  
504 performance of the system (**Fig. 7a**)<sup>79</sup>. In photoelectrochemical systems, incident photon-to-current  
505 efficiency should be calculated utilizing a monochromatic light source<sup>127</sup>. All experiments should be  
506 repeated several times, from at least three independent batches of experiments to allow appropriate  
507 determination of a mean and its associate standard deviation. Representative CA or CP graphs should also  
508 be shown, as this illustrates the catalyst stability with time (**Fig. 7b**). In the case of powder photocatalysis,  
509 the amount of product formed should be plotted versus time and a production value per hour and gram  
510 catalyst can be extracted. The amount of product formed must be correlated with the amount of incident  
511 photons reaching the reaction vessel by calculating the average quantum yield [G] (or quantum efficiency),  
512 which is measured with monochromatic light sources or cut-off filters at a wavelength relevant to the  
513 monitored species<sup>128,129</sup>.

514 As rigorous product detection is key to appropriately evaluating activity of (photo)electrochemical  
515 catalysts, product concentrations should be verified using at least two independent detection methods and  
516 quantitative agreement must be observed with each method over multiple points<sup>130</sup>. Typically, this strategy  
517 involves comparing results from colorimetric methods with results from isotope labelled experiments<sup>76</sup>.  
518 Ideally, the amount of product measured using appropriately cleaned  $^{15}N_2$  (**Fig. 7c**) can reproduce the  
519 amount measured using  $^{14}N_2$  quantitatively over numerous points, and a linear increase in detected product  
520 as a function of time or charge passed is observed (**Fig. 7d**).

521

### 522 [H3] Issues hindering progress in (photo)electrochemical $N_2$ activation

523 Reported yields and Faradaic efficiencies are very low for both electrochemical  $N_2$  reduction and oxidation  
524 owing to the selectivity challenge and the activity issue. The reported partial current densities towards  $NH_3$   
525 are  $\lesssim 1 \text{ mA cm}_{geo}^{-2}$  with up to 60% Faradaic efficiency. However, great care must be taken with  
526 experimentation to avoid false positives because  $NH_3$  is ubiquitous in the environment<sup>131</sup> in concentrations  
527 similar to or greater than those reported. Many reports in **Fig. 6c** now include isotopic labelling  
528 experimentation (crossed points), which reflects the shift towards utilizing isotopes that has occurred over  
529 the previous 2 years<sup>76</sup>. Unfortunately, many of these reports only perform isotopic labeling in a single  
530 experiment<sup>95,132-138</sup>, which does not demonstrate reproducibility as this is not enough to prove beyond doubt  
531 that synthesis of the product takes place. Also, the isotopically labelled gas typically contains  $^{15}NH_3$  and  
532  $^{15}NO_x$  impurities<sup>97</sup>, and most of these recent reports do not clean the gas prior to conducting the  
533 measurements, or if gas cleaning is reported it was done incorrectly<sup>102</sup>. Many of these reports are aqueous  
534 systems (non-asterisked), which typically suffer from low selectivity due to the competing  $H_2$  evolution  
535 reaction<sup>32</sup> and could therefore be contaminated. The flagged Bi report<sup>95</sup> demonstrates the possibility of



536 inflated yield rates due to contamination: therefore researchers should reexamine high catalytic activity  
537 results via a rigorous experimentation<sup>76,102</sup> (see Experimentation). The Li-mediated system (denoted  
538  $\text{Li}_x\text{N}/\text{xx}$ )<sup>139,140</sup> has recently gained renewed interest as it has proven effective via rigorous isotope sensitive  
539 experimentation<sup>76</sup>. This system is displaying comparatively increased partial current density towards  $\text{NH}_3$ <sup>81</sup>,  
540 but it requires very negative potentials owing to the necessity of Li plating, making it energy inefficient.

541 For  $\text{N}_2$  oxidation (squares, **Fig. 6c**), the partial current densities to  $\text{NO}_3^-$  are  $\lesssim 10 \mu\text{Acm}^{-2}_{\text{geo}}$ <sup>50</sup>, and the highest  
542 activity catalysts tend to correspond to  $\lesssim 1\%$  Faradaic efficiencies<sup>56,141</sup>. The field of electrochemical  $\text{N}_2$   
543 oxidation is novel and small, with only a handful of published papers<sup>50-52,56,141</sup>. However, there is hope of  
544 a significant increase in the selectivity because  $\text{H}_2$  evolution is not a competing reaction to  $\text{N}_2$  oxidation as  
545 it is for  $\text{N}_2$  reduction. More theory to elucidate the reaction mechanisms is needed, along with a  
546 standardization and rigour regarding measurement, as the yields and product concentrations achieved are  
547 still very low.

548 In the case of photon-driven  $\text{N}_2$  fixation, there is a general lack of rigorous testing<sup>116</sup>. The activity of titania  
549 is highly dependent on supplier, which has been attributed to differences in oxygen vacancy abundance<sup>142</sup>  
550 or carbon contaminants<sup>143</sup>. Nonetheless, there is an increasing number of reports of photochemical  $\text{N}_2$   
551 fixation on titania and numerous other materials<sup>64,116</sup>. Literature results in photochemical  $\text{N}_2$  fixation must  
552 be viewed in the context of experimental rigour, which not only includes mere isotope labelling experiments  
553 but also tangible efforts to account for contamination sources, including the elimination of  $^{15}\text{NH}_3$  and  $^{15}\text{NO}_x$   
554 impurities in gas streams. The necessity of isotope-labelled experiments is a consequence of the inherent  
555 measurement challenges, similar to those within electrochemical systems. For instance, some of the most  
556 widely utilized semiconductor photocatalysts for  $\text{N}_2$  reduction are based on carbon nitride materials<sup>144,145</sup>,  
557 which contain many amine terminal moieties and a generally high N content that can lead to producing  
558 meaningful amounts of  $\text{NH}_3$  upon degradation<sup>146</sup>. Additionally, residual alcohols, amines and/or organic  
559 solvents can interfere with  $\text{NH}_3$  quantification and result in an unreliable determination of  $\text{NH}_3$  yields<sup>116,147</sup>.  
560 Photochemical studies in which isotope labelling shows quantitative agreement between  $^{14}\text{N}_2$  and  $^{15}\text{N}_2$  over  
561 multiple points (i.e. as a function of illumination time), along with proper gas cleaning to scrub away  $^{15}\text{NH}_3$   
562 and  $^{15}\text{NO}_x$  impurities, have yet to be reported. Nonetheless, theoretical works suggest that photo-excited  
563 holes or electrons may facilitate N fixation more easily than metal electrodes, as the adsorbates at the  
564 electrodes may not be in equilibrium with the charge carriers<sup>32</sup>.

## 565 [H2] Thermochemical $\text{N}_2$ Reduction

### 566 [H3] Reporting metrics of experimental results

567 The effects of temperature, pressure, and space velocity on catalytic activity as well as stability testing  
568 should be measured to evaluate a catalyst. The typical reports of catalytic performance are shown in **Fig. 8**.  
569 A temperature-dependent activity test within a certain temperature range (250-400 °C) should be conducted,  
570 and a benchmark catalyst (Cs-Ru/MgO) should also be tested under identical conditions. Special care  
571 should be given to the measurement of low-temperature activity (temperatures below 250 °C) as less  
572 product is formed due to lower activity, thereby being more prone to contamination issues and potentially  
573 not satisfying the criteria of  $\text{mass}_{\text{prod}} > 2 \text{mass}_{\text{sys}}$ . For some of N-containing catalysts, such as nitrides,  
574 amides, imides and N-doped carbonaceous support, the catalysts should be reduced/pretreated under  $\text{H}_2$  or  
575  $\text{H}_2/\text{N}_2$  at elevated temperature long enough to remove any reactive species from the catalyst. The stability  
576 is also crucial for evaluating the performance of a catalyst, and the activity data is only meaningful if there  
577 is stable performance. A life-time evaluation should show  $\text{NH}_3$  production that is greater than the amount

578 of N in the system, and the NH<sub>3</sub> concentration should be greater than 100 ppm in the outlet gas. Isotope  
579 sensitive measurements are necessary if these production levels are not observed.

580 Kinetic measurements should be conducted under conditions far from the thermodynamic equilibrium and  
581 in the absence of mass and heat transfer limitations (**Fig. 8c**). The reaction rate is affected by the partial  
582 pressures of all gaseous components (N<sub>2</sub>, H<sub>2</sub> and NH<sub>3</sub>) as is shown in the power-law rate equation

$$583 \quad r = kP_{NH_3}^{\alpha}P_{N_2}^{\beta}P_{H_2}^{\gamma} \quad (\text{eq. 8})$$

584 where  $r$  is the reaction rate,  $k$  is the rate constant,  $P$  is the partial pressure of the reactants or product,  $\alpha$ ,  $\beta$   
585 and  $\gamma$  are the reaction orders for NH<sub>3</sub>, N<sub>2</sub> and H<sub>2</sub>, respectively<sup>148,149</sup>. The reaction order of NH<sub>3</sub> ( $\alpha$ ) is  
586 obtained by measuring the NH<sub>3</sub> synthesis rates with varying total gas flow ( $F$ ) at constant H<sub>2</sub> and N<sub>2</sub> partial  
587 pressures. The reaction order of NH<sub>3</sub> ( $\alpha$ ) could be obtained by plotting  $\log(P_{NH_3})$  (or  $\log(C_{NH_3})$ , where  $C_{NH_3}$   
588 is the NH<sub>3</sub> outlet concentration) vs.  $\log(1/F)$  where the slope is  $1/(1-\alpha)$ . For a step-by-step derivation, readers  
589 are referred to the [Supplementary information](#).

590 For the reaction orders of N<sub>2</sub> ( $\beta$ ) and H<sub>2</sub> ( $\gamma$ ),  $\log(r)$  plotted against  $\log(P_{N_2})$  would give a slope of  $\beta$  and  
591  $\log(r)$  plotted against  $\log(P_{H_2})$  would give a slope of  $\gamma$  provided that the partial pressures of the other gasses  
592 are kept constant. In cases where it is difficult to keep the NH<sub>3</sub> partial pressure ( $P_{NH_3}$ ) constant by changing  
593 the flow rate while varying either the N<sub>2</sub> or the H<sub>2</sub> partial pressure independently, one may determine  $\beta$  and  
594  $\gamma$  by plotting  $\log(r) - \alpha\log(P_{NH_3})$  vs.  $\log(P_{N_2})$  or by plotting  $\log(r) - \alpha\log(P_{NH_3})$  vs.  $\log(P_{H_2})$  (**Fig. 8c**)  
595 respectively, however it is a less desired solution (see derivation in the [Supplementary Information](#)). It is  
596 worth noting that the term  $\alpha\log(P_{NH_3})$  cannot be omitted unless  $\alpha$  is close to zero or the partial pressure of  
597 NH<sub>3</sub> is kept constant. Calculating  $\beta$  or  $\gamma$  without accounting for NH<sub>3</sub> partial pressure variation may obtain  
598 inaccurate values of reaction orders and lead to a problematic interpretation of the reaction mechanism.

599 Generally, the N<sub>2</sub> order is positive and close to unity for the conventional oxide or carbon supported catalyst  
600 because the rate-determining step of these catalysts is the N<sub>2</sub> activation. However, H<sub>2</sub> and NH<sub>3</sub> orders can  
601 differ between various catalysts. For the iron-based catalysts, the H<sub>2</sub> order is positive and the NH<sub>3</sub> order is  
602 negative because of the strong adsorption of N<sup>150,151</sup>. In contrast, the H<sub>2</sub> order can be negative for some of  
603 the Ru-based catalysts due to the strong H<sub>2</sub> adsorption<sup>152</sup>.

604 In theory, the apparent activation energy ( $E_a$ ) should be determined by plotting  $\ln(k)$  vs.  $1/T$ , rather than  
605  $\ln(r)$  vs.  $1/T$  because the variation of NH<sub>3</sub> partial pressure has influence on the reaction rate according to  
606 the power-law rate equation. Thus,  $E_a$  should be measured at a constant NH<sub>3</sub> pressure. As shown in **Fig. 8d**,  
607 the apparent  $E_a$  values calculated at constant NH<sub>3</sub> pressure were greater than those determined at constant  
608 flow rate over RuCl<sub>3</sub>/γ-Al<sub>2</sub>O<sub>3</sub> catalysts<sup>153</sup>. The importance of NH<sub>3</sub> partial pressure should be considered in  
609 the kinetic measurements, as it could otherwise lead to inaccurate values. Moreover, we note the apparent  
610 activation energy is a complex function of both the activation energy for the rate-limiting step and the cost  
611 of freeing up sites. Thus,  $E_a$  cannot be directly compared to the activation enthalpy (nor the free energy) of  
612 the rate-limiting step.

613

614 [H3] Issues hindering progress in thermochemical N<sub>2</sub> reduction

615 Generally, catalysts operated at lower temperature are associated with a lower NH<sub>3</sub> synthesis rate. More  
616 recently, reactive catalytic materials have been employed for thermal NH<sub>3</sub> synthesis (**Fig. 6d**). Materials  
617 such as electrides<sup>112</sup>, hydrides<sup>78</sup>, nitrides<sup>154</sup> and oxy-hydrides<sup>155</sup> have been found effective in  
618 promoting/synergizing with transition metals, making early- and/or late-transition metals highly active.  
619 Some of the transition metal hydrides alone were also found to be catalytic active<sup>156,157</sup>. Those materials,  
620 however, have dynamic responses to the reacting environment. A recent neutron scattering investigation

621 reveals formation of H-containing species in the C12A7:e<sup>-</sup> lattice under reaction conditions<sup>158</sup>. The TiH<sub>2</sub>  
622 shows the potential nitridation of the surface during the reaction<sup>156</sup>. The VH<sub>0.39</sub> is most likely converted into  
623 VH<sub>0.44</sub>N<sub>0.16</sub> under reaction conditions, which is the stable active composition<sup>157</sup>. Amides, hydrides and  
624 nitrides of alkali/alkaline earth/rare earth metals can also react with H<sub>2</sub>, N<sub>2</sub> and/or NH<sub>3</sub><sup>159</sup>. Moreover,  
625 catalyst made of coordination-unsaturated transition metal atoms or clusters may alter its chemical  
626 composition or physical state in response to the reacting environment. Characterization on a catalyst  
627 quenched by the reaction being evaluated would be more meaningful to provide information on the  
628 composition and chemical state of the active phase/site. However, this means of catalyst evaluation has yet  
629 to be fully addressed.

630 Adventitious N sources can also be significant when claiming catalytic activity with NH<sub>3</sub> concentration  
631 below 100 ppm or  $mass_{prod} < 2 mass_{sys}$ . In addition to the possible sources of contamination discussed in  
632 electrochemical N<sub>2</sub> reduction/oxidation reactions, attention should also be given to reactive catalysts that  
633 would build up lattice or surface N species in situ under a N<sub>2</sub>- or NH<sub>3</sub>-rich atmosphere and elevated  
634 temperatures. Those N species have a chance to convert to NH<sub>3</sub> via a non-catalytic mechanism when the  
635 reaction condition allows for it, such as in an H<sub>2</sub>-rich environment or at a low temperature. This conversion  
636 might result in a false-positive, which calls for using isotope labelling in the activity test for verification.

## 637 [H2] Reporting and interpreting DFT results

638 Quantum mechanical simulations, typically based on **density functional theory [G]** (DFT), are useful in  
639 understanding the mechanisms of N<sub>2</sub> activation. In this section, best practices in creating free energy  
640 diagrams, assessing active site stability and rationalizing free energy diagrams are discussed.

## 641 [H3] Creating free energy diagrams

642 To ensure the overall reaction energy is independent of the catalytic material when creating free energy  
643 diagrams, it is critical to ensure that the initial and final states correspond to gas-phase N<sub>2</sub> and gas-  
644 phase/aqueous products (for liquid-phase systems vapor pressure of N<sub>2</sub> can be used), respectively. For  
645 electrochemical free energy diagrams, a convenient model of applied potential is the computational  
646 hydrogen electrode (CHE) model<sup>160</sup>, but more sophisticated models of applied potential may provide more  
647 accurate energies<sup>161,162</sup>.

648 Considering the free energy of species, rather than only the energy obtained directly from DFT, is critical  
649 whenever computed energies are compared to experimental values<sup>163</sup>. At 0 K, the free energy consists of  
650 the energy obtained from DFT and the **zero point energy [G]**. The temperature-dependent free energy  
651 includes additional contributions from enthalpy and entropy, which can be computed through statistical  
652 mechanics (this standard DFT textbook<sup>164</sup> describes how each term is calculated). The entropy can be  
653 computed by assuming the adsorbate acts as a harmonic oscillator as an approximate upper bound. This  
654 assumption can lead to over-estimation in the case of low-frequency modes because the entropy diverges  
655 as frequency goes to zero for a harmonic oscillator, calling the need for rigorous treating and reporting of  
656 low-frequency modes<sup>165</sup>. Compared to the DFT energies, the inclusion of all free energy terms generally  
657 causes surface states to be less favorable due to the vibrational energy of the adsorbed states and the loss of  
658 entropy as they are bound to the surface. The entropy loss of a gaseous reactant as it becomes bound on the  
659 surface needs to be accounted for when in evaluating the free energy barrier<sup>164</sup> (**Fig. 2a**). The importance  
660 of the full consideration of all free energy terms is more concretely illustrated in **Fig. 9a**. The \*N<sub>2</sub>H surface  
661 species gains 0.16 eV to be adsorbed on Ru (211) when considering only the DFT energy (grey). However,  
662 this \*N<sub>2</sub>H surface species is destabilized by 0.67 eV due to the entropy loss relative to the gas phase and by

0.16 eV owing to change in the zero-point energy of the bonds (while it is stabilized by 0.05 eV from the enthalpy change), all leading to an energy penalty of +0.62 eV for \*N<sub>2</sub>H adsorption. This difference between DFT and free energies reveals that not considering the relevant free energy can lead to qualitatively incorrect conclusions of the thermodynamic driving force(s) for elementary reaction steps and what the rate-limiting steps are.

### [H3] Assessing Active Site Stability

The feasibility of an active site model can be assessed in terms of at least two criteria: stability and reactivity. An active site's stability should be assessed by computing its surface energy using ab initio thermodynamics<sup>160</sup>. In general, activity and reactivity are related by a non-linear volcano plot relationship, where sites that are more reactive tend to be less stable. Therefore, it is necessary to find a trade-off between reactivity and stability<sup>166,167</sup>. An example of an activity-stability plot for surfaces toward O<sub>2</sub> reduction reaction on a number of Pt (111)-derived surfaces, where predicted current density represents activity and surface energy represents stability is shown in **Fig. 9b**. The most relevant surfaces form a **Pareto-optimal frontier [G]** along the activity/stability axes. Surfaces on the Pareto-optimal line represent optimal trade-offs between activity and stability, whereas surfaces below the line are sub-optimal, and surfaces further to the right are less stable and thus more challenging to generate under the atmospheric conditions used as the reference state. However, the stoichiometry of active sites can vary, and their relative stability will vary depending on the chemical potential of the environment. Therefore, it is critical to consider the relevant chemical potentials when assessing active site stability. Competitive adsorption is also an important component of active site stability. For example, analysis of N<sub>2</sub> adsorption free energy often assumes that there is no competitive adsorption from abundant spectator species such as \*H, which may prohibit adsorption and reaction<sup>73</sup>. Surface phase diagrams provide a useful tool to assess stability and coverage of competing intermediates as a function of chemical potential<sup>168</sup>.

### [H3] Rationalizing free energy diagrams

When reading free energy diagrams, a distinction should be made between electrochemical steps and non-electrochemical steps. The thermodynamic barrier  $\Delta G_{step}$ , which is the most uphill step in free energy along the reaction pathway, can be set as a lower bound for the true activation energy,  $\Delta G^\ddagger$ . As mentioned, a free energy diagram for electrochemical N<sub>2</sub> fixation with a thermodynamic barrier greater than  $\Delta G_{step} = 1.5$  eV under ambient conditions should be treated with skepticism.

Moreover, it is also important to consider the adsorption free energy of the inert N<sub>2</sub> molecule, an essential first step of N<sub>2</sub> fixation. N<sub>2</sub> **physisorbing [G]** to the surface results in an energy penalty of 0.67 eV<sup>169</sup> at 25 °C owing to the gas-phase entropy loss, and thus must be compensated by an enthalpic gain. To assess the point where N<sub>2</sub> adsorption becomes rate-limiting, collision theory can be used to obtain the rate of collisions between a gas and a surface<sup>63</sup>. Thus, the number of successful collisions per unit time per area becomes:

$$r \sim \frac{P_{N_2}}{N_A \sqrt{2\pi m k_B T}} \exp\left(-\frac{\Delta G_{*N_2}}{k_B T}\right) [\text{mol}_{N_2} \text{ cm}_{\text{geo}}^{-2} \text{ s}^{-1}] \quad (\text{eq. 9})$$

where  $P_{N_2}$  is the partial pressure of N<sub>2</sub>,  $m$  is the mass of N<sub>2</sub> molecule,  $k_b$  is the Boltzmann constant,  $T$  is the temperature,  $N_A$  is the Avogadro constant, and  $\Delta G_{*N_2}$  is the thermodynamic N<sub>2</sub> adsorption free energy, which is a lower bound for the true adsorption barrier. To obtain the number of successful collisions per site per second, the rate can be multiplied by  $N_A$  and divided by the site density  $N_s$ .

$$r \sim \frac{P_{N_2}}{N_s \sqrt{2\pi m k_B T}} \exp\left(-\frac{\Delta G_{*N_2}}{k_B T}\right) [\text{s}^{-1}] \quad (\text{eq. 10})$$

Using a typical site density<sup>63</sup> of  $N_o = 1.5 \times 10^{15}$  sites  $\text{cm}_{\text{geo}}^{-2}$  and 1 bar of  $N_2$ , the barrier corresponding to 1 successful collision per site per second (turnover frequency of  $1 \text{ s}^{-1}$ ) becomes roughly 0.5 eV at 25 °C. The collision rate can be estimated by using the concentration of dissolved  $N_2$  at standard conditions ( $P_{N_2} = 0.012$  bar) with respect to aqueous solutions, in which case the  $N_2$  adsorption free energy should be below 0.35 eV to ensure that  $N_2$  adsorption is not rate limiting.

## [H1] Applications

Electrochemical, photo(electro)chemical and thermochemical  $N_2$  fixations have primarily been discussed in this Primer due to the size of interest and research efforts in these fields, and the possibilities they offer to sustainably produce high value N-containing chemicals. Particularly power-to- $NH_3$  is an attractive process, as  $NH_3$  is the only other viable carbon-free green fuel to  $H_2$  with significant advantages: it has ~70% higher H density than  $H_2$  in liquid form, it can be liquefied under moderate conditions (20 °C at 0.86 MPa) for a more economical delivery, and it can be stored in benign, low-cost metal halide salts, which are mature, safe and reversible storage systems<sup>170</sup>. It can be used as fuel in gas turbines and power generators, or the  $NH_3$  can be split, thereby providing a source of  $H_2$  gas for fuel-cell based vehicles and marine transportation<sup>171,172</sup>.

Centralized  $NH_3$  production via the Haber-Bosch process is currently slowly replacing steam-methane reforming (Gen 1  $NH_3$ ) with wind or solar-powered water electrolysis to generate  $H_2$  (Gen 2, **Fig. 1**)<sup>28</sup>. Gen 2 facilities would significantly reduce the carbon footprint of  $NH_3$  production<sup>12</sup>. Thermochemical  $N_2$  reduction is a crucial key point, as lowering the required pressure and temperatures of the Haber-Bosch process enables smaller and thereby cheaper production facilities<sup>11</sup>. For fully decentralized  $NH_3$  production, such that there would be one device per farm for fertilizer production, significant breakthrough in electrochemical or photo(electro)chemical  $N_2$  activation (Gen 3, **Fig. 1**) is necessary<sup>173</sup>. These advanced processes could significantly reduce the dependence on Haber-Bosch on a local scale, as the only inputs should be air, water and renewable electricity on a small-scale device. Breakthroughs on the small-system scales (on the order of 1 device per farm or greenhouse) would also lead to electricity storage as  $NH_3$ , aiding the intermittency issue of renewable electricity sources, and more advances in overall power-to-X technologies, as more infrastructure and reliance on Gen 3  $NH_3$  will increase understanding of general electricity conversion, energy storage, and reconversion pathways.

Furthermore,  $N_2$  activation has widespread use across many different fields, as N-containing chemicals is pivotal in the pharmaceutical industry, the synthesis of polymer materials, dye manufacture, and the field of organic synthesis<sup>174</sup>. Direct synthesis of compounds such as urea<sup>175</sup>, the most commonly used and highest N-containing solid fertilizer by weight, via electrochemistry from  $N_2$  and  $CO_2$  in  $H_2O$  would skip the intermediate step of  $NH_3$  synthesis coupled with further processing, enabling decentralized production of a high-value chemical. One could even dream of direct electrochemical synthesis of higher complexity N-containing compounds, such as acetonitrile, pyridines, amino acids, etc.<sup>11</sup>. Understanding  $N_2$  activation as the critical first step can therefore tremendously impact the chemical and pharmaceutical industry.

## [H1] Reproducibility and data deposition

### [H2] The importance of reproducibility

Ensuring complete account and mitigation of contamination sources is key to improving reproducibility in  $N_2$  activation. Given the ubiquity of N-impurities, results of catalytic performance must be accompanied with experimental details showing how contamination sources have been mitigated. To this end, performing complete isotope-labelling experiments, with time-dependent product quantification and proper cleaning of



746 the  $^{15}\text{N}_2$  gas stream, is imperative to ensure unambiguous certainty of successful  $\text{N}_2$  fixation. Additional  
747 rigor needs to be applied when performing electrochemical and photo(electro)chemical measurements and  
748 detecting product formation from these processes, especially when the reported selectivity is very low. For  
749 electrochemical measurements, the pre- and post-test Ohmic resistance can differ substantially (See  
750 [Experimentation](#)) such that the shift in potential should be properly adjusted<sup>76</sup>. Similarly, in thermochemical  
751 studies, catalyst preparation-pretreatment and activity measurements are two main factors influencing the  
752 reproducibility of the experiments, so reporting the associated experimental details is imperative.

753 The reported data should highlight  $n \geq 3$  reproductions, which include at least three repeated measurements  
754 in product detection for each catalytic activity point, three independent activity tests, and three  
755 independently prepared catalyst batches. The mean and spread of each data point must be reported,  
756 acknowledging errors from activity measurements and product detection, with the appropriate number of  
757 significant digits. This is significant as several studies report an excessive number of digits beyond the  
758 precision usually attainable in catalysis.

## 759 [H2] Data deposition and reporting

760 Transparency in reporting and data deposition are essential. Useful figures of merit regarding the catalytic  
761 performance and details of the experimental conditions, as elaborated in **Table 2**, must be reported to enable  
762 a thorough assessment of the experimental rigor and aid comparisons of data collected under different  
763 conditions. Ultimately, these efforts are aimed at evaluating the product mass relative to the system size of  
764 the experiment. Kinetic measurements such as the determination of reaction orders and activation energy  
765 may be required according to the need of these mechanistic details. Lastly, pre- and post-measurement  
766 (and/or in situ) characterization of the catalyst may be necessary to ascertain changes associated with the  
767 reaction conditions.

768 In a move towards open data, raw calibration and test data associated with catalytic activity measurements  
769 should be openly shared, also including the relevant data analysis scripts where possible, and results such  
770 as converged atomic coordinates and vibrational frequencies when a DFT calculation is performed.

## 771 [H1] Limitations and Optimizations

### 772 [H2] Cost of isotope experiments

773 For repeated isotope labelled experiments, the cost of  $^{15}\text{N}_2$  can be prohibitively expensive, as a single long-  
774 term experiment can easily cost upwards to 2,300 USD for 5 L. This high cost can be circumvented by  
775 introducing a glass circulation pump. Once a high enough  $^{15}\text{N}_2$  atmosphere is achieved in the system, the  
776 glass pump will continuously circulate the gas, without the need to supply more throughout the experiment.  
777 Furthermore, the circulation pump has the added benefit of not introducing contaminants over time, if the  
778 gas stream contains any  $\text{NH}_3$  or  $\text{NO}_x$  species, decreasing the possibility of false positives. The glass  
779 circulation pump can be made in-house<sup>176</sup> as seen in **Fig. 10a**, or purchased commercially.

780 Isotopically labelled  $^{15}\text{N}_2$  can contain significant amounts of both  $^{15}\text{NH}_3$ , and  $^{15}\text{NO}_x$  species that reduce  
781 easily, leading to isotopically labelled contamination<sup>97</sup>. We do not advocate the use of aqueous solutions to  
782 clean  $\text{N}_2$ , as they would not trap all contaminants<sup>177</sup>. The residence time of the bubbles compared to the  
783 diffusion time inside the bubbles would need to be ideal, with a certain probability of uptake. The bubbles  
784 need to be tiny, so they rise slowly and have fast internal mixing and large surface/volume ratio<sup>102</sup>.  
785 Furthermore, it is unclear how  $\text{NO}_x$  species would be trapped in acid<sup>134</sup>. We found that a home-made  
786 reduced Cu catalyst combined with a freeze trap to be efficacious for removing impurities, on the basis of  
787 the measured level of all  $\text{NH}_3$  and  $\text{NO}_x$  impurities removed before and after the cleaning<sup>76</sup>. The reduced Cu  
788 catalyst will catch all  $\text{NO}_x$  species, while the cold trap freezes out  $\text{NH}_3$ . Commercial gas purifiers down to

789 parts per trillion per volume fraction (pptV) level are also available for purchase. A complete home-built  
790 and inexpensive system for both the glass circulation pump and the reduced Cu catalyst is shown in **Fig.**  
791 **10b**.

## 792 [H2] Access to NMR

793 NMR is the most commonly reported technique for isotope labelling experiments, as it can distinguish  
794 between  $^{14}\text{NH}_3$  and  $^{15}\text{NH}_3$ . Not all will have access to a high-field 800 MHz NMR, but the use of the more  
795 commonly available 400 MHz NMR can achieve similar sensitivity, covered in more detail in REF<sup>76</sup>.

## 796 [H3] Overcoming mass-transport limitations

797 Mass-transport of  $\text{N}_2$  to the catalyst surface is one of the main limitations in electrochemical and  
798 photo(electro)chemical systems. However, using a gas diffusion electrode (GDE) in a flow-cell system  
799 creates triple-phase (solid, liquid and gaseous) boundary points where  $\text{N}_2$  is readily available for reaction  
800 at the surface of the electrode, which can help circumvent this limitation. Using this GDE is advantageous  
801 over the more common H-cell or single compartment cells that rely on  $\text{N}_2$  solubility in the electrolyte, which  
802 is typically quite low for most liquids<sup>178</sup>. For the electrochemical Li-mediated  $\text{N}_2$  reduction in an H-cell<sup>81</sup>,  
803 the equivalent flow-cell system has been proven to significantly increase the Faradaic efficiency and current  
804 density via application of a slight overpressure on the backside of the GDE<sup>80</sup>.

## 805 [H1] Outlook

### 806 [H2] Adoption of standardized test protocols

807  $\text{N}_2$  reduction and oxidation at low temperature and pressure are reactions with immense technological  
808 significance. Unfortunately, much published research lacks rigorous and standardized testing, leading to  
809 possible contamination and false positives. The possibility of contamination is particularly prominent for  
810 reports with low product formation rates, spanning all electrochemical and photo(electro)chemical systems  
811 to date, as well as some low temperature thermochemical systems. The only conclusive proof of productive  
812  $\text{N}_2$  activation is via repeated and quantified isotope labelled testing coupled with proper gas cleaning. In  
813 this Primer, the cut-off necessitating the use of the crucial  $^{15}\text{N}_2$  quantitative isotope labelling  
814 experimentation for all  $\text{N}_2$  activation reactions has been defined; both  $mass_{prod} > 2 mass_{sys}$  ( $mass_{sys}$  is based  
815 on experimentally measured N in the system) and  $C_{prod} > 100$  ppm must be satisfied. This defined caliber  
816 should prevent reporting false positives, which hinder development of the  $\text{N}_2$  activation field.

817 Beyond electrochemical, photo(electro)chemical and thermochemical systems, efforts on non-thermal  
818 plasma  $\text{N}_2$  fixation have been pursued in recent years<sup>179</sup>. Generally, the plasma-driven  $\text{N}_2$  fixation studies  
819 report product concentrations of hundreds of ppm and up to ~5% of the gas stream<sup>36</sup>, dwarfing the  
820 detrimental contribution of labile N-species from various contamination sources. However, with the field's  
821 primary focus on achieving higher energy efficiency, several studies using dielectric barrier discharges as  
822 the most common plasma source show worryingly low  $\text{NH}_3$  production ( $C_{prod} < 100$  ppm)<sup>35</sup>, possibly dipping  
823 into the range of contaminants. The mechanochemical method of  $\text{NH}_3$  synthesis has also emerged as a new  
824 direction for  $\text{N}_2$  activation<sup>39,40</sup>, with similarly high reported  $\text{NH}_3$  yields, but the field can benefit from the  
825 critical assessment of the potential size of N-contaminants. Researchers in these exploratory areas should  
826 adapt the protocol in this Primer by comparing the product mass with the system size and performing  
827 quantitative isotopic-labelling verification technique at the low-yield data points.

### 828 [H2] In situ mechanistic insight

829 Insight into the reaction mechanisms on  $\text{N}_2$  reduction has largely been built on theoretical  
830 investigations<sup>69,73,180</sup>. In-situ and in-operando techniques to probe intermediate species can validate or  
831 challenge established paradigm, and provide valuable considerations for future catalyst designs. In **Box 2**,



832 we discuss four techniques which can be utilized for electrochemical and thermochemical N<sub>2</sub> activation,  
833 but other spectro(electro)chemical techniques such as Differential Electrochemical Mass Spectrometry  
834 (DEMS) among others in development may be useful. All of these techniques can be complemented with  
835 Raman and core-level spectroscopies to gain an understanding of the underlying mechanistic processes  
836 enabling N<sub>2</sub> activation. However, adoption of the rigorous protocol takes precedence to ensure what is being  
837 detected is not associated with the presence and redox processes of adventitious N sources.

## 838 [H2] Commercialization

839 The reported false positives and likely unreliability of many prior publications in N<sub>2</sub> fixation have  
840 undoubtedly affected the reputation of the field. In the immediate future, the scientific community should  
841 aim to restore the field's integrity and eliminate the emergence and propagation of unreliable results. An  
842 increase in rigor of experimental practices, efforts to reproduce reported results, cross-pollination of  
843 knowledge and best practices across laboratories, and a more deliberate regard toward fundamental  
844 concepts and principles will support this restoration.

845 In the next 5-10 years, we anticipate researchers will focus on addressing the field-specific needs (**Box 3**),  
846 ultimately finding breakthrough catalysts with practically relevant and reliably demonstrated yield rates,  
847 selectivity, stability and energy efficiency to enable industrial deployment of sustainably-produced NH<sub>3</sub>.  
848 The obsessive pursuit of breakthrough results must go hand-in-hand with robust fundamental studies to  
849 identify reaction mechanisms, active sites and reaction kinetics, aided by experimental mechanistic studies  
850 and quantum chemistry or other computational methods. Ultimately, concerted efforts from experimental  
851 and theoretical communities will be key to discovering practical solutions to decarbonize the activation of  
852 N<sub>2</sub>.

## 854 [bH1] Box 1. Sources of system N mass

855 [bH2]  $mass_{N,cat}$ 

856 The amount of measured N in the catalyst and support, which must be experimentally determined. This  
857 measure is important, even if the catalyst does not intrinsically contain N, as substantial levels of  $NO_3^-$  and  
858 nitrides can contaminate commercial metal sources<sup>107,181,182</sup>, despite manufacturer's claims otherwise.  
859 The simple 2-step procedure of alkaline and acidic treatment of the catalyst should be conducted,  
860 followed by HPLC or UV-vis analysis or any equivalent method for determining N-content.<sup>182</sup> Special care  
861 should be taken regarding N-buildup on the catalyst if pretreated with an N-containing procedural step.  
862 These N-species could contaminate the catalyst, and convert to  $NH_3$  via a non-catalytic route<sup>183,91</sup>.  
863 Therefore, examining the N-content of the catalyst as bought, after any pre-treatment, and after catalysis  
864 should be a routine practice. If the N-content of the catalyst is not experimentally determined, one should  
865 consider  $mass_{N,cat}$  as at least 25% of the whole mass of the catalyst, unless the catalyst is intrinsically N-  
866 containing (for example, a nitride), in which case 100% of the mass should be considered.

867 [bH2]  $mass_{N,electrolyte}$ 

868 The measured amount of N in the electrolyte. Electrochemical and photo(electro)chemical systems  
869 submerge the catalyst in electrolyte, and if the electrolyte itself contains N species, these must be  
870 considered as sources of contamination, owing to possible electrolyte breakdown. However, the  
871 electrolyte itself may also be contaminated, as chemicals and membranes (for example, Nafion) readily  
872 soak up  $NH_3$  from the surroundings<sup>76</sup>, and both  $NO_x$  and  $NH_3$  blank measurements of the electrolyte should  
873 be included with each batch of electrolyte.

874 [bH2]  $mass_{N,absorber}$ 

875 The measured amount of N in the photoabsorber present in photo(electro)chemical system. This may  
876 contain sources of activated N as a contaminant, which should be determined experimentally.

877 [bH2]  $mass_{N,gas}$ 

878 The total calculated N impurities of the  $N_2$  gas stream<sup>97,102</sup>. If the purity of the  $N_2$  is 99.999%, one must  
879 consider 0.001% of the total gas used to be entirely contamination, and calculate the mass of this based  
880 on flow rate and duration. Alternatively, a proper gas cleaning procedure, with reported  $NH_3$  and  $NO_x$   
881 contamination of the gas before and after cleaning can be used.

882

883

884 [bH1] Box 2. In-situ and operando techniques for N<sub>2</sub> fixation

885 [bH2] Surface enhanced infrared spectroscopy (SEIRAS)

886 SEIRAS can detect the adsorbates in electrochemical N<sub>2</sub> fixation in operando. The infrared adsorption  
887 peaks can be attributed to vibrational modes of reaction intermediates, and these signals can be enhanced  
888 on metal surfaces by the SEIRA effect (enhancement of infrared adsorption as a result of enhanced optical  
889 fields on a surface<sup>184</sup>. Several studies have attempted SEIRAS for electrochemical N<sub>2</sub> reduction<sup>185,186</sup>, but  
890 contributions from contamination to the detected species are highly probable. Nonetheless, successful  
891 in-situ Fourier transform infrared (FTIR) spectroscopy for electrochemical NH<sub>3</sub> oxidation on Pt electrode  
892 has been reported<sup>187</sup>. Here, various bands, detected at different voltages, were ascribable to the HNH  
893 bending mode of \*NH<sub>3</sub>, NH<sub>2</sub> wagging mode of \*N<sub>2</sub>H<sub>4</sub>, absorption of NO bridged species and HOH bending  
894 mode of \*OH groups.

895 [bH2] Electron Paramagnetic Resonance Spectroscopy (EPR)

896 EPR allows the monitoring on paramagnetic species - having unpaired electrons - as a function of potential  
897 in an electrochemical process, detectable upon rapid freezing of the electrodes. EPR spectra have  
898 detected nitrous oxides in redox processes in biomolecules<sup>188</sup> and during alcohol oxidation.<sup>189</sup>.  
899 Electrochemical EPR could detect absorbed paramagnetic surface-adsorbed NO (\*NO) species formed  
900 during N<sub>2</sub> oxidation.

901 [bH2] N<sub>2</sub> isotopic exchange reaction (N<sub>2</sub>-IER)

902 N<sub>2</sub>-IER (<sup>15</sup>N<sub>2</sub> + <sup>14</sup>N<sub>2</sub> → 2<sup>15</sup>N<sup>14</sup>N) has been used to probe the reaction mechanisms and the rate-determining  
903 step of the thermochemical NH<sub>3</sub> synthesis, by introducing <sup>14</sup>N<sub>2</sub>/<sup>15</sup>N<sub>2</sub> gas mixtures and monitoring the <sup>14</sup>N<sub>2</sub>,  
904 <sup>15</sup>N<sub>2</sub> and <sup>14</sup>N<sup>15</sup>N gas phase composition. Examples confirming N<sub>2</sub> dissociation as the rate-determining step  
905 using N<sub>2</sub>-IER for NH<sub>3</sub> synthesis have been reported on Fe<sup>190</sup> and Ru<sup>191,192</sup>. A N<sub>2</sub>-IER study on cobalt  
906 molybdenum nitride<sup>193</sup> demonstrates the possible participation of lattice N in a Mars-van Krevelen  
907 mechanism involving the hydrogenation of lattice N to evolve NH<sub>3</sub>, and the refilling of lattice N vacancies  
908 by N<sub>2</sub> gas<sup>194</sup>.

909 [bH2] Steady State Isotopic Transient Kinetic Analysis (SSITKA)

910 SSITKA is performed under steady-state conditions and involves introducing a step change in the isotopic  
911 content of the reactant and monitoring the transient responses of the isotopically labeled species<sup>195</sup>.  
912 SSITKA has been used to study the kinetics of NH<sub>3</sub> synthesis on commercial Fe<sup>196</sup> and Ru<sup>197-200</sup> catalysts. A  
913 study on commercial Fe catalysts reveals \*N as the most abundant reactive intermediate<sup>196</sup>. The role of  
914 potassium promoter over Ru catalysts, investigated by SSITKA, is revealed to induce surface site  
915 heterogeneity on Ru/SiO<sub>2</sub>, creating super-active sites responsible for enhanced catalytic activity<sup>197</sup>.

916

917

918 [bH1] Box 3. Field-specific progress, needs, and insight

919 [bH2] Thermochemical N<sub>2</sub> reduction

920 The thermochemical N<sub>2</sub> reduction is the most advanced in terms of technological readiness, as there are  
921 a variety of newly developed catalysts shown to produce NH<sub>3</sub> at low pressures (1-10 bar) and low  
922 temperatures (< 300 °C). However, higher operation temperatures (compared to ambient conditions) and  
923 pure H<sub>2</sub> as the feed gas are still required, necessitating an additional H<sub>2</sub> cleaning step. Therefore, major  
924 efforts include exploring unconventional, highly active and electron-rich materials as catalysts or catalyst  
925 supports to optimize the reaction rate and decrease the temperature further. Elucidating the active site  
926 and reaction mechanism should also be a focus area. Any progress in fundamental insight and/or  
927 practical transformation in thermochemical NH<sub>3</sub> synthesis would have a profound impact on the field of  
928 heterogeneous catalysis.

929 [bH2] Electrochemical and photo(electro)chemical N<sub>2</sub> reduction

930 The requirements for high yields comparable to the Haber-Bosch process or even to thermochemical  
931 systems are not necessary, as the focus is on creating completely decentralized systems<sup>28</sup>. Unfortunately,  
932 the validation of aqueous results using rigorous protocols<sup>76,102</sup> is necessary in light of the sheer selectivity  
933 challenge in aqueous environments and the ubiquity of contaminants. Once these systems are  
934 experimentally validated, efforts towards increased catalytic activity, selectivity and number of active  
935 sites can be considered<sup>125</sup>.

936 The non-aqueous Li-mediated N<sub>2</sub> reduction process is proven to work, achieving record high energy  
937 efficiencies<sup>79-82</sup>. However, a vast majority of the reported literature still remains focused on aqueous  
938 systems (**Fig. 6**), which is most likely due to the numerous experimental challenges for non-aqueous  
939 systems, such as Ohmic drop compensation and high over-potentials, evaporation of organic solvents,  
940 compatibility of colorimetric methods, etc. Furthermore, this system has significant kinetic challenges due  
941 to mass-transport limitations that need to be overcome, which is possible with the use of GDEs in flow-  
942 cell type systems (see Limitations and Optimizations). Further research in these systems would enable  
943 scientists to tackle these challenges as breakthroughs occur, thereby increasing the feasibility of the  
944 system for practical commercial use.

945 [bH2] Electrochemical N<sub>2</sub> oxidation

946 Electrochemical aqueous N<sub>2</sub> oxidation is piquing the curiosity of the scientific community. Nonetheless,  
947 this field is in its infancy, with ample opportunity for fundamental insight and step improvements to  
948 catalyst performance.

949

950

951

## Tables

952

**Table 1 Electrochemical and photo(electro)chemical systems contaminations sources and solutions.**

953

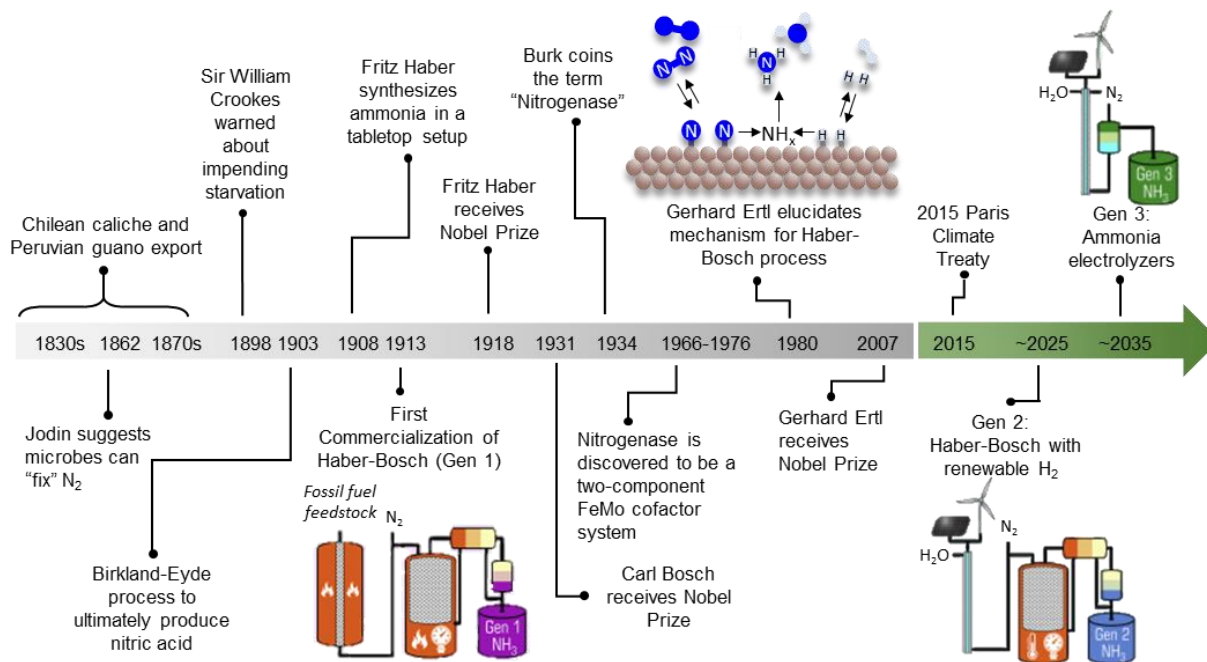
Methods adapted from Liu et al.<sup>107</sup>

Sources of Contamination	Nitrogen form	Method of Elimination
Feed gas <sup>97</sup>	NO <sub>x</sub> , N <sub>2</sub> O and NH <sub>3</sub>	Use of home-made reduced Cu catalyst and a freeze trap, or commercial gas purifier.
Impurities in the catalyst <sup>91,181,182</sup>	NO <sub>x</sub> <sup>-</sup> and NH <sub>4</sub> <sup>+</sup>	Complete removal via pre-reduction of the catalyst before N <sub>2</sub> reduction testing. <sup>107</sup>
Uptake/release from the membrane <sup>76,106,107</sup>	NH <sub>3</sub>	Replace with contamination-free membrane, such as Celgard <sup>107</sup> .
Electrolyte	NH <sub>4</sub> <sup>+</sup> , NO <sub>2</sub> <sup>-</sup> and NO <sub>3</sub> <sup>-</sup>	Removal via annealing of electrolyte salt or other cleaning methods. <sup>107</sup>
Glassware, tubes, laboratory air, etc. <sup>201</sup>	NH <sub>3</sub>	Ensure the entire system is properly cleaned between uses; by boiling in ultra-pure water and drying in oven.

954

**Table 2. Required reporting standards for catalyzed N<sub>2</sub> reduction and oxidation.**

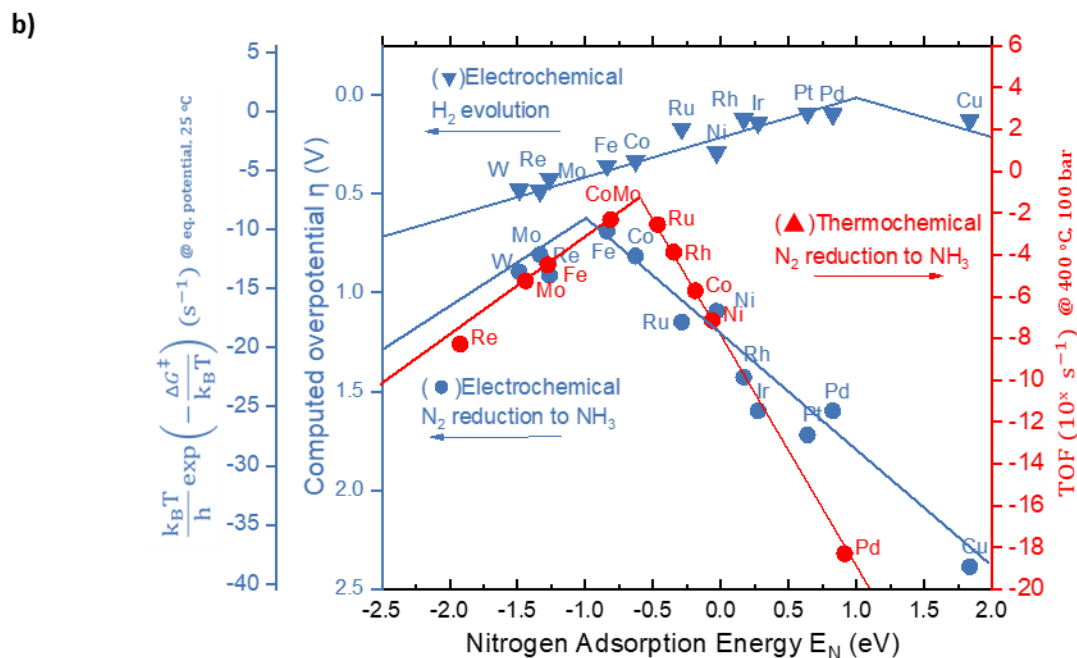
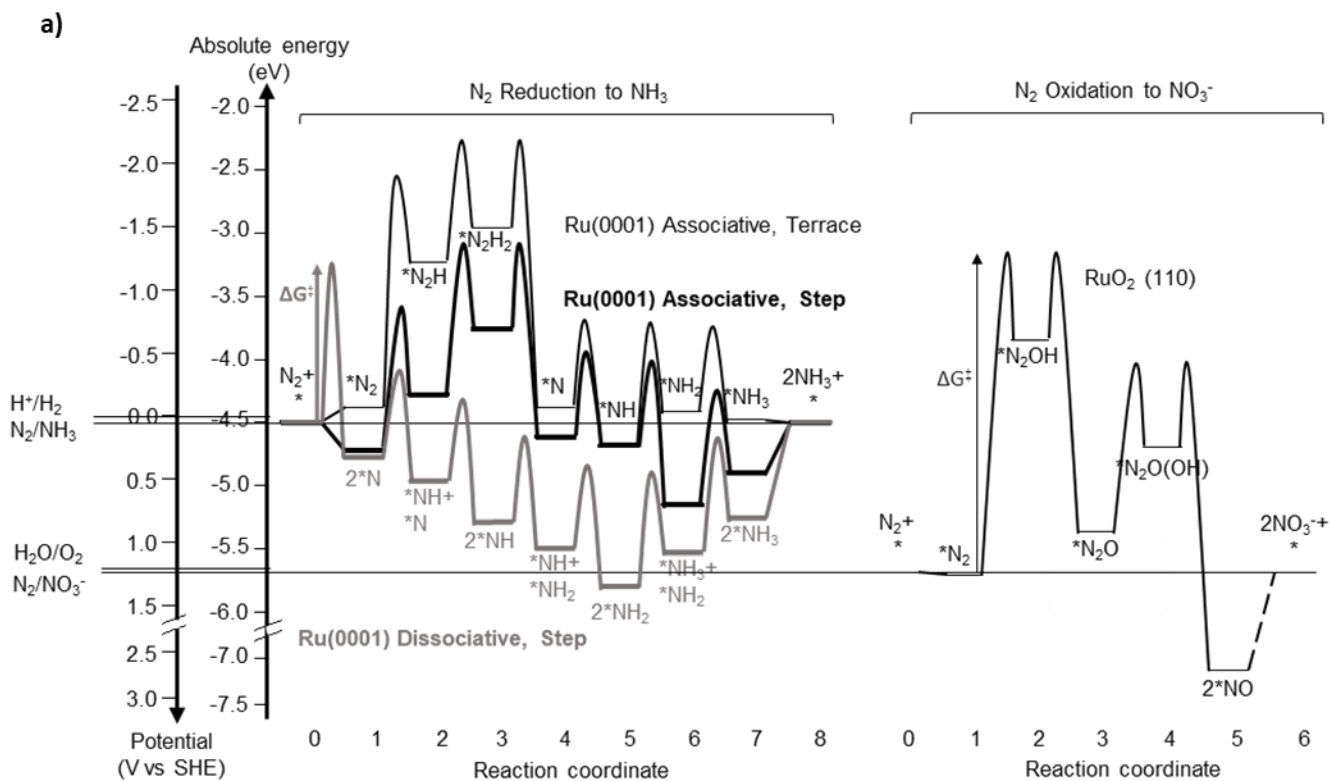
Data type	Definition	System type
<b>Reporting of catalyst performance</b>		
Yield rate	Amount of product formed in a given time interval.	All systems
Area-normalized activity	Yield rate normalized to either geometric or electrochemically active surface area.	Electrochemical
Mass-normalized activity	Yield rate normalized by the mass of catalyst.	All systems
Turnover frequency	Rate of chemical conversion normalized to number of actives per unit of time.	All systems
Faradaic efficiency	Ratio of charges employed for the synthesis of a given product relative to the total amount of charge passed through the circuit.	(Photo)electrochemical
Stability	Capability of a catalyst to perform in prolonged time intervals without detriment in its intrinsic activity	All systems
Energy efficiency	Ratio of converted energy relative to the initial energy input.	All systems
Average Quantum yield	Ratio of electrons transferred towards product relative to the incident photons reaching the sample at a given wavelength.	Photo(electro)chemical
Incident photon-to-current efficiency	Ratio of produced photocurrent versus the incident photon flux at a given wavelength.	Photo(electro)chemical
Reaction orders	The power dependence of reaction rate on reactant concentration.	All systems
Activation energy	The minimum amount of energy required to activate reactants to a state in which they can undergo a chemical reaction.	All systems
<b>Reporting of experimental conditions</b>		
Catalyst loading	Mass of catalyst employed in a single experiment.	All systems
Gas purity & flow rate	Purity and flow rate of the <sup>14/15</sup> N <sub>2</sub> , H <sub>2</sub> and Ar gases.	All systems
Time	Length of time of the experiment.	All systems
Potential	The operating potential of working electrode during reaction.	Electrochemical
Electrolyte volume	The volume of the supporting electrolyte used in electrolysis.	(Photo)electrochemical
Temperature and pressure	The temperature of the catalyst bed and the total pressure of the reaction gases.	All systems
Photon intensity	Photon flux reaching the sample per second and illumination area.	Photo(electro)chemical
Illumination area/distribution	Available surface for the incident photon flux to reach the sample.	Photo(electro)chemical
Weight hourly space velocity	Flow rate of the reaction gas fed to the reactor, divided by the mass of catalyst.	Thermochemical (most relevant)
<b>Essential Information</b>		
Gas cleaning procedure	An account of how impurities are removed in the gas streams.	All systems
Technical specifications of materials	Details such as manufacturer and purity of commercial catalyst and reagents used in catalyst synthesis; purity of electrolytes and ionic salts; additive content (for non-organic solvents).	All systems
Key experimental details	Details such as the use of glovebox during electrolysis, cleaning of system impurities, solvent-handling (drying steps), and residual water traces (non-aqueous systems).	(Photo)electrochemical
Catalyst characterization	Structural or chemical information pre- and post- catalytic measurement to inform changes to the catalyst.	All systems



957

958 **Fig. 1. Historical development of N<sub>2</sub> activation.** Nature mainly produces activated N-species via the  
 959 nitrogenase enzyme<sup>6</sup>. The source of N-containing fertilizer first originated from caliche deposits and  
 960 guano, both predicted to be unsustainable<sup>8</sup>. Two commercial N<sub>2</sub> activation processes emerged in early  
 961 20<sup>th</sup> century: the Birkland-Eyde and Haber-Bosch process, and the latter has since dominated the N<sub>2</sub>  
 962 activation industry<sup>7</sup>, with 3 Nobel prizes given for its discovery<sup>14</sup>. With the global commitment to tackle  
 963 climate change, the decarbonization of N<sub>2</sub> fixation is envisioned to involve two technology generations:  
 964 coupling the Haber-Bosch process with renewable H<sub>2</sub> (Gen 2) and electrochemical NH<sub>3</sub> synthesis (Gen 3)<sup>28</sup>.  
 965 Components coloured orange represent process steps requiring elevated temperatures. Schematics of  
 966 Gen 1, 2 and 3 technologies were adapted with permission from REF<sup>28</sup>, Elsevier.

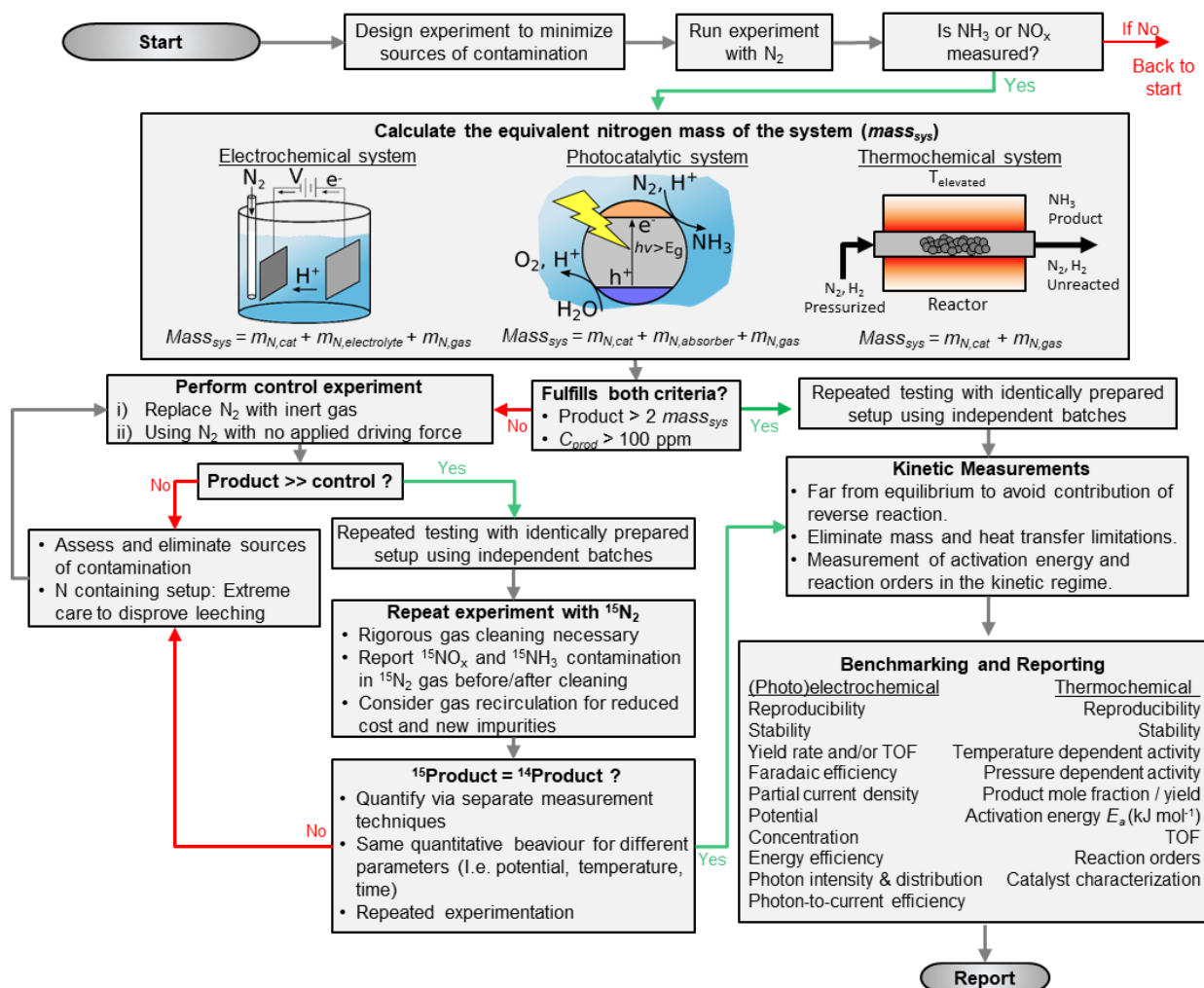




967

968 **Fig. 2. The fundamental challenges of  $N_2$  activation.** a) Standard equilibrium potentials for  $N_2$  and  $H_2O$   
 969 redox are aligned with the electron energy (0  $V_{SHE}$  equals -4.44 eV on the absolute scale where electron in  
 970 vacuum is 0 eV<sup>42</sup>). The free energy diagrams for  $N_2$  reduction<sup>74</sup> and oxidation<sup>56</sup> on selected surfaces are  
 971 plotted at the equilibrium potentials referenced to standard conditions, 1 bar  $NH_{3(g)}$  and 1M  $H^+NO_3^-(aq)$ . \*X  
 972 refers to surface adsorbed intermediates. The energy difference between two states (for example, step

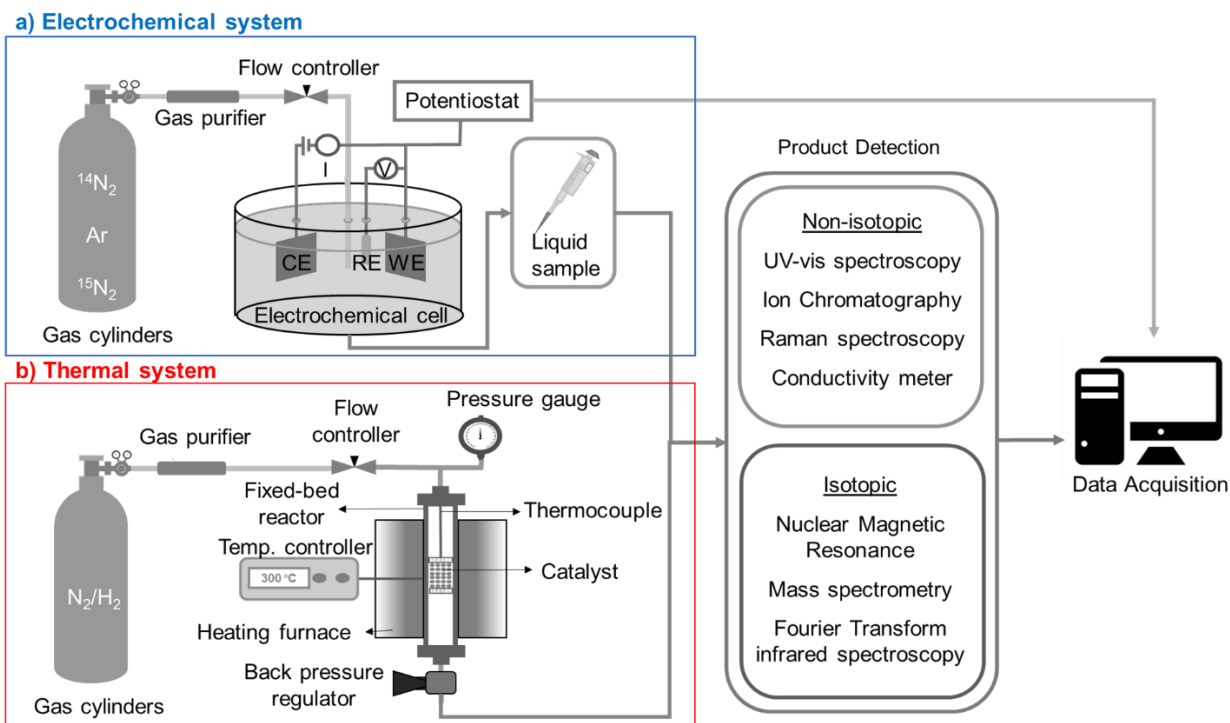
973 1-2 of associative N<sub>2</sub> reduction) corresponds to the thermodynamic barrier and can be lowered by  
974 applying potential if the step involves an electron transfer. An additional activation barrier may be  
975 present, shown as bumps between steps, whereby the value 0.7 eV is chosen for all coupled proton-  
976 electron transfer steps (consistent with Singh et al<sup>66</sup>). The N-N dissociation barrier follows ref<sup>202</sup> in which  
977 the zero-point energy and the gas phase entropy loss of N<sub>2</sub> have been included. The overall reaction  
978 barrier can be approximated by the step with the highest barrier ( $\Delta G^\ddagger$ ), which is much slower than other  
979 elementary steps thus governing the rate. b) Limiting potential analysis<sup>66</sup> (blue) for electrochemical N<sub>2</sub>  
980 reduction and H<sub>2</sub> evolution (overpotentials referenced to N<sub>2(g)</sub>/NH<sub>3(g)</sub> and H<sup>+(aq)</sup>/H<sub>2(g)</sub> standard potentials)  
981 as a function of N binding energy on transition metal terraces. For electrochemical N<sub>2</sub> reduction,  
982 N<sub>2</sub>+\*+H<sup>+</sup>+e<sup>-</sup>→\*N<sub>2</sub>H (Step 0-2 in panel a) and \*NH+H<sup>+</sup>+e<sup>-</sup>→\*NH<sub>2</sub> (Step 5-6) define the right and left legs  
983 respectively. For H<sub>2</sub> evolution, \*+H<sup>+</sup>+e<sup>-</sup>→\*H and \*H+H<sup>+</sup>+e<sup>-</sup>→H<sub>2</sub> define the right and left legs. The rate  
984 constants are shown in the second blue axis, where k<sub>B</sub>T/h equals 10<sup>13</sup> at 25 °C. The red points correspond  
985 to the calculated turnover frequencies (TOF) on transition metal FCC/HCP (211), computed using a micro-  
986 kinetic model by considering the dissociative mechanism as described in ref<sup>69</sup>. The synthesis condition is  
987 400 °C, 100 bar, gas composition H<sub>2</sub>:N<sub>2</sub>=3:1 containing 5% NH<sub>3</sub>. The N<sub>2</sub> reduction energy diagrams in panel  
988 a were adopted with permission from REF<sup>74</sup>, Royal Society of Chemistry, and the N<sub>2</sub> oxidation diagram  
989 with permission from REF<sup>56</sup>, Wiley. In panel b, the electrochemical N<sub>2</sub> reduction and H<sub>2</sub> evolution plots  
990 are adapted with permission from REF<sup>66</sup>, Elsevier and adapted with permission from Singh, A. R. *et al.*  
991 *Strategies toward Selective Electrochemical Ammonia Synthesis. ACS Catal.* **9**, 8316–8324 (2019).  
992 Copyright 2019 American Chemical Society. The turnover frequency data points for thermochemical N<sub>2</sub>  
993 reduction are reproduced with permission from REF<sup>69</sup>



994

995 **Fig. 3. General flow chart of experimentation.** The total equivalent mass of the system,  $mass_{sys}$ , must be  
 996 determined, which will be compared with the amount of product ( $NH_3$  or  $NO_3^-$ ) measured,  $mass_{prod}$ , in  
 997 order to determine the need for isotope labelled experiments. The  $mass_{sys}$  is the summation of the  
 998 relevant N-containing masses, which includes the experimentally measured N in the catalyst ( $m_{N,catalyst}$ ), the  
 999 mass of N in the electrolyte ( $mass_{N,electrolyte}$ ), the mass of the N-containing absorber ( $mass_{N,absorber}$ ), and the  
 1000 calculated or measured mass of impurities in the gas stream ( $mass_{N,gas}$ ).

1001



1002

1003

1004

1005

1006

1007

1008

1009

1010

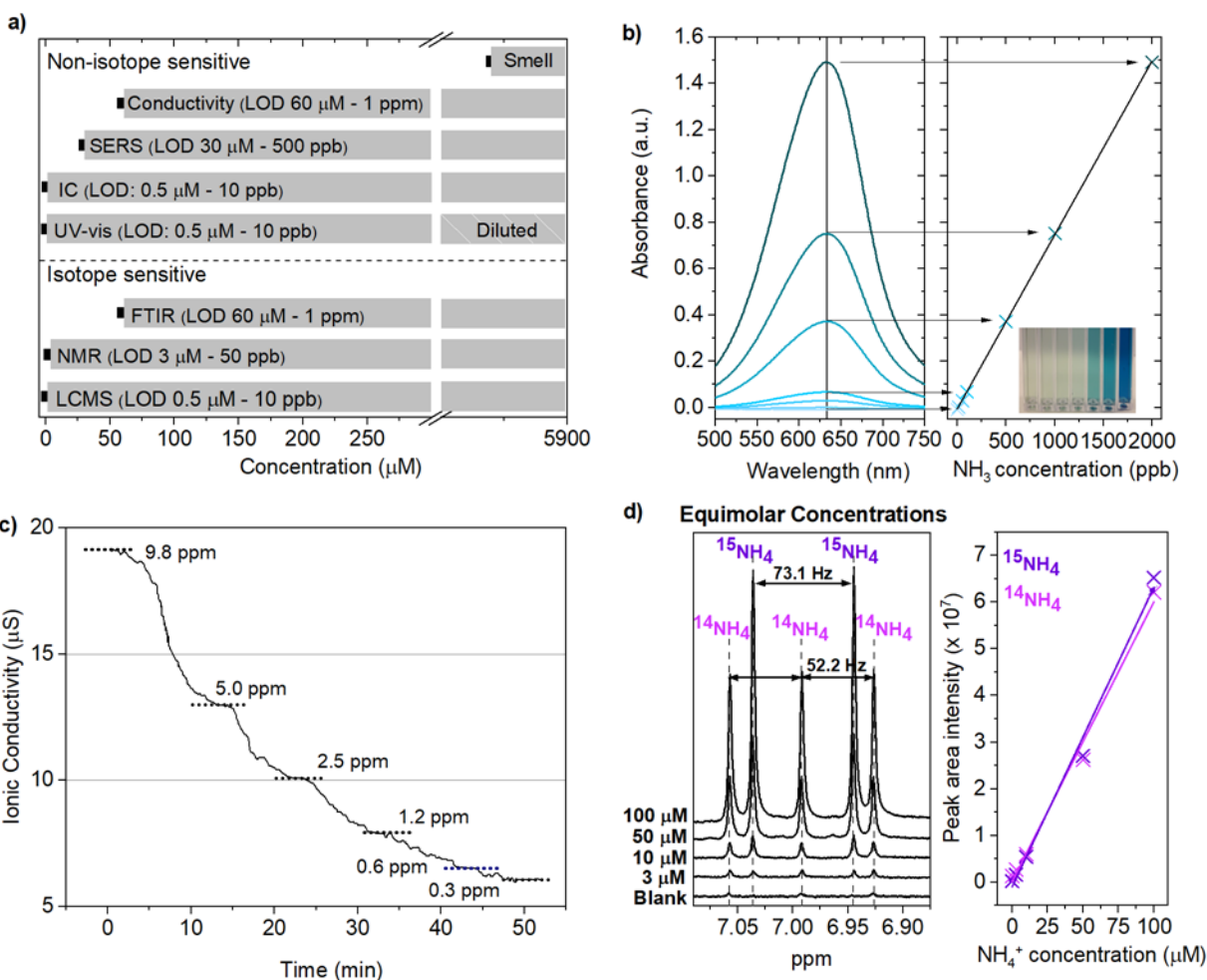
1011

1012

1013

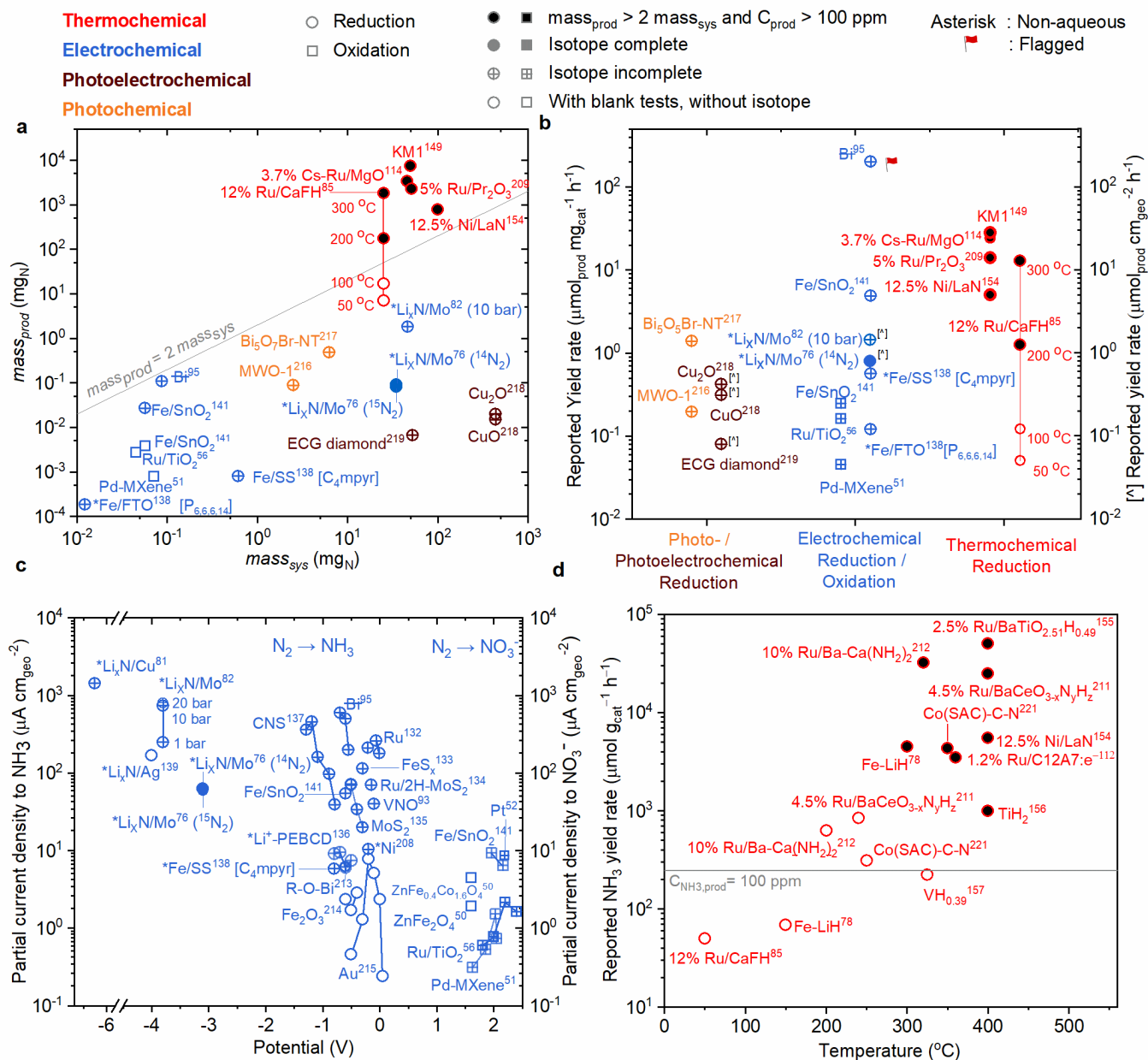
1014

**Fig. 4. Experimental setup for electrochemical and thermochemical  $\text{N}_2$  activation.** a) Experimental setup for electrochemical  $\text{N}_2$  reduction or oxidation reactions. The gas passes through a gas cleaner (either a reduced metal catalyst and freeze trap, or a commercial purifier), then flows into the electrochemical cell with a defined flow rate. The setup can be adapted for photoelectrochemical systems by using a photoelectrochemical cell with an illumination source. The reaction of interest is undertaken by controlling the potential across the electrodes via a potentiostat. For photochemical systems, the setup does not require a potentiostat, and the cell typically contains a suspension of particles or a surface with the active catalyst, and an illumination source is used to drive the reaction. b) Activity measurement system for thermal  $\text{NH}_3$  synthesis. The setup contains a fixed-bed reactor, a furnace with a temperature controller, a thermocouple placed on the top of catalyst bed, gas purifiers, a flow meter, a pressure gauge and a back-pressure regulator. Then, the product of catalysis is detected via either non-isotope or isotope-sensitive techniques if necessary.



1015

1016 **Fig. 5. Isotopic and non-isotopic NH<sub>3</sub> detection methods.** a) Detection limits of well-known techniques  
 1017 for NH<sub>3</sub> quantification. The bar at 5882 μM (100 ppm) corresponds to NH<sub>3</sub> concentrations in liquid where  
 1018 olfactory detection is possible beyond any doubt<sup>96</sup>. UV-vis<sup>76</sup>, Conductivity meter<sup>120</sup>, and nuclear magnetic  
 1019 resonance (NMR)<sup>76</sup> is discussed in text, Fourier transform infrared spectroscopy (FTIR)<sup>83</sup>, liquid  
 1020 chromatography mass spectroscopy (LCMS)<sup>203</sup>, surface enhanced Raman spectroscopy (SERS)<sup>204</sup> and ion  
 1021 chromatography (IC)<sup>205</sup> is discussed in the Supplementary Information. b) UV-vis spectra of indophenol  
 1022 blue method, showing quantification via calibrated samples from 10 to 2000 ppb NH<sub>3</sub> in H<sub>2</sub>O. Straight line  
 1023 is fitted based on peak absorbance of each sample, displaying linearity with sample concentration<sup>206</sup>. c)  
 1024 Conductivity measurement curve showing sensitivity of the NH<sub>3</sub> concentration from 9.8 to 0.3 ppm in  
 1025 purified H<sub>2</sub>O<sup>207</sup>. Due to the intensity of the conductivity baseline, it is difficult to detect an NH<sub>3</sub>  
 1026 concentration below 1 ppm. d) Example of NMR spectra of increasing equimolar <sup>14</sup>NH<sub>3</sub> and <sup>15</sup>NH<sub>3</sub>  
 1027 concentrations, clearly showing the respectively distinct triplet and doublet peaks. Calibration curve for  
 1028 <sup>14</sup>NH<sub>3</sub> and <sup>15</sup>NH<sub>3</sub> based on area under peaks, respectively, the triplet and doublet peaks from the NMR  
 1029 spectra<sup>76</sup>. Panel c is reprinted with permission from REF<sup>207</sup>, Elsevier. Panel d is reprinted from REF<sup>76</sup>,  
 1030 Springer Nature Limited.



103.

1032 **Fig. 6. State-of-the-art literature overview of electrochemical, photo(electro)chemical, and**  
 1033 **thermochemical  $\text{N}_2$  activation.** Evaluation of experimental conditions for thermochemical (red),  
 1034 electrochemical (blue), photochemical (orange), and photoelectrochemical (brown)  $\text{N}_2$  fixation.  
 1035 Experimental details can be found in **Table S1-3**. Circle represents reduction, square represents oxidation.  
 1036 Unfilled symbol represents data with simple background tests. Cross represents data with either  
 1037 qualitative or quantitative isotope labelled experiments at a single point, without measuring or cleaning  
 1038 gas contaminants. Filled symbol represents repeated isotope labelled experiments with rigorous gas  
 1039 cleaning. Black-filled data satisfy both  $mass_{prod} > 2mass_{sys}$  and  $C_{prod} > 100 \text{ ppm}$ . Asterisk points contain  
 1040 non-aqueous electrolytes. Flagged data raise suspicion of contamination based on non-reproducible  
 1041 results. a) Comparison of  $mass_{prod}$  with  $mass_{sys}$  for different catalytic systems.  $mass_{N,cat}$  is calculated based



1042 on 25% catalyst weight for non-N-containing catalysts, and 100% for N-containing catalysts.  
1043 Thermochemical data at 400 °C and 1 bar unless otherwise specified: Cs-Ru/MgO<sup>114</sup> at 9 bar, Ru/Pr<sub>2</sub>O<sub>3</sub><sup>209</sup>  
1044 at 390 °C and 9 bar, KM1<sup>149</sup> at 10 bar. b) Comparison of reported mass-specific activity. Yield rates of data  
1045 points annotated by [^] are expressed in  $\mu\text{mol cm}_{\text{geo}}^{-2} \text{h}^{-1}$ . c) Literature overview of partial current density  
1046 towards NH<sub>3</sub> (left y-axis) or NO<sub>3</sub><sup>-</sup> (right y-axis) from product detection as a function of potential vs RHE,  
1047 unless otherwise specified. Fe on Stainless Steel (Fe/SS) and Fe/FTO<sup>138</sup> reported vs NHE, Li<sub>x</sub>N/Cu<sup>81</sup> total  
1048 cell potential with Ohmic correction, Ni<sup>208</sup> vs Ag wire in 0.1 M LiCl/EDA, Li<sub>x</sub>N/Ag<sup>139</sup> is vs Ag/AgCl/AgCl (sat),  
1049 LiCl, LiClO<sub>4</sub>/THF reference. d) Literature overview of thermochemical NH<sub>3</sub> synthesis catalyzed by “reactive”  
1050 materials whose composition or active phase may change during or after reaction. The line  $C_{\text{NH}_3\text{-prod}} = 100$   
1051 ppm was calculated with the assumption of WHSV= 60,000 ml  $\text{g}_{\text{cat}}^{-1} \text{h}^{-1}$ . Data at 10 bar unless otherwise  
1052 specified: Ru/CaFH<sup>85</sup> at 1 bar, TiH<sub>2</sub><sup>156</sup> at 50 bar, 2.5%Ru/BaTiO<sub>2.51</sub>H<sub>0.49</sub><sup>155</sup> at 50 bar, 4.5%Ru/BaCeO<sub>3-x</sub>N<sub>y</sub>H<sub>z</sub><sup>211</sup>  
1053 at 9 bar, Ru/Ba-Ca(NH<sub>2</sub>)<sub>2</sub><sup>212</sup> at 9 bar, 12.5%Ni/LaN<sup>154</sup> at 1 bar, VH<sub>0.39</sub><sup>157</sup> at 50 bar.

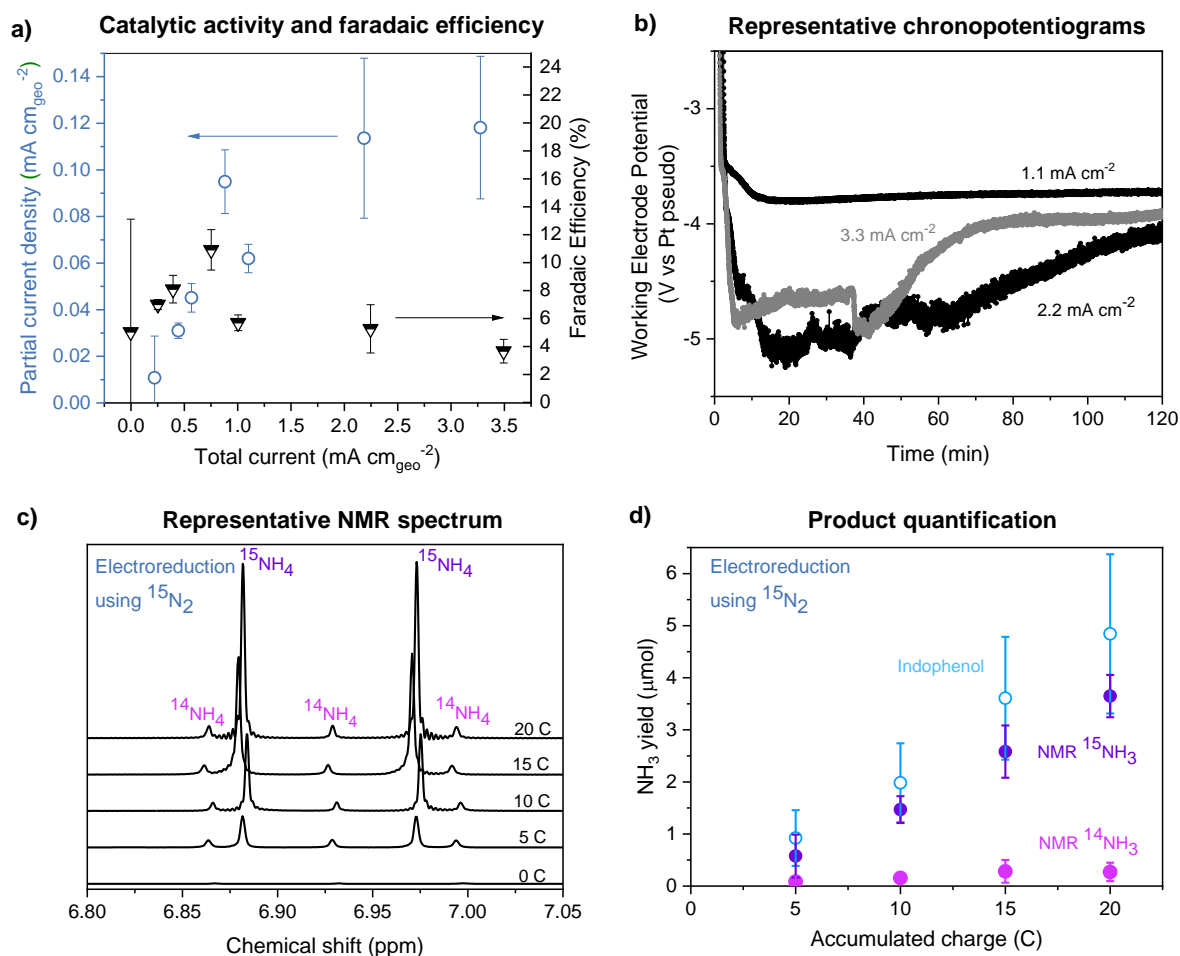
1054

1055

1056

1057

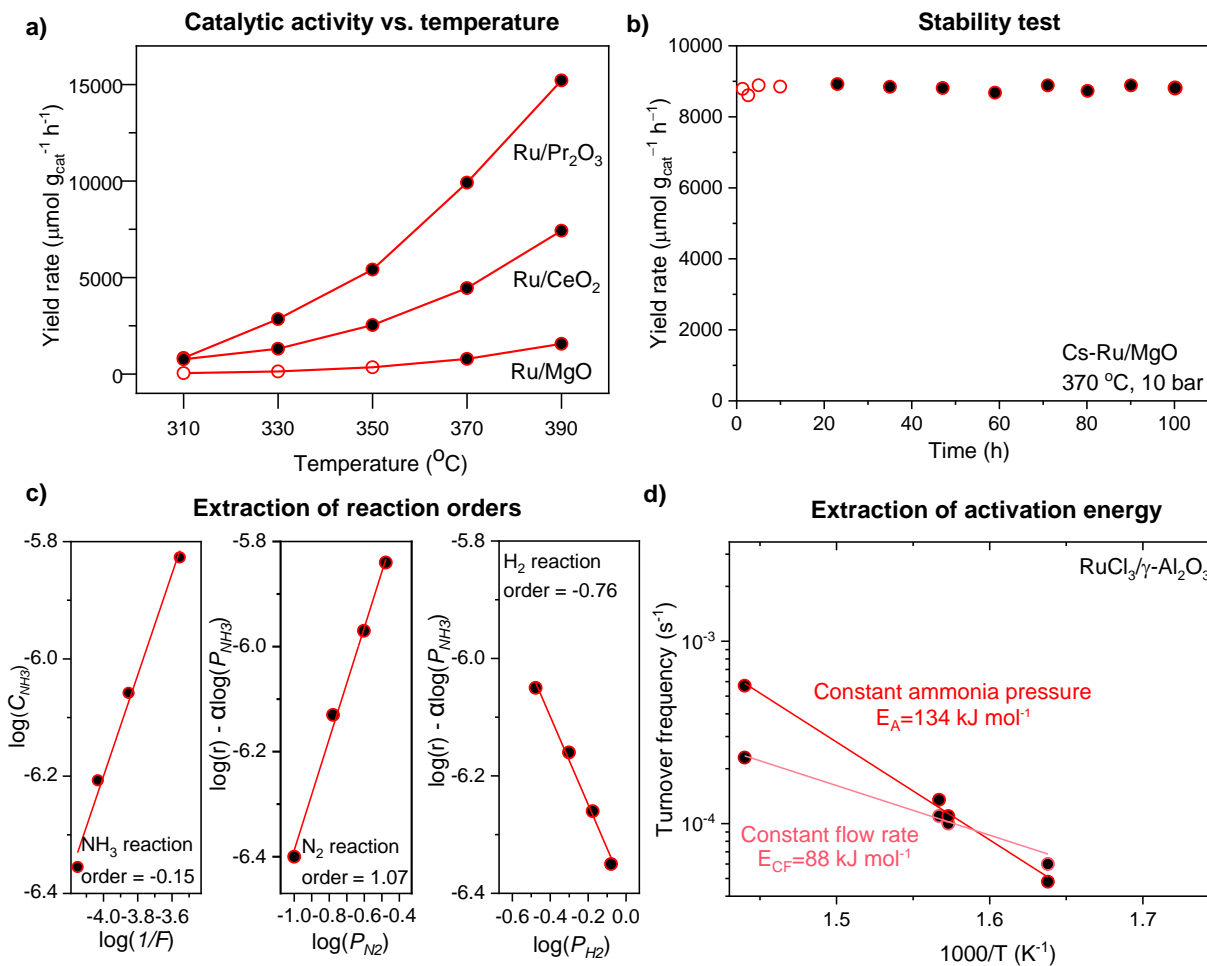
1058



1059

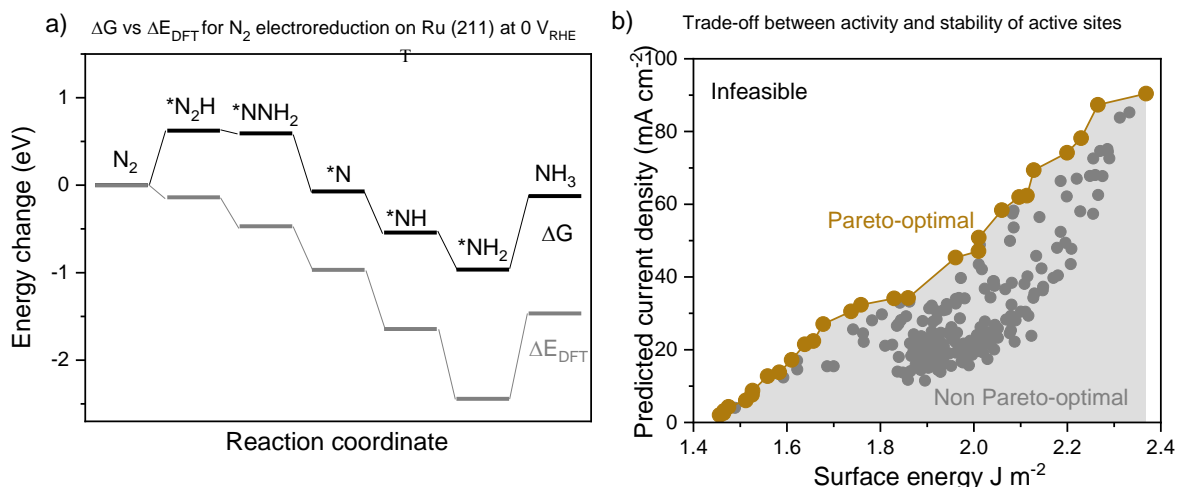
1060 **Fig. 7. Example data of Li-mediated  $\text{NH}_3$  synthesis in THF with  $\text{LiClO}_4$  salt and EtOH as the proton source.**

1061 a) Partial current density to  $\text{NH}_3$  ( $i_{\text{NH}_3}$ , left y-axis) and Faradaic efficiency ( $FE_{\text{NH}_3}$ , right y-axis) as a function  
 1062 of total applied current. b) Representative CPs for experiments plotted in panel a. c) Representative NMR  
 1063 data from a single measurement, with samples taken every 5 Coulomb of charge passed (C) using cleaned  
 1064  $^{15}\text{N}_2$  as feed-gas. d) Yield of  $\text{NH}_3$  as a function of charge passed, showing quantitative agreement between  
 1065 isotope sensitive results (purple and pink) with non-isotope sensitive result (blue). Error bars signify mean  
 1066 and standard deviation of 3 repeated identical but independently prepared experiments. Panels a and b  
 1067 are reprinted with permission from REF<sup>79</sup>, Wiley. Panels c and d are reprinted from REF<sup>76</sup>, Springer Nature  
 1068 Limited.



1069

1070 **Fig. 8. Recommended reports of catalytic performances for thermal NH<sub>3</sub> synthesis.** (a) NH<sub>3</sub> synthesis rate  
 1071 as a function of temperature<sup>209</sup>; (b) Stability test of NH<sub>3</sub> synthesis rate<sup>114</sup> (c) extraction of reaction orders  
 1072 with respect to NH<sub>3</sub>, N<sub>2</sub>, and H<sub>2</sub><sup>221</sup>. (d). Arrhenius plots at constant NH<sub>3</sub> pressure (red) and at constant flow  
 1073 rate (lighter red) resulting in a difference in the extracted activation energy<sup>153</sup>. Dark-filled points satisfy  
 1074 both  $mass_{prod} > 2mass_{sys}$  and  $C_{prod} > 100$  ppm criteria. Panel a is reprinted from REF<sup>209</sup>, CC BY 3.0  
 1075 (<https://creativecommons.org/licenses/by/3.0/>). Panel b is adapted with permission from Wu, S. et al.  
 1076 Removal of Hydrogen Poisoning by Electrostatically Polar MgO Support for Low-Pressure NH<sub>3</sub> Synthesis  
 1077 at a High Rate over the Ru Catalyst. *ACS Catal.* **10**, 5614–5622 (2020). Copyright 2020 American Chemical  
 1078 Society. Panel c is reprinted from REF<sup>221</sup>, CC BY 3.0 (<https://creativecommons.org/licenses/by/3.0/>). Panel  
 1079 d is reprinted with permission from REF<sup>153</sup>, Elsevier.



1080

1081 **Fig. 9. Density functional theory results.** (a) An energy diagram of N<sub>2</sub> reduction on Ru (211) showing the

1082 free energies and DFT energies respectively (black and grey respectively<sup>65</sup>). (b) The surface energy plotted

1083 against the predicted current density for the O<sub>2</sub> reduction reaction (ORR) on defected Pt (111) surfaces.

1084 Beige points represent points on the Pareto Frontier, grey points represent non Pareto-optimal surfaces.

1085 The grey area represents sub optimal surfaces whereas the white region represents unobtainable

1086 surfaces<sup>166</sup>. The current density (*i*) is calculated using the expression  $i = i_c \exp(-\Delta G_{ORR}/kT)$ , where *i<sub>c</sub>* is an

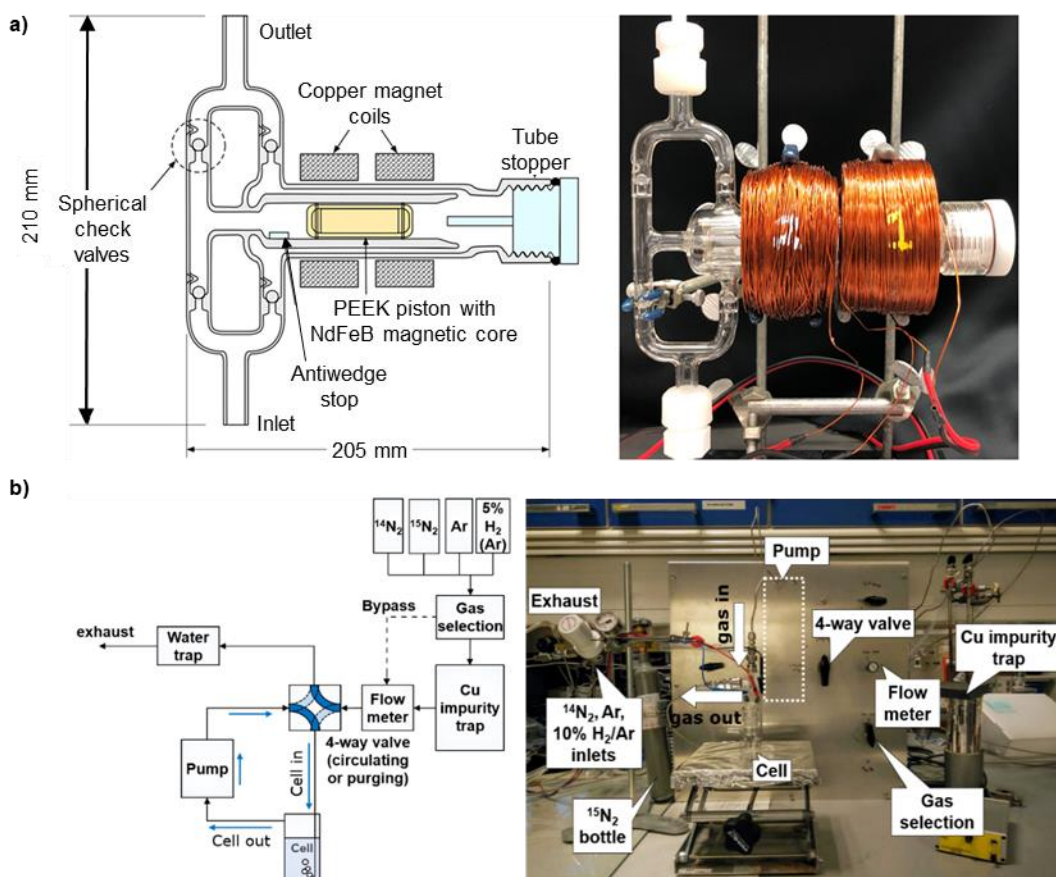
1087 experimental value  $3.68 \times 10^{11}$  kA mol<sup>-1</sup> at cell potential 0.9 V, and  $\Delta G_{ORR}$  is the change in Gibbs energy of

1088 the limiting step. The surface energy of each defected surface is calculated by dividing the formation

1089 energy by the surface area. The full methodology can be found in REF<sup>166</sup>. In panel a,  $\Delta G$  data were adopted

1090 with permission from REF<sup>73</sup>, Royal Society of Chemistry, and the DFT energy points were acquired from J.

1091 Montoya. Panel b is reprinted from REF<sup>166</sup>, Springer Nature Limited.



1092

1093 **Fig. 10. Home-built glass circulation pump and full gas recirculating setup with home-built activated Cu**  
 1094 **catalyst for gas cleaning.** a) Glass circulation pump, enabling long-duration experiments without supplying  
 1095 continuous  $^{15}\text{N}_2$ . b) Inexpensive gas cleaning system with a reduced Cu catalyst, freeze trap and glass  
 1096 circulation pump for cheap  $^{15}\text{N}_2$  experimentation. Panel a is adapted with permission from REF<sup>176</sup>  
 1097 Nielander, A. C. *et al.* Readily Constructed Glass Piston Pump for Gas Recirculation. *ACS Omega* **5**, 16455–  
 1098 16459 (2020). Copyright 2020 American Chemical Society. Panel b is reprinted from REF<sup>76</sup>, Springer Nature  
 1099 Limited.

1100

## 1101 Acknowledgment

1102 Y.S.-H gratefully acknowledges the support by Toyota Research Institute through the Accelerated Materials  
1103 Design and Discovery Program. H.I. acknowledges support from the Imperial-MIT Department of  
1104 Materials Exchange Program S.Z.A. and I.C. gratefully acknowledge the funding by Villum Fonden, part  
1105 of the Villum Center for the Science of Sustainable Fuels and Chemicals (V-SUSTAIN grant 9455) and  
1106 Innovationsfonden (E-ammonia grant 9067-00010B). P.C. and X.L. were supported by the National Natural  
1107 Science Foundation of China (Grant Nos. 21633011 and 21988101). The material based upon work by  
1108 A.J.M. and B.C. was supported by the National Science Foundation under Grant No.1943707. I.E.L.S. and  
1109 J.B. would like to acknowledge financial support from the Engineering and Physical Sciences Research  
1110 Council (EP/M0138/1), the European Research Council (ERC) under the European Union's Horizon 2020  
1111 research and innovation programme (grant agreement No. 866402) and the National Research Council  
1112 Canada through the Materials for Clean Fuels Challenge Program. We thank Marta Hatzell and Zhichuan  
1113 J. Xu for the insightful discussion regarding N<sub>2</sub> oxidation. We thank Vahid Shadravan for helpful advice  
1114 on thermochemical catalysis. We would like to acknowledge Joseph Montoya for providing data on the  
1115 vibrational frequencies and free energy calculations for N<sub>2</sub> reduction on Ru (211) for Fig. 9a.

## 1116 Competing interests

1117 The authors declare no competing interests.

## 1118 Author Contributions

1119 Introduction (H.I., S.Z.A., and Y. S.-H.); Experimentation (S.Z.A., H.I., X.Z., J.B., P.C., I.E.L.S., I.C., and  
1120 Y. S.-H.); Results (S.Z.A., H.I., X.Z., B.M.C., J.B., P.C., I.C., A.J.M., and Y. S.-H.); Applications (H.I. and  
1121 S.Z.A.); Reproducibility and data deposition (H.I. and I.C.); Limitations and optimizations (S.Z.A.);  
1122 Outlook (H.I., S.Z.A., J.B., X.Z. and I.E.L.S.); Overview of the Primer (H.I., S.Z.A., and Y. S.-H.). All  
1123 authors discussed and edited the full manuscript.

1124



## References

- 1125  
1126 1. Cottrell, T. L. The Strengths of Chemical Bonds, 2nd Ed. *Prop. atoms, radicals, Bond* (1966).
- 1127 2. Jia, H.-P. & Quadrelli, E. A. Mechanistic aspects of dinitrogen cleavage and hydrogenation to  
1128 produce ammonia in catalysis and organometallic chemistry: relevance of metal hydride bonds and  
1129 dihydrogen. *Chem. Soc. Rev.* **43**, 547–564 (2014).
- 1130 3. Noxon, J. F. Atmospheric nitrogen fixation by lightning. *Geophys. Res. Lett.* (1976).
- 1131 4. Rivera Ortiz, J. M. & Burris, R. H. Interactions among substrates and inhibitors of nitrogenase. *J.*  
1132 *Bacteriol.* (1975).
- 1133 5. Yang, Z. Y. *et al.* Evidence That the Pi Release Event Is the Rate-Limiting Step in the Nitrogenase  
1134 Catalytic Cycle. *Biochemistry* (2016).
- 1135 6. Hoffman, B. M., Lukoyanov, D., Yang, Z., Dean, D. R. & Seefeldt, L. C. Mechanism of Nitrogen  
1136 Fixation by Nitrogenase: The Next Stage. *Chem. Rev.* **114**, 4041–4062 (2014).
- 1137 7. Smil, V. *Enriching the Earth: Fritz Haber, Carl Bosch, and the Transformation of World Food*  
1138 *Production.* (The MIT Press, 2001).
- 1139 8. Hager, T. *The Alchemy of Air: A Jewish Genius, a Doomed Tycoon, and the Discovery that*  
1140 *Changed the Course of History.* Broadway Books (Broadway Books, 2008).
- 1141 9. Science and Food Supplies. *Nature* **126**, 193–194 (1930).
- 1142 10. Ihde, A. J. *The Development of Modern Chemistry (Dover Books on Chemistry).* (Dover  
1143 Publications, 1984).
- 1144 11. Chen, J. G. *et al.* Beyond fossil fuel–driven nitrogen transformations. *Science* (80-. ). **360**,  
1145 eaar6611 (2018).
- 1146 **This review covers the thermochemistry of all nitrogen transformation reactions, and the**  
1147 **challenges and opportunities associated with these reactions in overcoming reliance on fossil**  
1148 **fuels.**
- 1149 12. Smith, C., Hill, A. K. & Torrente-Murciano, L. Current and future role of Haber–Bosch ammonia  
1150 in a carbon-free energy landscape. *Energy Environ. Sci.* (2020).
- 1151 13. Aika, K. & Tamara, K. Ammonia Synthesis over Non-Iron Catalysts and Related Phenomena. in  
1152 *Ammonia* (1995).
- 1153 14. Ertl, G. Reactions at Surfaces: From Atoms to Complexity (Nobel Lecture). *Angew. Chemie Int.*  
1154 *Ed.* **47**, 3524–3535 (2008).
- 1155 15. Erisman, J. W., Sutton, M. a., Galloway, J., Klimont, Z. & Winiwarter, W. How a century of  
1156 ammonia synthesis changed the world. *Nat. Geosci.* **1**, 636–639 (2008).
- 1157 16. Smil, V. Nitrogen and Food Production: Proteins for Human Diets. *AMBIO A J. Hum. Environ.*  
1158 **31**, 126–131 (2002).
- 1159 17. Stewart, W. M., Dibb, D. W., Johnston, A. E. & Smyth, T. J. The Contribution of Commercial  
1160 Fertilizer Nutrients to Food Production. *Agron. J.* **97**, 1–6 (2005).
- 1161 18. USGS National Minerals Information Center. *Nitrogen Statistics and Information, U.S. Geological*  
1162 *Survey, Mineral Commodity Summaries, January 2020.* (2020).
- 1163 19. Apodaca, L. E. Nitrogen (fixed) — Ammonia. 116–117 (2021).

- 1164 <https://www.usgs.gov/centers/nmic/nitrogen-statistics-and-information>
- 1165 20. Smil, V. Detonator of the population explosion. *Nature* **400**, 415–415 (1999).
- 1166 21. Schlögl, R. Ammonia Synthesis. in *Handbook of Heterogeneous Catalysis* 2501 (Wiley-VCH  
1167 Verlag GmbH & Co. KGaA, 2008).
- 1168 22. IHS Markit. *Ammonia - Chemical Economics Handbook (CEH) | IHS Markit. IHSmarkit.com*  
1169 (2020).
- 1170 23. Klerke, A., Christensen, C. H., Nørskov, J. K. & Vegge, T. Ammonia for hydrogen storage:  
1171 challenges and opportunities. *J. Mater. Chem.* **18**, 2304 (2008).
- 1172 24. Zamfirescu, C. & Dincer, I. Using ammonia as a sustainable fuel. *J. Power Sources* **185**, 459–465  
1173 (2008).
- 1174 25. Brightling, J. Ammonia and the Fertiliser Industry: The Development of Ammonia at Billingham  
1175 A history of technological innovation from the early 20th century to the present day. *Johnson*  
1176 *Matthey Technol. Rev.* (2018).
- 1177 26. Brown, T. Ammonia production causes 1% of total global GHG emissions. Ammoniaindustry.  
1178 [https://ammoniaindustry.com/ammonia-production-causes-1-percent-of-total-global-ghg-](https://ammoniaindustry.com/ammonia-production-causes-1-percent-of-total-global-ghg-emissions/)  
1179 [emissions/](https://ammoniaindustry.com/ammonia-production-causes-1-percent-of-total-global-ghg-emissions/)
- 1180 27. Soloveichik, G. Electrochemical synthesis of ammonia as a potential alternative to the Haber–  
1181 Bosch process. *Nature Catalysis* (2019) doi:10.1038/s41929-019-0280-0.
- 1182 28. MacFarlane, D. R. *et al.* A Roadmap to the Ammonia Economy. *Joule* **4**, 1186–1205 (2020).
- 1183 **This paper covers 3 different generations of technological advancement needed to produce**  
1184 **ammonia sustainably.**
- 1185 29. Stephens, I. & Nilsson, A. Research needs towards sustainable production of fuels and chemicals.  
1186 *Energy-X, Chapter 5* (2019). <https://www.energy-x.eu/research-needs-report/>
- 1187 30. Erisman, J. W., Bleeker, A., Galloway, J. & Sutton, M. S. Reduced nitrogen in ecology and the  
1188 environment. *Environ. Pollut.* **150**, 140–149 (2007).
- 1189 31. Good, A. G. & Beatty, P. H. Fertilizing nature: A tragedy of excess in the commons. *PLoS Biol.* **9**,  
1190 1–9 (2011).
- 1191 32. Singh, A. R. *et al.* Electrochemical Ammonia Synthesis - The Selectivity Challenge. *ACS Catal.* **7**,  
1192 706–709 (2017).
- 1193 **This viewpoint elucidates the selectivity challenge by covering a qualitative analysis of**  
1194 **electrochemical ammonia synthesis and suggests strategies to circumvent the issue.**
- 1195 33. Comer, B. M. *et al.* Prospects and Challenges for Solar Fertilizers. *Joule* (2019).
- 1196 34. Ummary, S. Renewable Energy to Fuels Through Utilization of EnergyDense Liquids (REFUEL)  
1197 Program Overview. 1–16 (2016). [https://arpa-](https://arpa-e.energy.gov/sites/default/files/documents/files/REFUEL_ProgramOverview.pdf)  
1198 [e.energy.gov/sites/default/files/documents/files/REFUEL\\_ProgramOverview.pdf](https://arpa-e.energy.gov/sites/default/files/documents/files/REFUEL_ProgramOverview.pdf)
- 1199 35. Rouwenhorst, K. H. R., Kim, H. H. & Lefferts, L. Vibrationally Excited Activation of N<sub>2</sub> in  
1200 Plasma-Enhanced Catalytic Ammonia Synthesis: A Kinetic Analysis. *ACS Sustain. Chem. Eng.*  
1201 (2019).
- 1202 36. Rouwenhorst, K. H. R. *et al.* Plasma-driven catalysis: Green ammonia synthesis with intermittent  
1203 electricity. *Green Chem.* (2020) doi:10.1039/d0gc02058c.

- 1204 37. Kim, H. H., Teramoto, Y., Ogata, A., Takagi, H. & Nanba, T. Atmospheric-pressure nonthermal  
1205 plasma synthesis of ammonia over ruthenium catalysts. *Plasma Process. Polym.* (2017)  
1206 doi:10.1002/ppap.201600157.
- 1207 38. Mehta, P. *et al.* Overcoming ammonia synthesis scaling relations with plasma-enabled catalysis.  
1208 *Nat. Catal.* (2018).
- 1209 39. Han, G.-F. *et al.* Mechanochemistry for ammonia synthesis under mild conditions. *Nat.*  
1210 *Nanotechnol.* (2020).
- 1211 40. Tricker, A. W. *et al.* Mechanocatalytic Ammonia Synthesis over TiN in Transient  
1212 Microenvironments. *ACS Energy Lett.* **5**, 3362–3367 (2020).
- 1213 41. IHS. *Nitric acid - Chemical Economics Handbooks (CEH)* | IHS Markit. IHSmarkit.com (2015).
- 1214 42. Bard, a & Faulkner, L. Chapter 2, Electrochemical Methods: Fundamentals and Applications,  
1215 New York: , 2001. *Russ. J. Electrochem.* (2002).
- 1216 43. Patil, B. S., Rovira Palau, J., Hessel, V., Lang, J. & Wang, Q. Plasma Nitrogen Oxides Synthesis  
1217 in a Milli-Scale Gliding Arc Reactor: Investigating the Electrical and Process Parameters. *Plasma*  
1218 *Chem. Plasma Process.* **36**, 241–257 (2016).
- 1219 44. Birkeland, K. R. On the oxidation of atmospheric nitrogen in electric arcs. *Trans. Faraday Soc.*  
1220 (1906).
- 1221 45. Eyde, S. Oxidation of atmospheric nitrogen and development of resulting industries in norway.  
1222 *Ind. Eng. Chem.* (1912).
- 1223 46. Cherkasov, N., Ibhaddon, A. O. & Fitzpatrick, P. A review of the existing and alternative methods  
1224 for greener nitrogen fixation. *Chemical Engineering and Processing: Process Intensification*  
1225 (2015).
- 1226 47. Hessel, V. *et al.* Industrial applications of plasma, microwave and ultrasound techniques:  
1227 Nitrogen-fixation and hydrogenation reactions. *Chem. Eng. Process. Process Intensif.* (2013).
- 1228 48. Rusanov, V. D., Fridman, A. A. & Sholin, G. V. The Physics of a Chemically Active Plasma With  
1229 Nonequilibrium Vibrational Excitation of Molecules. *Sov. Phys. - Uspekhi* (1981).
- 1230 49. Li, S., Medrano, J. A., Hessel, V. & Gallucci, F. Recent progress of plasma-assisted nitrogen  
1231 fixation research: A review. *Processes* (2018).
- 1232 50. Dai, C., Sun, Y., Chen, G., Fisher, A. C. & Xu, Z. J. Electrochemical Oxidation of Nitrogen  
1233 towards Direct Nitrate Production on Spinel Oxides. *Angew. Chemie Int. Ed.* **59**, 9418–9422  
1234 (2020).
- 1235 51. Fang, W. *et al.* Boosting efficient ambient nitrogen oxidation by a well-dispersed Pd on MXene  
1236 electrocatalyst. *Chem. Commun.* **56**, 5779–5782 (2020).
- 1237 52. Wang, Y., Yu, Y., Jia, R., Zhang, C. & Zhang, B. Electrochemical synthesis of nitric acid from air  
1238 and ammonia through waste utilization. *Natl. Sci. Rev.* **6**, 730–738 (2019).
- 1239 53. Lun Pang, C., Lindsay, R. & Thornton, G. Chemical reactions on rutile TiO<sub>2</sub>(110). *Chem. Soc.*  
1240 *Rev.* (2008).
- 1241 54. Bickley, R. I. & Vishwanathan, V. Photocatalytically induced fixation of molecular nitrogen by  
1242 near UV radiation [6]. *Nature* (1979).
- 1243 55. Yuan, S. J. *et al.* Nitrate formation from atmospheric nitrogen and oxygen photocatalysed by  
1244 nano-sized titanium dioxide. *Nat. Commun.* (2013).

- 1245 56. Kuang, M. *et al.* Efficient Nitrate Synthesis via Ambient Nitrogen Oxidation with Ru-Doped TiO  
1246 2 /RuO<sub>2</sub> Electrocatalysts. *Adv. Mater.* **32**, 2002189 (2020).
- 1247 57. Wang, S. *et al.* Universal transition state scaling relations for (de)hydrogenation over transition  
1248 metals. *Phys. Chem. Chem. Phys.* (2011).
- 1249 58. Bozso, F., Ertl, G., Grunze, M. & Weiss, M. Interaction of nitrogen with iron surfaces. I. Fe(100)  
1250 and Fe(111). *J. Catal.* (1977).
- 1251 59. Bozso, F., Ertl, G. & Weiss, M. Interaction of nitrogen with iron surfaces. II. Fe(110). *J. Catal.*  
1252 (1977).
- 1253 60. Ertl, G., Lee, S. B. & Weiss, M. Adsorption of nitrogen on potassium promoted Fe(111) and (100)  
1254 surfaces. *Surf. Sci.* (1982).
- 1255 61. Honkala, K. *et al.* Ammonia synthesis from first-principles calculations. *Science* (80-. ). (2005).
- 1256 62. Dahl, S. *et al.* Role of steps in N<sub>2</sub> activation on Ru(0001). *Phys. Rev. Lett.* (1999).
- 1257 63. Chorkendorff, I. & Niemantsverdriet, J. W. Chapter 3: Reaction Rate Theory. in *Concepts of*  
1258 *Modern Catalysis and Kinetics* (John Wiley and Sons, 2003).
- 1259 64. Medford, A. J. & Hatzell, M. C. Photon-Driven Nitrogen Fixation: Current Progress,  
1260 Thermodynamic Considerations, and Future Outlook. *ACS Catal.* **7**, 2624–2643 (2017).
- 1261 65. Comer, B. M. & Medford, A. J. Analysis of Photocatalytic Nitrogen Fixation on Rutile TiO<sub>2</sub>(110).  
1262 *ACS Sustain. Chem. Eng.* **6**, 4648–4660 (2018).
- 1263 66. Singh, A. R. *et al.* Strategies toward Selective Electrochemical Ammonia Synthesis. *ACS Catal.* **9**,  
1264 8316–8324 (2019).
- 1265 67. Medford, A. J. *et al.* Assessing the reliability of calculated catalytic ammonia synthesis rates.  
1266 *Science* (80-. ). (2014).
- 1267 68. Wellendorff, J. *et al.* Density functionals for surface science: Exchange-correlation model  
1268 development with Bayesian error estimation. *Phys. Rev. B - Condens. Matter Mater. Phys.* (2012).
- 1269 69. Medford, A. J. *et al.* From the Sabatier principle to a predictive theory of transition-metal  
1270 heterogeneous catalysis. *J. Catal.* **328**, 36–42 (2015).
- 1271 **This paper discusses scaling relations, activity maps, and the d-band model, thereby**  
1272 **mapping out the development of trends in transition-metal catalysts.**
- 1273 70. Bare, S. R., Strongin, D. R. & Somorjai, G. A. Ammonia synthesis over iron single-crystal  
1274 catalysts: The effects of alumina and potassium. *J. Phys. Chem.* (1986).
- 1275 71. Dahl, S., Taylor, P. A., Törnqvist, E. & Chorkendorff, I. The synthesis of ammonia over a  
1276 ruthenium single crystal. *J. Catal.* (1998).
- 1277 72. Singh, A. R. *et al.* Computational Design of Active Site Structures with Improved Transition-State  
1278 Scaling for Ammonia Synthesis. *ACS Catal.* (2018).
- 1279 73. Montoya, J. H., Tsai, C., Vojvodic, A. & Nørskov, J. K. The Challenge of Electrochemical  
1280 Ammonia Synthesis: A New Perspective on the Role of Nitrogen Scaling Relations.  
1281 *ChemSusChem* **8**, 2180–2186 (2015).
- 1282 **This paper presents insights from DFT calculations that describe limitations on the low-**  
1283 **temperature electrocatalytic production of ammonia from dinitrogen.**

- 1284 74. Skúlason, E. *et al.* A theoretical evaluation of possible transition metal electro-catalysts for N<sub>2</sub>  
1285 reduction. *Phys. Chem. Chem. Phys.* **14**, 1235–1245 (2012).
- 1286 75. Rostamikia, G., Maheshwari, S. & Janik, M. J. Elementary kinetics of nitrogen electroreduction to  
1287 ammonia on late transition metals. *Catal. Sci. Technol.* (2019).
- 1288 76. Andersen, S. Z. *et al.* A rigorous electrochemical ammonia synthesis protocol with quantitative  
1289 isotope measurements. *Nature* **570**, 504–508 (2019).
- 1290 **This letter provides a rigorous protocol from which the source of activated nitrogen can be**  
1291 **determined.**
- 1292 77. Suryanto, B. H. R. *et al.* Challenges and prospects in the catalysis of electroreduction of nitrogen  
1293 to ammonia. *Nat. Catal.* **2**, 290–296 (2019).
- 1294 78. Wang, P. *et al.* Breaking scaling relations to achieve low-temperature ammonia synthesis through  
1295 LiH-mediated nitrogen transfer and hydrogenation. *Nat. Chem.* **9**, 64–70 (2017).
- 1296 **This study designed a two-active-center strategy using TM(N)-LiH composite catalysts to**  
1297 **create an energy-efficient pathway that allows NH<sub>3</sub> synthesis under mild conditions.**
- 1298 79. Schwalbe, J. A. *et al.* A Combined Theory-Experiment Analysis of the Surface Species in  
1299 Lithium-Mediated NH<sub>3</sub> Electrosynthesis. *ChemElectroChem* **7**, 1542–1549 (2020).
- 1300 80. Lazouski, N., Chung, M., Williams, K., Gala, M. L. & Manthiram, K. Non-aqueous gas diffusion  
1301 electrodes for rapid ammonia synthesis from nitrogen and water-splitting-derived hydrogen. *Nat.*  
1302 *Catal.* **3**, 463–469 (2020).
- 1303 81. Lazouski, N., Schiffer, Z. J., Williams, K. & Manthiram, K. Understanding Continuous Lithium-  
1304 Mediated Electrochemical Nitrogen Reduction. *Joule* **3**, 1127–1139 (2019).
- 1305 82. Andersen, S. Z. *et al.* Increasing stability, efficiency, and fundamental understanding of lithium-  
1306 mediated electrochemical nitrogen reduction. *Energy Environ. Sci.* **13**, 4291–4300 (2020).
- 1307 83. McEnaney, J. M. *et al.* Ammonia synthesis from N<sub>2</sub> and H<sub>2</sub>O using a lithium cycling  
1308 electrification strategy at atmospheric pressure. *Energy Environ. Sci.* **10**, 1621–1630 (2017).
- 1309 84. Kim, K. *et al.* Lithium-Mediated Ammonia Electro-Synthesis: Effect of CsClO<sub>4</sub> on Lithium  
1310 Plating Efficiency and Ammonia Synthesis. *J. Electrochem. Soc.* (2018).
- 1311 85. Hattori, M., Iijima, S., Nakao, T., Hosono, H. & Hara, M. Solid solution for catalytic ammonia  
1312 synthesis from nitrogen and hydrogen gases at 50 °C. *Nat. Commun.* **11**, 2001 (2020).
- 1313 86. Davy, H. The Bakerian Lecture, on some chemical agencies of electricity. *Philos. Trans. R. Soc.*  
1314 *London* **97**, 1–56 (1807).
- 1315 87. Rayleigh, Lord. XIII.—Observations on the oxidation of nitrogen gas. *J. Chem. Soc., Trans.* **71**,  
1316 181–186 (1897).
- 1317 88. Boucher, D. L., Davies, J. A., Edwards, J. G. & Mennad, A. An investigation of the putative  
1318 photosynthesis of ammonia on iron-doped titania and other metal oxides. *J. Photochem. Photobiol.*  
1319 *A Chem.* **88**, 53–64 (1995).
- 1320 89. Shipman, M. A. & Symes, M. D. A re-evaluation of Sn(II) phthalocyanine as a catalyst for the  
1321 electrosynthesis of ammonia. *Electrochim. Acta* **258**, 618–622 (2017).
- 1322 90. Licht, S. *et al.* Retraction. *Science (80-. )*. **369**, 780 (2020).
- 1323 91. Du, H.-L., Gengenbach, T. R., Hodgetts, R., MacFarlane, D. R. & Simonov, A. N. Critical



- 1324 Assessment of the Electrocatalytic Activity of Vanadium and Niobium Nitrides toward Dinitrogen  
1325 Reduction to Ammonia. *ACS Sustain. Chem. Eng.* **7**, 6839–6850 (2019).
- 1326 92. Choi, J. *et al.* Promoting nitrogen electroreduction to ammonia with bismuth nanocrystals and  
1327 potassium cations in water. *ChemRxiv, Prepr.* (2020).
- 1328 93. Yang, X. *et al.* Quantification of Active Sites and Elucidation of the Reaction Mechanism of the  
1329 Electrochemical Nitrogen Reduction Reaction on Vanadium Nitride. *Angew. Chemie* **131**, 13906–  
1330 13910 (2019).
- 1331 94. Bao, D. *et al.* Electrochemical Reduction of N<sub>2</sub> under Ambient Conditions for Artificial N<sub>2</sub>  
1332 Fixation and Renewable Energy Storage Using N<sub>2</sub>/NH<sub>3</sub> Cycle. *Adv. Mater.* **29**, 1604799 (2017).
- 1333 95. Hao, Y.-C. *et al.* Promoting nitrogen electroreduction to ammonia with bismuth nanocrystals and  
1334 potassium cations in water. *Nat. Catal.* **2**, 448–456 (2019).
- 1335 96. Smeets, M. A. M. *et al.* Odor and Irritation Thresholds for Ammonia: A Comparison between  
1336 Static and Dynamic Olfactometry. *Chem. Senses* **32**, 11–20 (2007).
- 1337 97. Dabundo, R. *et al.* The Contamination of Commercial <sup>15</sup>N<sub>2</sub> Gas Stocks with <sup>15</sup>N–Labeled Nitrate  
1338 and Ammonium and Consequences for Nitrogen Fixation Measurements. *PLoS One* **9**, e110335  
1339 (2014).
- 1340 **This paper shows that commercial isotope labelled <sup>15</sup>N<sub>2</sub> contains significant contamination**  
1341 **across lot numbers and different manufacturers.**
- 1342 98. Giordano, L. *et al.* PH dependence of OER activity of oxides: Current and future perspectives.  
1343 *Catal. Today* **262**, 2–10 (2016).
- 1344 99. Shinagawa, T., Garcia-Esparza, A. T. & Takanabe, K. Insight on Tafel slopes from a microkinetic  
1345 analysis of aqueous electrocatalysis for energy conversion. *Sci. Rep.* **5**, 13801 (2015).
- 1346 100. Limaye, A., Zeng, J. S., Willard, A. & Manthiram, K. Bayesian Data Analysis Reveals No  
1347 Preference for Cardinal Tafel Slopes in CO<sub>2</sub> Reduction Electrocatalysis. *ChemRxiv* (2020).
- 1348 101. Neyerlin, K. C., Gu, W., Jorne, J. & Gasteiger, H. A. Determination of Catalyst Unique  
1349 Parameters for the Oxygen Reduction Reaction in a PEMFC. *J. Electrochem. Soc.* **153**, A1955  
1350 (2006).
- 1351 102. Choi, J. *et al.* Identification and elimination of false positives in electrochemical nitrogen  
1352 reduction studies. *Nat. Commun.* **11**, 5546 (2020).
- 1353 **This perspective assesses a wide range of electrocatalytic nitrogen reduction reports**  
1354 **identifying false positives and providing an experimental protocol for ensuring rigorous**  
1355 **ammonia quantification in upcoming works.**
- 1356 103. Wei, C. *et al.* Recommended Practices and Benchmark Activity for Hydrogen and Oxygen  
1357 Electrocatalysis in Water Splitting and Fuel Cells. *Adv. Mater.* **31**, 1806296 (2019).
- 1358 104. Ledezma-Yanez, I., Díaz-Morales, O., Figueiredo, M. C. & Koper, M. T. M. Hydrogen Oxidation  
1359 and Hydrogen Evolution on a Platinum Electrode in Acetonitrile. *ChemElectroChem* **2**, 1612–  
1360 1622 (2015).
- 1361 105. Raccichini, R., Amores, M. & Hinds, G. Critical review of the use of reference electrodes in li-ion  
1362 batteries: A diagnostic perspective. *Batteries* (2019) doi:10.3390/batteries5010012.
- 1363 106. Ren, Y. *et al.* Is It Appropriate to Use the Nafion Membrane in Electrocatalytic N<sub>2</sub> Reduction?  
1364 *Small Methods* **3**, 1900474 (2019).



- 1365 107. Liu, H., Zhang, Y. & Luo, J. The removal of inevitable NO species in catalysts and the selection of  
1366 appropriate membrane for measuring electrocatalytic ammonia synthesis accurately. *J. Energy*  
1367 *Chem.* **49**, 51–58 (2020).
- 1368 108. Hongsirikarn, K., Goodwin, J. G., Greenway, S. & Creager, S. Influence of ammonia on the  
1369 conductivity of Nafion membranes. *J. Power Sources* **195**, 30–38 (2010).
- 1370 109. Halseid, R., Vie, P. J. S. & Tunold, R. Influence of Ammonium on Conductivity and Water  
1371 Content of Nafion 117 Membranes. *J. Electrochem. Soc.* **151**, A381 (2004).
- 1372 110. Lindley, B. M., Appel, A. M., Krogh-Jespersen, K., Mayer, J. M. & Miller, A. J. M. Evaluating the  
1373 Thermodynamics of Electrocatalytic N<sub>2</sub> Reduction in Acetonitrile. *ACS Energy Lett.* **1**, 698–704  
1374 (2016).
- 1375 111. Guo, J. *et al.* Lithium imide synergy with 3d transition-metal nitrides leading to unprecedented  
1376 catalytic activities for ammonia decomposition. *Angew. Chemie, Int. Ed. English* **54**, 2950–2954  
1377 (2015).
- 1378 112. Kitano, M. *et al.* Ammonia synthesis using a stable electride as an electron donor and reversible  
1379 hydrogen store. *Nat. Chem.* **4**, 934–940 (2012).
- 1380 113. Ma, Z., Zhao, S., Pei, X., Xiong, X. & Hu, B. New insights into the support morphology-  
1381 dependent ammonia synthesis activity of Ru/CeO<sub>2</sub> catalysts. *Catal. Sci. Technol.* **7**, 191–199  
1382 (2017).
- 1383 114. Wu, S. *et al.* Removal of Hydrogen Poisoning by Electrostatically Polar MgO Support for Low-  
1384 Pressure NH<sub>3</sub> Synthesis at a High Rate over the Ru Catalyst. *ACS Catal.* **10**, 5614–5622 (2020).
- 1385 115. Searle, P. L. The berthelot or indophenol reaction and its use in the analytical chemistry of  
1386 nitrogen. A review. *Analyst* **109**, 549 (1984).
- 1387 116. Zhao, Y. *et al.* Ammonia Detection Methods in Photocatalytic and Electrocatalytic Experiments:  
1388 How to Improve the Reliability of NH<sub>3</sub> Production Rates? *Adv. Sci.* **6**, (2019).
- 1389 117. Zhou, L. & Boyd, C. E. Comparison of Nessler, phenate, salicylate and ion selective electrode  
1390 procedures for determination of total ammonia nitrogen in aquaculture. *Aquaculture* **450**, 187–193  
1391 (2016).
- 1392 118. Giner-Sanz, J. J., Leverick, G. M., Pérez-Herranz, V. & Shao-Horn, Y. Salicylate Method for  
1393 Ammonia Quantification in Nitrogen Electroreduction Experiments: The Correction of Iron III  
1394 Interference. *J. Electrochem. Soc.* **167**, 134519 (2020).
- 1395 119. Murray, E. *et al.* A colorimetric method for use within portable test kits for nitrate determination  
1396 in various water matrices. *Anal. Methods* **9**, 680–687 (2017).
- 1397 120. Hayashi, M. Temperature-electrical conductivity relation of water for environmental monitoring  
1398 and geophysical data inversion. *Environ. Monit. Assess.* **96**, 119–128 (2004).
- 1399 121. Bruker. What Is NMR? *Bruker BioSpin* 145–158 (2010).
- 1400 122. Nielander, A. C. *et al.* A Versatile Method for Ammonia Detection in a Range of Relevant  
1401 Electrolytes via Direct Nuclear Magnetic Resonance Techniques. *ACS Catal.* **9**, 5797–5802  
1402 (2019).
- 1403 **This paper reports on a frequency-selective pulse nuclear magnetic resonance method for**  
1404 **the accurate determination of ammonia.**
- 1405 123. Mooney, E. F. & Winson, P. H. Nitrogen Magnetic Resonance Spectroscopy. *Annu. Reports NMR*

- 1406 *Spectrosc.* **2**, 125–152 (1969).
- 1407 124. Giddey, S., Badwal, S. P. S. & Kulkarni, A. Review of electrochemical ammonia production  
1408 technologies and materials. *Int. J. Hydrogen Energy* **38**, 14576–14594 (2013).
- 1409 125. Seh, Z. W. *et al.* Combining theory and experiment in electrocatalysis: Insights into materials  
1410 design. *Science (80-. )*. **355**, eaad4998 (2017).
- 1411 126. Choi, J. *et al.* Electroreduction of Nitrates, Nitrites, and Gaseous Nitrogen Oxides: A Potential  
1412 Source of Ammonia in Dinitrogen Reduction Studies. *ACS Energy Lett.* **5**, 2095–2097 (2020).
- 1413 127. Li, J. & Wu, N. Semiconductor-based photocatalysts and photoelectrochemical cells for solar fuel  
1414 generation: A review. *Catalysis Science and Technology* (2015).
- 1415 128. Kisch, H. Semiconductor Photocatalysis-Mechanistic and Synthetic Aspects. *Angew. Chemie Int.*  
1416 *Ed.* **52**, 812–847 (2013).
- 1417 129. Chen, X., Shen, S., Guo, L. & Mao, S. S. Semiconductor-based Photocatalytic Hydrogen  
1418 Generation. *Chem. Rev.* **110**, 6503–6570 (2010).
- 1419 130. Kibsgaard, J., Nørskov, J. K. & Chorkendorff, I. The Difficulty of Proving Electrochemical  
1420 Ammonia Synthesis. *ACS Energy Lett.* **4**, 2986–2988 (2019).
- 1421 131. Turner, C., Španěl, P. & Smith, D. A longitudinal study of ammonia, acetone and propanol in the  
1422 exhaled breath of 30 subjects using selected ion flow tube mass spectrometry, SIFT-MS. *Physiol.*  
1423 *Meas.* **27**, 321–337 (2006).
- 1424 132. Tao, H. *et al.* Nitrogen Fixation by Ru Single-Atom Electrocatalytic Reduction. *Chem* **5**, 204–214  
1425 (2019).
- 1426 133. Xiong, W. *et al.* Facile, cost-effective plasma synthesis of self-supportive FeS<sub>x</sub> on Fe foam for  
1427 efficient electrochemical reduction of N<sub>2</sub> under ambient conditions. *J. Mater. Chem. A* **7**, 19977–  
1428 19983 (2019).
- 1429 134. Suryanto, B. H. R. *et al.* MoS<sub>2</sub> Polymorphic Engineering Enhances Selectivity in the  
1430 Electrochemical Reduction of Nitrogen to Ammonia. *ACS Energy Lett.* **4**, 430–435 (2019).
- 1431 135. Li, X. *et al.* Boosted Electrocatalytic N<sub>2</sub> Reduction to NH<sub>3</sub> by Defect-Rich MoS<sub>2</sub> Nanoflower.  
1432 *Adv. Energy Mater.* **8**, (2018).
- 1433 136. Chen, G.-F. *et al.* Ammonia Electrosynthesis with High Selectivity under Ambient Conditions via  
1434 a Li<sup>+</sup> Incorporation Strategy. *J. Am. Chem. Soc.* **139**, 9771–9774 (2017).
- 1435 137. Song, Y. *et al.* A physical catalyst for the electrolysis of nitrogen to ammonia. *Sci. Adv.* **4**,  
1436 e1700336 (2018).
- 1437 138. Zhou, F. *et al.* Electro-synthesis of ammonia from nitrogen at ambient temperature and pressure in  
1438 ionic liquids. *Energy Environ. Sci.* **10**, 2516–2520 (2017).
- 1439 139. Tsuneto, A., Kudo, A. & Sakata, T. Lithium-mediated electrochemical reduction of high pressure  
1440 N<sub>2</sub> to NH<sub>3</sub>. *J. Electroanal. Chem.* **367**, 183–188 (1994).
- 1441 140. Tsuneto, A., Kudo, A. & Sakata, T. Efficient Electrochemical Reduction of N<sub>2</sub> to NH<sub>3</sub> Catalyzed  
1442 by Lithium. *Chem. Lett.* **22**, 851–854 (1993).
- 1443 141. Zhang, L. *et al.* A Janus Fe-SnO<sub>2</sub> Catalyst that Enables Bifunctional Electrochemical Nitrogen  
1444 Fixation. *Angew. Chemie Int. Ed.* **59**, 10888–10893 (2020).
- 1445 142. Hirakawa, H., Hashimoto, M., Shiraishi, Y. & Hirai, T. Photocatalytic Conversion of Nitrogen to

- 1446 Ammonia with Water on Surface Oxygen Vacancies of Titanium Dioxide. *J. Am. Chem. Soc.* **139**,  
1447 10929–10936 (2017).
- 1448 143. Comer, B. M. *et al.* The Role of Adventitious Carbon in Photo-catalytic Nitrogen Fixation by  
1449 Titania. *J. Am. Chem. Soc.* (2018).
- 1450 144. Wang, Z. *et al.* Recent Developments in Polymeric Carbon Nitride-Derived Photocatalysts and  
1451 Electrocatalysts for Nitrogen Fixation. *ACS Catalysis* (2019).
- 1452 145. Lv, C. *et al.* Defect Engineering Metal-Free Polymeric Carbon Nitride Electrocatalyst for  
1453 Effective Nitrogen Fixation under Ambient Conditions. *Angew. Chemie - Int. Ed.* (2018).
- 1454 146. Hu, B., Hu, M., Seefeldt, L. & Liu, T. L. Electrochemical Dinitrogen Reduction to Ammonia by  
1455 Mo<sub>2</sub>N: Catalysis or Decomposition? *ACS Energy Lett.* **4**, 1053–1054 (2019).
- 1456 147. Liu, Q. *et al.* Photocatalytic N<sub>2</sub> reduction: Uncertainties in the determination of ammonia  
1457 production. *ACS Sustain. Chem. Eng.* (2021).
- 1458 148. Bielawa, H., Hinrichsen, O., Birkner, A. & Muhler, M. The ammonia-synthesis catalyst of the next  
1459 generation: Barium-promoted oxide-supported ruthenium. *Angew. Chemie-International Ed.* **40**,  
1460 1061- (2001).
- 1461 149. Hagen, S. *et al.* New efficient catalyst for ammonia synthesis: barium-promoted cobalt on carbon.  
1462 *Chem. Commun.* **11**, 1206–1207 (2002).
- 1463 150. Kojima, R. & Aika, K. Cobalt molybdenum bimetallic nitride catalysts for ammonia synthesis Part  
1464 2. Kinetic study.pdf. *Appl. Catal. A Gen.* **218**, 121–128 (2001).
- 1465 **This article presents a typical kinetic study for thermocatalytic ammonia synthesis, including**  
1466 **the measurement conditions, derivation process of the equations, and the calculations.**
- 1467 151. Hagen, S. Ammonia synthesis with barium-promoted iron–cobalt alloys supported on carbon. *J.*  
1468 *Catal.* **214**, 327–335 (2003).
- 1469 152. Aika, K. Role of alkali promoter in ammonia synthesis over ruthenium catalysts—Effect on  
1470 reaction mechanism. *Catal. Today* **286**, 14–20 (2017).
- 1471 153. Holzman, P. R., Shiflett, W. K. & Dumesic, J. A. The importance of ammonia pressure in the  
1472 kinetics of ammonia synthesis over supported Ru. *J. Catal.* **62**, 167–172 (1980).
- 1473 **This study compared the results of apparent activation energies measured at constant**  
1474 **ammonia pressure and at constant flow rate, demonstrating the importance of ammonia**  
1475 **partial pressure for reaction kinetics.**
- 1476 154. Ye, T.-N. *et al.* Vacancy-enabled N<sub>2</sub> activation for ammonia synthesis on an Ni-loaded catalyst.  
1477 *Nature* **583**, 391–395 (2020).
- 1478 155. Tang, Y. *et al.* Metal-Dependent Support Effects of Oxyhydride-Supported Ru, Fe, Co Catalysts  
1479 for Ammonia Synthesis. *Adv. Energy Mater.* **8**, (2018).
- 1480 156. Kobayashi, Y. *et al.* Titanium-Based Hydrides as Heterogeneous Catalysts for Ammonia  
1481 Synthesis. *J. Am. Chem. Soc.* (2017).
- 1482 157. Cao, Y. *et al.* Vanadium Hydride as an Ammonia Synthesis Catalyst. *ChemCatChem* (2020).
- 1483 158. Kammert, J. *et al.* Nature of Reactive Hydrogen for Ammonia Synthesis over a Ru/C12A7  
1484 Electride Catalyst. *J. Am. Chem. Soc.* **142**, 7655–7667 (2020).
- 1485 159. Gao, W., Guo, J. & Chen, P. Hydrides, Amides and Imides Mediated Ammonia Synthesis and

- 1486 Decomposition. *Chinese J. Chem.* **37**, 442–451 (2019).
- 1487 160. Peterson, A. A., Abild-Pedersen, F., Studt, F., Rossmeisl, J. & Nørskov, J. K. How copper  
1488 catalyzes the electroreduction of carbon dioxide into hydrocarbon fuels. *Energy Environ. Sci.*  
1489 (2010).
- 1490 161. Sundararaman, R., Goddard, W. A. & Arias, T. A. Grand canonical electronic density-functional  
1491 theory: Algorithms and applications to electrochemistry. *J. Chem. Phys.* (2017).
- 1492 162. Kastlunger, G., Lindgren, P. & Peterson, A. A. Controlled-Potential Simulation of Elementary  
1493 Electrochemical Reactions: Proton Discharge on Metal Surfaces. *J. Phys. Chem. C* (2018).
- 1494 163. Govender, A., Curulla Ferré, D. & Niemantsverdriet, J. W. A density functional theory study on  
1495 the effect of zero-point energy corrections on the methanation profile on Fe(100). *ChemPhysChem*  
1496 (2012).
- 1497 164. Sholl, D. S. & Steckel, J. A. *Density Functional Theory: A Practical Introduction, Chapter 5, Pg.*  
1498 *113-130. Density Functional Theory: A Practical Introduction* (2009).
- 1499 **Book chapter covering zero point energy and entropy/enthalpy energy terms, and provides a**  
1500 **good overview of the theory.**
- 1501 165. Sprowl, L. H., Campbell, C. T. & Árnadóttir, L. Hindered translator and hindered rotor models for  
1502 adsorbates: Partition functions and entropies. *J. Phys. Chem. C* (2016).
- 1503 166. Núñez, M., Lansford, J. L. & Vlachos, D. G. Optimization of the facet structure of transition-metal  
1504 catalysts applied to the oxygen reduction reaction. *Nat. Chem.* **11**, 449–456 (2019).
- 1505 **This paper shows trade-offs between activity and stability.**
- 1506 167. Goldsmith, B. R., Sanderson, E. D., Bean, D. & Peters, B. Isolated catalyst sites on amorphous  
1507 supports: A systematic algorithm for understanding heterogeneities in structure and reactivity. *J.*  
1508 *Chem. Phys.* (2013).
- 1509 168. Wexler, R. B., Qiu, T. & Rappe, A. M. Automatic Prediction of Surface Phase Diagrams Using Ab  
1510 Initio Grand Canonical Monte Carlo. *J. Phys. Chem. C* (2019) doi:10.1021/acs.jpcc.8b11093.
- 1511 169. Shimanouchi, T. ‘Molecular Vibrational Frequencies’ in NIST Chemistry WebBook. *NIST*  
1512 *Standard Reference Database Number 69.*
- 1513 170. Makepeace, J. W. *et al.* Reversible ammonia-based and liquid organic hydrogen carriers for high-  
1514 density hydrogen storage: Recent progress. *Int. J. Hydrogen Energy* **44**, 7746–7767 (2019).
- 1515 171. Service, R. F. Liquid Sunshine. *Science* (80-. ). **361**, 120–123 (2018).
- 1516 172. Christensen, C. H., Johannessen, T., Sørensen, R. Z. & Nørskov, J. K. Towards an ammonia-  
1517 mediated hydrogen economy? *Catal. Today* **111**, 140–144 (2006).
- 1518 173. Soloveichik, G. ARPA-E REFUEL Program: Distributed Production of Ammonia and its  
1519 Conversion to Energy. in *2019 AIChE Annual Meeting* (AIChE, 2019).
- 1520 174. Kerru, N., Gummidi, L., Maddila, S., Gangu, K. K. & Jonnalagadda, S. B. A Review on Recent  
1521 Advances in Nitrogen-Containing Molecules and Their Biological Applications. *Molecules* **25**,  
1522 1909 (2020).
- 1523 175. Chen, C. *et al.* Coupling N<sub>2</sub> and CO<sub>2</sub> in H<sub>2</sub>O to synthesize urea under ambient conditions. *Nat.*  
1524 *Chem.* **12**, 717–724 (2020).
- 1525 176. Nielander, A. C. *et al.* Readily Constructed Glass Piston Pump for Gas Recirculation. *ACS Omega*

- 1526           **5**, 16455–16459 (2020).
- 1527 177. Tang, C. & Qiao, S.-Z. How to explore ambient electrocatalytic nitrogen reduction reliably and  
1528 insightfully. *Chem. Soc. Rev.* **48**, 3166–3180 (2019).
- 1529 178. Kang, C. S. M., Zhang, X. & MacFarlane, D. R. High Nitrogen Gas Solubility and  
1530 Physicochemical Properties of [C 4 mpyr][eFAP]–Fluorinated Solvent Mixtures. *J. Phys. Chem. C*  
1531 **123**, 21376–21385 (2019).
- 1532 179. Shi, R., Zhang, X., Waterhouse, G. I. N., Zhao, Y. & Zhang, T. The Journey toward Low  
1533 Temperature, Low Pressure Catalytic Nitrogen Fixation. *Adv. Energy Mater.* **10**, (2020).
- 1534 180. Munter, T. R., Bligaard, T., Christensen, C. H. & Nørskov, J. K. BEP relations for N<sub>2</sub> dissociation  
1535 over stepped transition metal and alloy surfaces. *Phys. Chem. Chem. Phys.* **10**, 5202 (2008).
- 1536 181. Yu, W. *et al.* Cathodic NH<sub>4</sub><sup>+</sup> + leaching of nitrogen impurities in CoMo thin-film electrodes in  
1537 aqueous acidic solutions. *Sustain. Energy Fuels* **4**, 5080–5087 (2020).
- 1538 182. Chen, Y. *et al.* Revealing nitrogen-containing species in commercial catalysts used for ammonia  
1539 electrosynthesis. *Nat. Catal.* **3**, (2020).
- 1540           **This paper shows that various commercially sold pure metals contain significant N-**  
1541 **containing contamination, and provides a way to measure these contaminants.**
- 1542 183. Hargreaves, J. S. J. Heterogeneous catalysis with metal nitrides. *Coord. Chem. Rev.* **257**, 2015–  
1543 2031 (2013).
- 1544 184. Krauth, O., Fahsold, G. & Lehmann, A. Surface-enhanced infrared absorption. *Surf. Sci.* **433**, 79–  
1545 82 (1999).
- 1546 185. Yao, Y., Zhu, S., Wang, H., Li, H. & Shao, M. A Spectroscopic Study on the Nitrogen  
1547 Electrochemical Reduction Reaction on Gold and Platinum Surfaces. *J. Am. Chem. Soc.* **140**,  
1548 1496–1501 (2018).
- 1549 186. Yao, Y., Wang, H., Yuan, X. Z., Li, H. & Shao, M. Electrochemical Nitrogen Reduction Reaction  
1550 on Ruthenium. *ACS Energy Lett.* **4**, 1336–1341 (2019).
- 1551 187. Matsui, T. *et al.* In Situ Attenuated Total Reflection Infrared Spectroscopy on Electrochemical  
1552 Ammonia Oxidation over Pt Electrode in Alkaline Aqueous Solutions. *Langmuir* **31**, 11717–  
1553 11723 (2015).
- 1554 188. Abdiaziz, K., Salvadori, E., Sokol, K. P., Reisner, E. & Roessler, M. M. Protein film  
1555 electrochemical EPR spectroscopy as a technique to investigate redox reactions in biomolecules.  
1556 *Chem. Commun.* **55**, 8840–8843 (2019).
- 1557 189. Bajada, M. A. *et al.* A Precious-Metal-Free Hybrid Electrolyzer for Alcohol Oxidation Coupled to  
1558 CO<sub>2</sub>-to-Syngas Conversion. *Angew. Chemie Int. Ed.* **59**, 15633–15641 (2020).
- 1559 190. Joris, G. G. & Taylor, H. S. Exchange reactions of nitrogen isotopes on iron and tungsten surfaces.  
1560 *J. Chem. Phys.* **7**, 893–898 (1939).
- 1561 191. Urabe, K. Activation of nitrogen by alkali metal-promoted transition metal II. Isotopic exchange in  
1562 molecular nitrogen over potassium-promoted ruthenium-carbon catalyst. *J. Catal.* **32**, 108–113  
1563 (1974).
- 1564 192. Urabe, K. Activation of nitrogen by alkali metal-promoted transition metal VI. Hydrogen effect on  
1565 isotopic equilibration of nitrogen and rate-determining step of ammonia synthesis on potassium-  
1566 promoted ruthenium catalysts. *J. Catal.* **42**, 197–204 (1976).



- 1567 193. Hunter, S. M. *et al.* A study of <sup>15</sup>N/<sup>14</sup>N isotopic exchange over cobalt molybdenum nitrides. *ACS*  
1568 *Catal.* **3**, 1719–1725 (2013).
- 1569 194. Hargreaves, J. S. J. Nitrides as ammonia synthesis catalysts and as potential nitrogen transfer  
1570 reagents. *Appl. Petrochemical Res.* (2014).
- 1571 195. Shannon, S. L. & Goodwin, J. G. Characterization of Catalytic Surfaces by Isotopic-Transient  
1572 Kinetics during Steady-State Reaction. *Chem. Rev.* **95**, 677–695 (1995).
- 1573 196. Nwalor, J. Steady-state isotopic transient-kinetic analysis of iron-catalyzed ammonia synthesis. *J.*  
1574 *Catal.* **117**, 121–134 (1989).
- 1575 197. Nwalor, J. U. & Goodwin, J. G. Isotopic tracing study of K promotion of NH<sub>3</sub> synthesis on Ru.  
1576 *Top. Catal.* **1**, 285–293 (1994).
- 1577 198. McClaine, B. Isotopic Transient Kinetic Analysis of Cs-Promoted Ru/MgO during Ammonia  
1578 Synthesis. *J. Catal.* **210**, 387–396 (2002).
- 1579 199. McClaine, B. C. & Davis, R. J. Importance of Product Readsorption during Isotopic Transient  
1580 Analysis of Ammonia Synthesis on Ba-Promoted Ru/BaX Catalyst. *J. Catal.* **211**, 379–386  
1581 (2002).
- 1582 200. Siporin, S. Isotopic transient analysis of ammonia synthesis over Ru/MgO catalysts promoted by  
1583 cesium, barium, or lanthanum. *J. Catal.* **222**, 315–322 (2004).
- 1584 201. Schlesinger, W. & Hartley, A. A global budget for atmospheric NH<sub>3</sub>. *Biogeochemistry* **15**, 191–  
1585 211 (1992).
- 1586 202. Vojvodic, A. *et al.* Exploring the limits: A low-pressure, low-temperature Haber-Bosch process.  
1587 *Chem. Phys. Lett.* (2014).
- 1588 203. Spinelli, J. B., Kelley, L. P. & Haigis, M. C. An LC-MS Approach to Quantitative Measurement  
1589 of Ammonia Isotopologues. *Sci. Rep.* **7**, 10304 (2017).
- 1590 204. Liu, Y. *et al.* Facile All-Optical Method for In Situ Detection of Low Amounts of Ammonia.  
1591 *iScience* **23**, 101757 (2020).
- 1592 205. Mou, S., Wang, H. & Sun, Q. Simultaneous determination of the three main inorganic forms of  
1593 nitrogen by ion chromatography. *J. Chromatogr. A* **640**, 161–165 (1993).
- 1594 206. Andersen, S. Z. Electrochemical Nitrogen Reduction Under (Near) Ambient Conditions. *Technical*  
1595 *University of Denmark* (2020).
- 1596 207. Timmer, B. H., van Delft, K. M., Otjes, R. P., Olthuis, W. & van den Berg, A. Miniaturized  
1597 measurement system for ammonia in air. *Anal. Chim. Acta* **507**, 137–143 (2004).
- 1598 208. Kim, K., Yoo, C.-Y., Kim, J.-N., Yoon, H. C. & Han, J.-I. Electrochemical Synthesis of Ammonia  
1599 from Water and Nitrogen in Ethylenediamine under Ambient Temperature and Pressure. *J.*  
1600 *Electrochem. Soc.* **163**, F1523–F1526 (2016).
- 1601 209. Sato, K. *et al.* A low-crystalline ruthenium nano-layer supported on praseodymium oxide as an  
1602 active catalyst for ammonia synthesis. *Chem. Sci.* **8**, 674–679 (2017).
- 1603 210. Chang, F. *et al.* Alkali and Alkaline Earth Hydrides-Driven N<sub>2</sub> Activation and Transformation  
1604 over Mn Nitride Catalyst. *J. Am. Chem. Soc.* **140**, 14799–14806 (2018).
- 1605 211. Kitano, M. *et al.* Low-Temperature Synthesis of Perovskite Oxynitride-Hydrides as Ammonia  
1606 Synthesis Catalysts. *J. Am. Chem. Soc.* **141**, 20344–20353 (2019).



- 1607 212. Kitano, M. *et al.* Self-organized Ruthenium-Barium Core-Shell Nanoparticles on a Mesoporous  
1608 Calcium Amide Matrix for Efficient Low-Temperature Ammonia Synthesis. *Angew. Chemie Int.*  
1609 *Ed.* **57**, 2648–2652 (2018).
- 1610 213. Wang, Y. *et al.* Generating Defect-Rich Bismuth for Enhancing the Rate of Nitrogen  
1611 Electroreduction to Ammonia. *Angew. Chemie Int. Ed.* **58**, 9464–9469 (2019).
- 1612 214. Kong, J. *et al.* Electrochemical Synthesis of NH<sub>3</sub> at Low Temperature and Atmospheric Pressure  
1613 Using a  $\gamma$ -Fe<sub>2</sub>O<sub>3</sub> Catalyst. *ACS Sustain. Chem. Eng.* **5**, 10986–10995 (2017).
- 1614 215. Shi, M.-M. *et al.* Au Sub-Nanoclusters on TiO<sub>2</sub> toward Highly Efficient and Selective  
1615 Electrocatalyst for N<sub>2</sub> Conversion to NH<sub>3</sub> at Ambient Conditions. *Adv. Mater.* **29**, 1606550  
1616 (2017).
- 1617 216. Zhang, N. *et al.* Refining Defect States in W<sub>18</sub>O<sub>49</sub> by Mo Doping: A Strategy for Tuning N<sub>2</sub>  
1618 Activation towards Solar-Driven Nitrogen Fixation. *J. Am. Chem. Soc.* **140**, 9434–9443 (2018).
- 1619 217. Wang, S. *et al.* Light-Switchable Oxygen Vacancies in Ultrafine Bi<sub>5</sub>O<sub>7</sub>Br Nanotubes for Boosting  
1620 Solar-Driven Nitrogen Fixation in Pure Water. *Adv. Mater.* **29**, 1701774 (2017).
- 1621 218. Jang, Y. J., Lindberg, A. E., Lumley, M. A. & Choi, K. S. Photoelectrochemical Nitrogen  
1622 Reduction to Ammonia on Cupric and Cuprous Oxide Photocathodes. *ACS Energy Lett.* **5**, 1834–  
1623 1839 (2020).
- 1624 219. Zhu, D., Zhang, L., Ruther, R. E. & Hamers, R. J. Photo-illuminated diamond as a solid-state  
1625 source of solvated electrons in water for nitrogen reduction. *Nat. Mater.* **12**, 836–841 (2013).
- 1626 220. Wang, X. *et al.* Insight into dynamic and steady-state active sites for nitrogen activation to  
1627 ammonia by cobalt-based catalyst. *Nat Commun* **11**, 653 (2020).
- 1628 221. Ogura, Y. *et al.* Efficient ammonia synthesis over a Ru/La<sub>0.5</sub>Ce<sub>0.5</sub>O<sub>1.75</sub> catalyst pre-reduced  
1629 at high temperature. *Chem. Sci.* **9**, 2230–2237 (2018).
- 1630 222. Hodgetts, R. Y. *et al.* Refining Universal Procedures for Ammonium Quantification via Rapid <sup>1</sup>H  
1631 NMR Analysis for Dinitrogen Reduction Studies. *ACS Energy Lett.* **5**, 736–741 (2020).

1632 **This paper assesses the sensitivity of nuclear magnetic resonance towards the detection of**  
1633 **ammonia in solutions with different proton concentration**

1634

1635 

## Glossary Terms

1636 **Faradaic Efficiency:** The efficiency at which charge, in the form of electrons, participate in a specific  
1637 electrochemical reaction

1638 **Activation barriers:** The minimal amount of energy required for reactants to undergo a chemical  
1639 reaction This is the energy difference between the reactant and the transition state.

1640 **Standard potential:** The potential (V) of a reversible electrode at standard state with ions at an effective  
1641 1 M concentration at the pressure of 1 atm.

1642 **Electrochemical half-cell reactions:** Either an oxidation reaction on the anode electrode where an  
1643 electron is lost or a reduction reaction on the cathode electrode where an electron is gained.

1644 **Electric arc-generated hot plasma:** A discharge of electric current across a spatial gap, sustained by the  
1645 presence of a thermally ionized plasma, which allows for the flow of said current.

1646 **Reaction orders:** the power dependence of the rate on the concentration of each reactant, which is an  
1647 experimentally determined parameter that can have fraction values.

1648 **Tafel analysis:** is used to determine an electrochemical systems transfer coefficient via voltammograms,  
1649 thereby providing information about the electrochemical mechanism and catalytic activity.

1650 **Ohmic correction:** Accounting for the Ohmic resistance of the media to accurately determine the  
1651 potential at the surface of the electrode.

1652 **Quantum yield:** Determining the number of times a specific event occurs per absorbed photon by the  
1653 system in question.

1654 **Density functional theory:** a computational quantum mechanical modelling method used to investigate  
1655 the electronic structure of many-body systems.

1656 **Zero point energy:** The lowest possible energy that a quantum mechanical system contains, which  
1657 includes fluctuations in the lowest energy state from the Heisenberg uncertainty principle.

1658 **Pareto-optimal frontier:** A curve which contains physically possible optimal trade-offs between activity  
1659 and stability

1660 **Physisorption:** Also called physical adsorption, is a weak intermolecular attraction via van der Waals  
1661 forces, which results in the development of monolayers or multilayers of adsorbates upon a surface.

1662

1663

RAT

1664 *Nature Reviews Methods Primers* thanks ref name, ref name and the other, anonymous, reviewer(s) for  
1665 their contribution to the peer review of this work.

1666

1667

## TOC blurb

1668 This Primer highlights the range of new strategies for sustainable N<sub>2</sub> activation and the step-by-step  
1669 protocol necessary for evaluating genuine activity. The required metrics and how to interpret data  
1670 alongside the best practices to improve reproducibility and enable the development of practical  
1671 technologies are discussed.